THEORETICAL AND EXPERIMENTAL INVESTIGATION OF THE IMPACT OF SURFACES ON DNA MELTING TEMPERATURE

by

Ayse Bilge Ozel

A dissertation submitted in partial fulfillment
of the requirements for the degree of
Doctor of Philosophy
(Chemical Engineering)
in The University of Michigan
2009

Doctoral Committee:

Professor Erdogan Gulari, Chair
Professor Mark A. Burns
Associate Professor Joerg Lahann
Associate Professor Shuichi Takayama

To my family – Mom, dad, brother, aunt and uncle

ACKNOWLEDGMENTS

I would like to thank Professor Erdogan Gulari for his advise, supervision and support throughout my dissertation. I also thank my doctoral committee members for their guidance on this work. Special thanks to all past and present Gulari members for making it an enjoyable journey, especially to Dr Onnop Srivannavit for his time and help.

I also would like to thank all of the Chemical Engineering staff members for their assistance, and also my friends for their continuous motivation.

I would like to dedicate this work to my family: my dad and mom, brother, aunt and her family, uncle and his family. The completion of this work would be impossible without their endless support, encouragement and inspiration.

TABLE OF CONTENTS

DEDICATION ii
ACKNOWLEDGEMENTS iii
LIST OF FIGURES vii
LIST OF TABLES xii
ABSTRACT xiii

CHAPTER

I. INTRODUCTION 1
1.1 Motivation 1
1.2 Theoretical Studies Investigating DNA Hybridization on the Surface 4
1.3 Experimental Approaches Investigating DNA Hybridization 5
1.3.1 Melting Temperature in Solution 5
1.3.2 Adaptation of Melting Temperature Definition on Surface 8
1.3.3 Experimental Studies Investigating DNA Hybridization on the Surface 9
1.4 Research Scope 12
1.5 Bibliography 14

II. THEORY OF ELECTROSTATIC AND ENTROPIC BLOCKING 24
2.1 Introduction 24
2.2 Materials and Methods 27
2.3 Theory 28
2.3.1 Electrostatic Blocking 28
2.3.2 Entropic Blocking 35
2.4 Results and Discussion 41
2.4.1 Zeta Potential Experiments 41
2.4.2 Electrostatic Blocking 44
2.4.3 Entropic Blocking 49

2.5 Conclusions 51
2.6 Appendix 53
2.6.1 Electrostatic Blocking 53
2.6.2 Entropic Blocking 54
2.7 Bibliography 55

III. DEVELOPMENT OF AN EXPERIMENTAL APPROACH TO GENERATE DNA MELTING CURVES ON THE SURFACE 58

3.1 Introduction 58
3.2 Experimental System Development 59
3.2.1 Experimental Set-up 59
3.2.2 Experimental Design 74
3.3 Data Analysis and Quality Assessment 77
3.3.1 Synthesis Quality Assessment 77
3.3.2 Melting Curve Analysis 79
3.3.3 Performance of the Analysis Method 83
3.4 Conclusions 86
3.5 Appendix 87
3.6 Bibliography 89

IV. THE EFFECT OF INITIAL TARGET CONCENTRATION 93

4.1 Introduction 93
4.2 Materials and Methods 96
4.3 Results and Discussion 98
4.3.1 The Effect of Target Concentration on the Melting Temperature on the Surface 98
4.3.2 Assessing the Synthesis Imperfections using Melting Curves 113
4.4 Conclusions 117
4.5 Bibliography 119

V. THE EFFECT OF SPACER LENGTH AND PROBE DENSITY 123

5.1 Introduction 123
5.2 Materials and Methods 126

5.3 Results and Discussion 128
5.3.1 Effect of Spacer Length on Melting Temperature 128
5.3.2 Effect of Probe Density on Melting Temperature 134
5.3.3 The Comparison of the Effects of Spacer Length and Probe Density on Melting Temperature 138
5.4 Conclusions 143
5.5 Bibliography 145
VI. CONCLUSIONS AND RECOMMENDATIONS 148
6.1 Conclusions 148
6.2 Recommendations for Future Work 152
6.3 Bibliography 154

LIST OF FIGURES

Figure

1-1 An experimental UV melting curve of a bimolecular duplex oligomer dissolve in 1 M NaCl-phosphate buffer, at C_{TOTAL} = 2 μM, pH = 7.0 6

2-1 Potential distribution around a charged particle in an ionic solution. 29

2-2 (a) The distribution of electrolyte ions (Na^+ and Cl^-) across a negatively charged, ion-penetrable polyelectrolyte layer (i.e. spacer) on a solid planar surface (b) The electric potential distribution across a negatively charged, ion-penetrable polyelectrolyte layer (i.e. spacer) on a solid planar surface. 32

2-3 Zeta potential measurements with different bead concentrations in 2 ml of 1X SSPE, pH = 6.7 at 23°C. 42

2-4 Average measured Zeta potential values with 0.001 mg glass beads at different steps during synthesis measured in 2ml of 0.01X (0.0016 M NaCl), 0.1X (0.016 M NaCl), 1X (0.16 M NaCl) SSPE, pH = 6.7 at 23°C. 42

2-5 Calculated surface potentials for 0.001 mg glass beads at different steps during synthesis measured in 2ml of 0.01X (0.0016 M NaCl), 0.1X (0.016 M NaCl), 1X (0.16M NaCl) SSPE, pH = 6.7 at 23°C, using Poisson-Boltzmann theory for hard spheres without ion penetration. 45

2-6 The comparison of the calculated potential at the half of the Debye length on a surface with a 15 dT spacer using the Poisson Boltzmann approach with ion penetration, and measured zeta potentials for 0.001 mg glass beads at the end of 15 dT spacer synthesis in 2 ml of 0.01X (0.0016 M NaCl), 0.1X (0.016 M NaCl), 1X (0.16 M NaCl) SSPE, pH 6.7 at 23°C. 46

2-7 Electrostatic free energy penalty experienced by a target hybridizing in a probe layer with a surface coverage of 0.5, at 23°C and 1 M NaCl concentration (a) with respect to spacer lengths of 2 dT, 15 dT, 25 dT at different probe densities, (b) with respect to probe densities of $5*10^{12}$ molecules/cm^2, $5*10^{13}$ molecules/cm^2 and $5*10^{14}$ molecules/cm^2 at different spacer lengths. 48

2-8 Entropic free energy penalty experienced by a target hybridizing in a probe layer with a surface coverage of 0.5, at 23°C and 1 M NaCl concentration (a) with respect to spacer lengths of 2 dT, 15 dT, 25 dT at different probe densities, (b) with respect to probe densities of $5*10^{12}$ molecules/cm^2, $5*10^{13}$ molecules/cm^2 and $5*10^{14}$ molecules/cm^2 at different spacer lengths..... 50

2-9 Electrostatic free energy penalty felt by a target (25mer) coming into the probe (25mer) layer at different surface coverages with probe densities of $5*10^{12}$ molecules/cm^2, $5*10^{13}$ molecules/cm^2, $5*10^{14}$ molecules/cm^2 at spacer lengths (Ns) of 2 dT, 15 dT, 25 dT, at 23°C and 1 M ionic (NaCl) concentration 53

2-10 Entropic free energy penalty felt by a target (25mer) coming into the probe (25mer) layer at different surface coverages with probe densities of $5*10^{12}$ molecules/cm^2, $5*10^{13}$ molecules/cm^2, $5*10^{14}$ molecules/cm^2 at spacer lengths (Ns) of 2 dT, 15 dT, 25 dT, at 23°C and 1 M ionic (NaCl) concentration 54

3-1 The experimental set-up comprising of a custom-designed holder housing a microfluidic chip, heater chip, temperature probe and the necessary fluidic and electrical connections; a temperature controller to check the temperature, a pump to circulate the hybridization solution, and a fluorescence scanner for detection. 60

3-2 The holder housing the microfluidic chip with the probes synthesized; a microfabricated heater chip for heating; a temperature probe for temperature

measurement; fluidic connections through which the target constantly recirculates; electrical connections with the temperature controller. 60

3-3 (a) Optical set-up within the fluorescence scanner (b) Representation of the TIRF mechanism and evanescent waves on the glass surface during the detection of the fluorescence signal off the targets hybridized with the probes on the glass surface and flowing free in solution. 63

3-4 A phosphoramidite DNA synthesis cycle. 69

3-5 Parallel synthesis using acid-labile protecting groups. The DNA chain is deprotected in a spatially controlled manner using photogenerated acid (PGA) (b and d), followed by coupling and oxidation reactions (c and e). This cycle is repeated until the desired lengths and sequences are obtained (f). 71

3-6 (a) Observed changes in the signal intensities on the surface at temperatures of 25°C, 40°C and 55°C at constant PMT voltage, brightness and contrast settings. (b) A melting curve of a perfect match duplex reproduced from the net signal intensities of the duplex at increasing temperatures. 76

3-7 (a) The signal distribution within a cross-section of a 50 μm spot with Cy3 labeled targets hybridized with the probes on the surface. (b) The overall signal intensity change on the chip with respect to the length of the Cy3 labeled synthesis controls on the surface. 78

3-8 (a) An example of the change in the fluorescence signal of the empty spots with respect to temperature. (b) Comparison of the experimental empty spot intensity change with the signal intensities derived from the Equation 3-4 at different temperatures. 81

3-9 Addressing the method performance with simulated data. The originally created curve has the following parameters: a_1 = 55,000, a_2 = 150, x_0 = 57, dx = 5. Various signal to noise ratio values are obtained via assigning the parameter x_0 different values ranging from 46 to 70. 84

3-10 The effect of PMT voltage and temperature on the average signal intensity at a target solution concentration of 0.05 nM. 87

3-11 The effect of PMT voltage and temperature on the average signal intensity at a target solution concentration of 0.5 nM. 88

3-12 The effect of PMT voltage and temperature on the average signal intensity at a target solution concentration of 1 nM. 88

4-1 The melting temperature trends observed on the surface and predicted in solution (using Nearest Neighbor method) with respect to different target concentrations at perfect match probe amounts of (a) 0.82 pmoles (b) 0.59 pmoles and (c) 0.03 pmoles on 10^{18} $Å^2$ surface. 100

4-2 3-dimensional representation of the variation in melting temperature of a duplex formed on surface as a function of the maximum extent of hybridization and initial target-to-probe concentration ratio at fixed initial hybridization temperature (23°C), standard enthalpy change of transition (ΔH^0(23°C) = - 104.7 kcal/mole) and specific heat capacity change (ΔC_p^0 = 12.5 cal/mole.bp.K). 109

4-3 Trends in melting temperature with respect to maximum extents of hybridization at two different initial target-to-probe ratios, as extracted from the plot in Figure 4-2. 110

4-4 Free energy contribution of electrostatic and entropic blocking terms encountered by a hybridizing target, as reproduced from the theoretical model presented in Chapter 2, and simulated with the system parameters (spacer length = 15 dT, probe length = target length = 25 nt, probe density = $5*10^{12}$ molecules/cm^2). 112

4-5 Experimentally observed melting curves of two duplexes formed on the surface with target concentrations of 15 nM and 5 nM with a constant probe concentration of 0.82 pmoles in 10^{18} $Å^2$ (from Experimental set 1). 112

4-6 A representative perfect-match duplex melting curve and the effect of pre-hybridization at 50°C for 5 h observed in Experimental Set 3 with target concentration of 0.0165 nM and probe concentration of 0.0165 pmoles in 10^{18} $Å^2$ 114

5-1 The comparison of the effect of spacer length on the melting temperature of the duplex on surface with predicted melting temperatures in solution at the same target-to-probe ratios. 129

5-2 Contributions of (a) Electrostatic blocking and (b) Entropic blocking on the free energy of duplex formation on the surface, with spacer lengths (2 dT, 15 dT, 25 dT) used in the experiments with respect to different surface coverages and a fixed probe density of $5*10^{12}$ molecules/cm^2, a salt concentration of 1M NaCl, and at 23°C. 131

5-3 The comparison of the effect of probe density on the melting temperature of the duplex on surface with predicted melting temperatures in solution at the same target-to-probe ratios. 135

5-4 The contribution of (a) electrostatic blocking and (b) entropic blocking on the free energy of duplex formation in the presence of different probe densities ($5*10^{12}$ molecules/cm^2, $5*10^{13}$ molecules/cm^2) used in the experiments with respect to different surface coverages and a fixed spacer length of 15 dT, a salt concentration of 1M NaCl, and at 23°C..... 136

5-5 Hybridization signal intensity change on the surface with respect to different probe densities. Hybridization conditions were 1 M NaCl, at 23°C and 100 nM target concentration. 139

5-6 The comparison of the effect of spacer length and probe density on the melting temperature of the duplex on surface with predicted melting temperatures in solution at the same target-to-probe ratios. 142

LIST OF TABLES

Table

1-1 Di-nucleotide Parameters in Nearest-Neighbor Method. 7

2-1 Predicted surface potential and charge values at salt concentrations of 0.0016 M, 0.016 M, and 0.16 M after the 15 dT spacer synthesis. 45

3-1 Effect of the changes in the concentration of the signal on the surface (C_1) and in solution (C_2) on the SI/I_o value. 65

3-2 Signal to noise ratio variation at different simulated x_0 parameters. 85

3-3 Average, standard deviation and regression coefficients of the melting temperatures calculated from the simulated data using the analysis method. 85

4-1 Summary of the Experiments Performed to Address the Effect of Target and Probe Concentrations on the Duplex Formation on the Surface 97

4-2 PMT Voltages Used in Experimental Set 1. 111

5-1 Summary of the Experiments on Spacer Length and Probe Density. 127

5-2 PMT voltages used in 635 nm wavelength to detect the probe-target duplex formed on the surface at equilibrium, at the end of initial hybridization, with different spacer lengths and target concentrations (at a probe density of $5*10^{12}$ molecules/cm^2). 132

5-3 PMT voltages used in 635 nm wavelength to detect the probe-target duplex formed on the surface at equilibrium, at the end of initial hybridization, with different probe densities and target concentrations. 137

ABSTRACT

The design of microarrays rely on studies geared towards sequence-specific recognition between complementary probe and target molecules in bulk solution. However, this proves to be insufficient to understand the duplex formation reaction on solid-phase. In this dissertation, influence of the surface on DNA duplex stability and melting temperature were theoretically and experimentally investigated. The theoretical approach represents electrostatic and entropic repulsions experienced by hybridizing targets. Electrostatic blocking stemming from surface charge was modeled through Electric Double Layer Theory and Surface Partition Model. Entropic blocking due to steric effects was modeled using polymer physics. Investigated experimental parameters were target concentration, spacer length and probe density. All the experiments gave reproducible melting temperatures with values lower on-surface than in-solution. In a representative set, a target concentration increase from 0.5 nM to 15 nM with 0.82 pmoles of probe at $5*10^{12}$ molecules/cm^2 density on 15 dT spacer resulted in approximately 8°C decrease in melting temperature, compared to 5°C increase in solution. This decreasing trend was supported by theory with increasing steric and electrostatic effects at increasing target concentrations leading to higher hybridization efficiencies. Additionally, at low target concentrations (0.0165 nM), we observed a multiple melting process in low temperature domains of melting curves due to low stability truncated probes; an indirect indication of synthesis quality. It was observed that as spacer length increases from 2 dT to 25 dT with 0.82 pmoles of probe at $5*10^{12}$ molecules/cm^2 density with target concentrations ranging from 0.36 nM to 1 nM, melting temperature increases; an observation theoretically explained by possible entropic blocking dominance. Probe density effect was tested at $5*10^{12}$ molecules/cm^2 and $5*10^{13}$ molecules/cm^2, on 15 dT spacer and target-to-probe

concentration ratios of 0.61:1 to 1.7:1. It was observed that high probe density resulted in lower melting temperature. This trend was theoretically supported by increasing electrostatic and crowding effects. Previously observed dependence of melting temperature on target concentration was also confirmed in all experiments. Melting temperature dependence on probe density seems to be stronger than the dependence on spacer length. The results of this work would lead to better experimental design and correct use of microarrays.

CHAPTER I

INTRODUCTION

1.1 Motivation

The completion of the human genome along with many different organisms opened a new era for humankind, providing vast number of opportunities for the scientific community. How well these opportunities can be utilized to extract the information underneath depends on the extent and applicability of the methods and techniques employed; and more importantly, how the biological basic principles are incorporated in them.

Nucleic acid hybridization is one of these basic principles used extensively in molecular biology. It is defined as the process that combines complementary single-stranded nucleic acids into a single molecule. Since the first hybridization experiment performed by Alexander Rich in the early 1960s [1], it is integrated in various methods, such as Southern and northern blotting, in nucleic acid amplifications such as the polymerase chain reaction (PCR), and more recently found its way into a more sophisticated technology, microarrays.

Microarrays are spatially ordered, miniaturized arrangement of a multitude of immobilized reagents on a planar two-dimensional support [2]. Among the variety of microarrays available, cDNA and oligonucleotide microarrays have been of particular interest, partly due to their assistance in the analysis of nucleic acids, which are considered as the central molecules in the transmission, expression and conservation of genetic information. Their increasing number of applications range from gene expression pattern analysis of different organisms (gene expression profiling) [3-5], genetic classifications [6-8] to pathway mapping

[9, 10], analysis of polymorphisms [11, 12], pathogen detection [13, 14] and predicting drug sensitivities and resistances [15-17] to individualize the medicinal approaches to make the treatments more effective.

With growing interest in understanding and analyzing the genomic and transcriptomic characteristics of the biological entities, more and more questions start to arise in different stages of this process, going down to the very fundamentals of what is really taking place on the microarrays. The answer revolves around one of the other reasons these microarrays found their way into the laboratory much faster than the others: their ease of incorporation into practice with the currently available knowledge about nucleic acid structures, properties and functions.

cDNA or oligonucleotide microarrays consists of a multitude of cDNA or oligonucleotides present on the surface (probes), which are designed to capture the free target DNA, RNA or oligonucleotide in solution. These probes are either immobilized on the surface through different immobilization techniques [18-20] or synthesized through in-situ synthesis [21-23]. The approach developed in our laboratory towards creating a unique way of synthesizing oligonucleotide arrays in a more efficient and economical manner [24] narrows the choice of platform of focus down to oligonucleotide microfluidic arrays.

Oligonucleotides are linear chains of nucleotides in a certain sequence, linked by phospodiester bonds. These chains form the backbone of the molecule, which is made from alternating phosphate-sugar residues. The nucleotides consist of the purine (adenine, A and guanine, G) or pyrimidine (cytosine, C or thymine, T) bases attached to the sugars (2'-deoxyribose or a ribose) and in turn the phosphate groups. These nucleotide repeats along the chain help the molecule form a double helical structure with an opposite anti-parallel, complementary strand, as it naturally exists in living organisms.

The stabilization of this double helix structure comes through various interactions existing between the two strands; mainly the hydrogen bonding between the opposite bases (inter-strand), and the base-stacking of the bases

with the neighboring bases on the same strand (intra-strand). Conceptually, the importance of stabilization plays the leading role in nucleic acid hybridization.

Within the complex environment this reaction takes place, it would be realistic to assume that the stability is affected by the many variables in the system: ionic concentrations, concentrations of the strands, concentrations of various chemical reagents, temperature; and the characteristics of the strands themselves: the composition, the sequence and the length [25]. These variables are inherent to in-solution hybridization processes, but on the surface of a microarray, additional ones need to be considered, which are: one of the strands being ‘attached’ on the surface; the presence of the surface; how densely packed the surface is; how far the reaction is taking place away from the surface; how long the attached strand is; how long the target in solution is; and where on the probe the target is forming the double helix.

The factors that control hybridization have been extensively studied for duplex formation in solution [26-28]. On the other hand, there are fewer investigations looking at the reaction between a free target in solution and an immobilized probe on the surface. This is one of the main reasons why current microarray design relies on the models used in solution [29-31]. However, this proves to be a problematic approach as recently shown in some of the experimental studies [32-34].

Two main design problems that interfere with the correct interpretation of the hybridization signal patterns on the surface are caused by false positive and false negative signals [34-37]. False positive signals are mainly the result of cross-hybridization, which results from the capture of the targets different than the probe is designed for, non-specifically. Due to sequence design or low stringency of the hybridization conditions to discriminate the specific and non-specific signals, this could lead to high background calculations or miscalculation of fold changes in gene expression studies [36]. On the other hand, false negative signals are mainly due to inefficient hybridization or low hybridization efficiency, the result of hybridization conditions that would create duplex structures with low stability and thus, signal intensity [38, 39]. This is a common

observation in the case of pathogens with low expression levels [35], which can lead to misidentification in genetic profiling [37]. Both of these situations seem to be due to the usage of sub-optimal conditions, given the surface characteristics, that can lead to results other than the objectives intended in the experiments.

Within the complex environment of nucleic acid hybridization on a solid-interphase, it is difficult to design experiments for an accurate outcome without prior knowledge of how the DNA strands would behave. This makes it necessary to investigate the effect of each system (i.e. spacer length, probe density) and experimental parameter (i.e. ionic concentration, target concentration) on DNA duplex formation on the surface, experimentally or theoretically, as an initial step.

1.2 Theoretical Studies Investigating DNA Hybridization on the Surface

Theoretical studies on DNA hybridization on the surface focus on different aspects of the reaction. The disruption of the DNA stability due to the presence of the surface is examined with the introduction of two hybridization blockage terms: electrostatic and entropic. Electrostatic blocking represents the interaction of the charges on the surface and the hybridizing target. Several approaches look at potential distribution around the surface to model this interaction [40-42], and some of them take into account the similarity of the DNA hybridization behavior with the protein adsorption on the surface and use Surface Partition Model [43]. Entropic blocking characterizes the entropic repulsion of the hybridizing target due to volume exclusion effects of the surface, the probes on the layer, and the effect of the immobilization of the probe. Work that has been done in this area utilizes the concepts behind polymer physics [43-45]. Some of these studies use their approaches to simulate the effect of different characteristics of the microarrays: probe and target length [43] and spacer length [46].

Alternatively, DNA hybridization on the surface is also studied using simulations. Molecular dynamics simulations are performed to obtain a more quantitative understanding of the salt gradients and DNA structures near surfaces [47, 48]. Monte Carlo simulations are utilized to examine the effects of

probe length, position of complementary segments, temperature of hybridization, target concentration and probe density on the specificity and sensitivity of the arrays [49, 50].

Surface hybridization is also modeled through physical models, which utilize concepts of thermodynamics, statistical mechanics, molecular physics and chemical kinetics to relate the experimentally observed probe intensities with the concentration of hybridized targets. Recent studies explore the sequence effects in the behavior of the perfect and mismatch probes, and attempt to establish a relationship between the probe signal intensities and these sequences [36, 38, 43, 45, 51].

1.3 Experimental Approaches Investigating DNA Hybridization

1.3.1 Melting Temperature in Solution

In solution, DNA hybridization and melting can be monitored using the parameter, melting temperature. It is defined as the temperature at which 50 percent of the duplexes initially present are denatured or unfolded into two single strands constituting it.

Spectroscopic or calorimetric melting experiments are commonly carried out to observe the conformational changes in the helical structure of DNA in the sample solution as it is heated and allowed to reach equilibrium over a range of temperature at a pre-determined rate. Depending on the experimental setup, these observations can be intensity signals of UV absorbance (hyperchromacity), fluorescence emission, molar ellipticity, NMR peaks, circular dichroism, or Raman. An example of a UV absorbance vs. temperature thermal denaturation curve can be seen in Figure 1-1 [52].

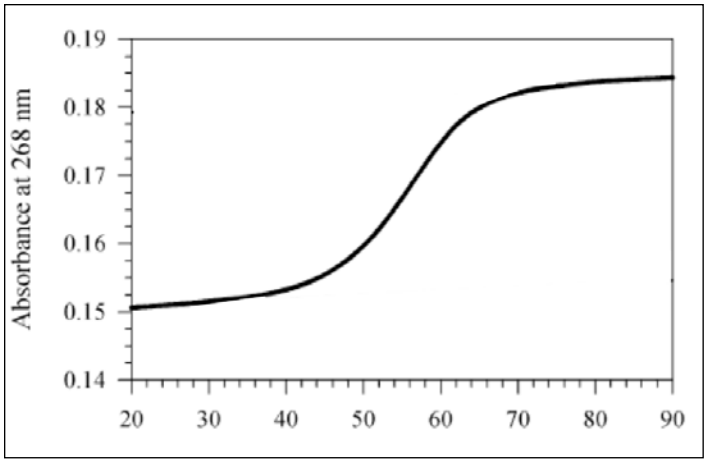

Figure 1-1 An experimental UV melting curve of a bimolecular duplex oligomer dissolve in 1 M NaCl-phosphate buffer, at C_{TOTAL} = 2 μM, pH = 7.0 [52].

Accuracy in the value of the melting temperature is prominent because many biological applications, such as, PCR, northern and Southern blots, and sequencing, require its utilization to determine the conditions (i.e. annealing temperature being 5-10ºC lower than the melting temperature) for optimum performance. This is especially critical for the techniques such as multiplex PCR, where large errors in the estimation of melting temperature can lead to the amplification of non-specific products [53].

Various theoretical and experimental approaches have been proposed and subsequently improved for a better prediction of the melting temperature value in solution. Initial methods look at the sequential compositions in the sequence [54].

An in-depth investigation of DNA structure and experimental melting temperatures of various oligonucleotides lead to the conclusion that the identity of the neighboring bases carries as much importance on the stability of the structure as the composition in the sequence [25, 55-57]. This germinated the well-known semi-empirical method of ‘Nearest Neighbor Model’. It revolves around the idea that the calculation of the melting temperature of a duplex is possible through the knowledge of all 10 di-nucleotide base stacking standard thermodynamical parameters, ΔG^o, ΔH^o, and ΔS^o [55, 58].

A set of these complementary pair-wise terms for all of the sequential combinations (dAA/dTT, dAT/dTA, dTA/dAT, dCA/dGT, dGT/dCA, dCT/dGA, dGA/dCT, dCG/dGC, dGC/dCG, dGG/dCC) were determined via an extensive experimental study looking at the UV- absorbance mediated melting curves of 44 oligonucleotides of 4 – 16 nt in length, in solution at 1 M NaCl concentration of neutral pH (6.5 – 8.5). The thermodynamical results from the curves are processed in matrices to extract the di-nucleotide values via linear regression analysis [25]. This set is further enhanced by including 222 more sequences of lengths 4 – 16 nt and the resulting parameters are presented as a unified set in Table 1-1.

Table 1-1 Di-nucleotide Parameters in Nearest-Neighbor Method [25].

Propagation sequence	ΔH° (kcal mol^{-1})	ΔS° (e.u.)	ΔG°_{37} (kcal mol^{-1})
AA/TT	−7.6	−21.3	−1.00
AT/TA	−7.2	−20.4	−0.88
TA/AT	−7.2	−21.3	−0.58
CA/GT	−8.5	−22.7	−1.45
GT/CA	−8.4	−22.4	−1.44
CT/GA	−7.8	−21.0	−1.28
GA/CT	−8.2	−22.2	−1.30
CG/GC	−10.6	−27.2	−2.17
GC/CG	−9.8	−24.4	−2.24
GG/CC	−8.0	−19.9	−1.84
Initiation	+0.2	−5.7	+1.96
Terminal AT penalty	+2.2	+6.9	+0.05
Symmetry correction	0.0	−1.4	+0.43

The melting temperature can be predicted easily by using the standard thermodynamic parameters of a particular sequence computed by utilizing the parameters in Table 1-1 for its coil-to-helix transition:

$$T_m(^oC) = \frac{\Delta H^o * 1000}{\Delta S^o + R * \ln(C_T / x)} - 273.15 + 16.6 \log\left[Na^+\right] \qquad \text{Equation 1-1}$$

where C_T is the total strand concentration (mol/l), R is the gas constant and x equals 4 for non-self-complementary and equals 1 for self-complementary duplexes, $[Na^+]$ is the salt concentration in solution. This formula follows the bimolecular equilibrium calculations with similar concentrations of both strands of the duplex in a two-state transition (coil-to-helix) without any intermediate formations.

1.3.2 Adaptation of Melting Temperature Definition on Surface

In microarrays, the strands forming the helical structure are distributed differently in the medium: one of them is free in solution and the other one is immobilized. As the duplexes are formed on the surface, and the hybridization reactions are affected by the presence of the surface, the definition of the melting temperature needs to be adapted to this interfacial system.

Melting temperature is an observable parameter that indicates the fraction of duplexes present at a given temperature. Thus, it is a function of both the stabilizing forces in the structure and the concentration of the strands. On the surface, the initial amount of probe-target duplexes, or the percent of hybridized probes on the surface, would vary depending on the experimental conditions [59-63], and thus, molecular interactions. Therefore, a correct redefinition of melting temperature for on-surface applications would be based on the maximum extent of hybridization at the initial hybridization temperature, and can be stated as the temperature at which 50 percent of the initially hybridized probes are denaturated [33].

1.3.3 Experimental Studies Investigating DNA Hybridization on the Surface

Different approaches have been used to investigate the effects of different surface characteristics; hybridization conditions; and design parameters on the extent of hybridization. The extent of hybridization is measured by the signal intensity obtained at the end of hybridization.

Surface characteristics have been tested on different strategies for the covalent attachment of pre-synthesized oligonucleotides to glass slides, gold films, polyacrylamide gel pads, polypyrrole films, and optical fibers [18, 63-67] as well as the surface material [51, 64, 68-70].

Hybridization conditions are also varied to examine the effect of the concentrations of the materials used in the solution, or the hybridization temperature. Changing the concentration of denaturants used, formamide in most cases, is a common application in microarrays to create stringent conditions for better discrimination at lower hybridization temperatures [22]. It is observed by Hughes *et al.* that for a 60mer oligonucleotide array, the highest specificity can be achieved with a formamide concentration of 32% [22]. A study by Peplies *et al.* uses the advantage of high hybridization temperature to get rid of false positive signals obtained at room temperature hybridizations [37].

Design parameters include the molecular variations imposed on the surface including, but not limited to, spacer length, probe density, probe length, and hybridization location of the target sequence on the probe, and probe sequence. An increase in the hybridization signal intensities is observed with increasing spacer length [71, 72]; while a denser probe layer results in lower signal intensities [60, 61, 73]. Longer probes are found to improve the sensitivity of the arrays, requiring lower amounts of target for detection [22, 59]. The study on the effect of the location of complementary sequence along the probe concluded that at higher probe densities, a lower hybridization efficiency is observed with probes having complementary sequences in close proximity to the surface; however, no difference is seen at lower surface densities [61]. A spike-in experiment with various target concentrations of different targets resulted in data

suggesting the influence of probe sequences on DNA hybridization on the surface [74, 75].

The effect of the design parameters is also examined through kinetic studies carried out during and after hybridization. Different studies look at the kinetics of specific (perfect-match) and non-specific hybridizations by introducing mismatch sequences [76-78]. These studies conclude that specific hybridizations take longer time to reach equilibrium, and a higher signal intensity is observed for the perfect match probes. Increasing probe lengths is found to give higher target adsorptions at the same experimental conditions [59, 79]. However, unexpected results are also obtained when a 20mer target is hybridized with 16mer, 18mer and 20mer probes on the surface; with 16mer and 18mer probes complementary to the mid-sections of the target. While an increase in hybridization signal intensity is observed going from 16mer to 18mer probes, a decrease is seen with 20mers. This result is attributed to the dangling end of the target when hybridizing with shorter probes, which could add stability to the duplex, and reduce the difference in stability between various probe lengths [32, 33, 80].

After the hybridization is completed, the hybridized probes can be washed out at increasing temperatures with solutions of different stringencies to obtain denaturation curves, which are 'non-equilibrium' melting curves. The denaturation curves are used to extract washing-time dependent denaturation temperatures. These curves are reproduced to look at the effect of mismatches in the sequence [39, 81, 82], different probe densities [83], and are utilized in the discrimination experiments using the same washing conditions [82].

However, the denaturation temperatures do not correctly represent the fraction of duplexes found at each temperature, a necessary value in the design of the experiments. The dependency of hybridization efficiency, or the maximum extent of hybridization on melting temperature is a better representation of the duplex formation at different temperatures, mainly because it represents equilibrium conditions, the goal to reach at the end of the hybridization reactions [38, 84-86]. While the value of melting temperature is a frequently used criterion in optimizing the experimental conditions in solution, there are very few studies in

literature that developed an experimental set-up to investigate the effect of different parameters on melting temperature [32]. This study includes the hybridization of a 20mer target flowing at a constant concentration over the array, hybridizing with probes of different lengths, and with one central mismatch. Target concentration was also varied. It is observed that probe length and target concentration have very little effect on the melting temperature. On the other hand, a central mismatch in shorter probes results in a higher depression in melting temperature, with higher discrimination ratios at higher temperatures. However, the low synthesis efficiency in their oligonucleotide synthesis (90%) as well as the utilization of the same equilibrium time interval at all temperature increments make these results questionable. For example, the percent of full length probes at different lengths with the given synthesis yield are 12%, 15% and 18%, respectively for 20mer, 18mer and 16mer probes on the surface. A monitoring method with low sensitivity (i.e. temperature intervals used by Forman *et al.*, with 5°C apart) could not be able to capture the differences these probe lengths would bring. Therefore, there is a need for an experimental set-up with better real-time capturing capabilities and automation as well as a robust analysis method for melting temperature extraction.

Overall goals of our research are to develop a theoretical approach to investigate the effect of the presence of the surface on DNA hybridization, use it as a foundation for general guidance in the experiments, and devise an experimental approach to observe the influence of the surface in terms of its contributions on the value of melting temperature with different design variables introduced in the system.

1.4 Research Scope

In Chapter 2, the effect of the surface on DNA hybridization is investigated theoretically, with the introduction of electrostatic and entropic blocking terms. Electrostatic blocking term represents the influence of the surface through electrostatic interactions between the charged surface and the hybridizing target in solution. The free energy penalty imposed by this term is calculated through the utilization of Electrical Double Layer theory, zeta potential experiments and Surface Partition Model. Entropic blocking term describes the entropic repulsion of the hybridizing target by the immobilized probes, hybridized targets, and the presence of the surface. Its free energy penalty is modeled using a Polymer Physics approach. The influences of spacer length and probe density are simulated with respect to different surface coverages, in their electrostatic and entropic contributions to the free energy of duplex formation on the surface.

In Chapter 3, the experimental set-up developed to generate melting curves of the duplexes formed on the surface, the analysis of these curves, and the quality assessment tools are described. This experimental set-up includes three main components: a holder consisting of a microfluidic chip on which the probes are synthesized and the labeled target is recirculated through the channels, a heater chip and a temperature probe; a temperature controller; and a fluorescence scanner to measure the signal intensity changes on the surface in real-time. The process is controlled and automated with a computer through a user-interface, in which the temperature ranges, increments and equilibrium times are input by the user at the beginning of the experiment. After the initial hybridization is completed, the melting curve is generated with the equilibrium signal intensities captured on the surface at increasing temperatures. The curves are then analyzed through background subtraction, normalization, temperature calibration, smoothing and curve fitting. The chip quality is assessed with synthesis quality controls, signal intensity distributions on the probes, and signal to noise ratios.

In Chapter 4, the influence of the surface on the dependence of the melting temperature on the target concentration is experimentally investigated.

Three different sets of experiments were carried out. In each set, the probe concentration was kept constant and the target concentration was varied. These sets include probe concentrations of 0.82 pmoles, 0.59 pmoles and 0.03 pmoles on 10^{18} $Å^2$ surface area, with a constant probe density of $5*10^{12}$ molecules/cm^2. The target concentrations used range from 0.5 nM to 15 nM; 0.36 nM to 1 nM; and 0.0165 nM to 0.027 nM, respectively. It is observed in all of the experiments that the melting temperatures on the surface are lower than in-solution values, and this discrepancy increases with increasing target concentration. It is also seen that the melting temperatures on the surface decrease with increasing target concentration, which is an opposite trend with respect to what is expected with in-solution predictions. This finding is explained using two approaches: a kinetic and thermodynamics model, and the electrostatic and entropic blocking terms presented in Chapter 2.

In Chapter 5, the influences of two surface characteristics, spacer length and probe density are experimentally examined. Each variation was accompanied with 3 different target concentrations, ranging from 0.36 nM to 1 nM. The spacer length was varied from 2 to 25 monomeric units (dT), and the probe densities tested were $5*10^{12}$ molecules/cm^2 (0.59 pmoles on 10^{18} $Å^2$ surface area) and $5*10^{13}$ molecules/cm^2 (5.9 pmoles on 10^{18} $Å^2$ surface area). All the on-surface melting temperatures are lower than in-solution predictions, and this discrepancy increases with increasing target concentrations. As the spacer molecule gets longer, the calculated melting temperatures on the surface increase. On the other hand, with a denser probe layer, the on-surface melting temperatures decrease. At the experimental conditions tested, probe density seems to have more influence in decreasing the duplex stability when compared to spacer length. These trends are explained with the utilization of electrostatic and entropic blocking terms derived in Chapter 2.

1.5 Bibliography

1. Kyogoku Y, Lord RC, Rich A, *Hydrogen bonding specificity of nucleic acid purines and pyrimidines in solution*. Science, 1966. 154: 518-520.
2. Pellois JP, *Photogenerated reagents and light-directed parallel synthesis of peptide microarrays*. University of Houston, Department of Chemistry, 2002. Ph.D.
3. Cheng KC, Stromvik MV, *SoyXpress: a database for exploring the soybean transcriptome*. BMC Genomics, 2008. 9: 368.
4. Hughes M, Deharo L, Pulivarthy SR, Gu J, Hayes K, Panda S, Hogenesch JB, *High-resolution time course analysis of gene expression from pituitary*. Cold Spring Harb Symp Quant Biol, 2007. 72: 381-386.
5. Schena M, Shalon D, Davis RW, Brown PO, *Quantitative monitoring of gene expression patterns with a complementary DNA microarray*. Science, 1995. 270: 467-470.
6. Absi TS, Sundt TMr, Tung WS, Moon M, Lee JK, Damiano RRJ, Thompson RW, *Altered patterns of gene expression distinguishing ascending aortic aneurysms from abdominal aortic aneurysms: complementary DNA expression profiling in the molecular characterization of aortic disease*. J Thorac Cardiovasc Surg, 2003. 126: 344-57; discission 357.
7. Milano A, Pendergrass SA, Sargent JL, George LK, McCalmont TH, Connolly MK, Whitfield ML, *Molecular subsets in the gene expression signatures of scleroderma skin*. PLoS ONE, 2008. 3: e2696.
8. Sengupta S, Onodera K, Lai A, Melcher U, *Molecular detection and identification of influenza viruses by oligonucleotide microarray hybridization*. J Clin Microbiol, 2003. 41: 4542-4550.
9. Cogburn LA, Wang X, Carre W, Rejto L, Aggrey SE, Duclos MJ, Simon J, Porter TE, *Functional genomics in chickens: development of integrated-systems microarrays for transcriptional profiling and discovery of regulatory pathways*. Comp Funct Genomics, 2004. 5: 253-261.

10. Pollack JR, Perou CM, Alizadeh AA, Eisen MB, Pergamenschikov A, Williams CF, Jeffrey SS, Botstein D, Brown PO, *Genome-wide analysis of DNA copy-number changes using cDNA microarrays*. Nat Genet, 1999. 23: 41-46.

11. D'Addabbo A, Latiano A, Palmieri O, Maglietta R, Annese V, Ancona N, *Regularized least squares classifiers may predict Crohn's disease from profiles of single nucleotide polymorphisms*. Ann Hum Genet, 2007. 71: 537-549.

12. Irving JA, Bloodworth L, Bown NP, Case MC, Hogarth LA, Hall AG, *Loss of heterozygosity in childhood acute lymphoblastic leukemia detected by genome-wide microarray single nucleotide polymorphism analysis*. Cancer Res, 2005. 65: 3053-3058.

13. Conejero-Goldberg C, Wang E, Yi C, Goldberg TE, Jones-Brando L, Marincola FM, Webster MJ, Torrey EF, *Infectious pathogen detection arrays: viral detection in cell lines and postmortem brain tissue*. Biotechniques, 2005. 39: 741-751.

14. Quinones B, Parker CT, Janda JMJ, Miller WG, Mandrell RE, *Detection and genotyping of Arcobacter and Campylobacter isolates from retail chicken samples by use of DNA oligonucleotide arrays*. Appl Environ Microbiol, 2007. 73: 3645-3655.

15. Anguiano A, Nevins JR, Potti A, *Toward the individualization of lung cancer therapy*. Cancer, 2008. 113: 1760-1767.

16. Chengalvala MV, Chennathukuzhi VM, Johnston DS, Stevis PE, Kopf GS, *Gene expression profiling and its practice in drug development*. Curr Genomics, 2007. 8: 262-270.

17. Lee CH, Macgregor PF, *Using microarrays to predict resistance to chemotherapy in cancer patients*. Pharmacogenomics, 2004. 5: 611-625.

18. Beaucage SL, *Strategies in the preparation of DNA oligonucleotide arrays for diagnostic applications*. Curr Med Chem, 2001. 8: 1213-1244.

19. Proudnikov D, Timofeev E, Mirzabekov A, *Immobilization of DNA in polyacrylamide gel for the manufacture of DNA and DNA-oligonucleotide microchips*. Anal Biochem, 1998. 259: 34-41.

20. Rogers YH, Jiang-Baucom P, Huang ZJ, Bogdanov V, Anderson S, Boyce-Jacino MT, *Immobilization of oligonucleotides onto a glass support via disulfide bonds: A method for preparation of DNA microarrays*. Anal Biochem, 1999. 266: 23-30.

21. Beier M, Hoheisel JD, *DNA microarray preparation by light-controlled in situ synthesis*. Curr Protoc Nucleic Acid Chem, 2005. Chapter 12: Unit 12.5.

22. Hughes TR, Mao M, Jones AR, Burchard J, Marton MJ, Shannon KW, Lefkowitz SM, Ziman M, Schelter JM, Meyer MR, Kobayashi S, Davis C, Dai H, He YD, Stephaniants SB, Cavet G, Walker WL, West A, Coffey E, Shoemaker DD, Stoughton R, Blanchard AP, Friend SH, Linsley PS, *Expression profiling using microarrays fabricated by an ink-jet oligonucleotide synthesizer*. Nat Biotechnol, 2001. 19: 342-347.

23. Gao X, LeProust E, Zhang H, Srivannavit O, Gulari E, Yu P, Nishiguchi C, Xiang Q, Zhou X, *A flexible light-directed DNA chip synthesis gated by deprotection using solution photogenerated acids*. Nucleic Acids Res, 2001. 29: 4744-4750.

24. Gao X, Gulari E, Zhou X, *In situ synthesis of oligonucleotide microarrays*. Biopol, 2004. 73: 579-596.

25. SantaLucia JJ, Allawi HT, Seneviratne PA, *Improved nearest-neighbor parameters for predicting DNA duplex stability*. Biochemistry, 1996. 35: 3555-3562.

26. Fish DJ, Horne MT, Brewood GP, Goodarzi JP, Alemayehu S, Bhandiwad A, Searles RP, Benight AS, *DNA multiplex hybridization on microarrays and thermodynamic stability in solution: a direct comparison*. Nucleic Acids Res, 2007. 35: 7197-7208.

27. Weckx S, Carlon E, DeVuyst L, Van Hummelen P, *Thermodynamic behavior of short oligonucleotides in microarray hybridizations can be described using Gibbs free energy in a nearest-neighbor model*. J Phys Chem B, 2007. 111: 13583-13590.

28. Pozhitkov A, Noble PA, Domazet-Loso T, Nolte AW, Sonnenberg R, Staehler P, Beier M, Tautz D, *Tests of rRNA hybridization to microarrays suggest that hybridization characteristics of oligonucleotide probes for species discrimination cannot be predicted*. Nucleic Acids Res, 2006. 34: e66.

29. Kane MD, Jatkoe TA, Stumpf CR, Lu J, Thomas JD, Madore SJ, *Assessment of the sensitivity and specificity of oligonucleotide (50mer) microarrays*. Nucleic Acids Res, 2000. 28: 4552-4557.

30. Murphy D, *Gene expression studies using microarrays: principles, problems, and prospects*. Adv Physiol Educ, 2002. 26: 256-270.

31. Rouillard JM, Zuker M, Gulari E, *OligoArray 2.0: design of oligonucleotide probes for DNA microarrays using a thermodynamic approach*. Nucleic Acids Res, 2003. 31: 3057-3062.

32. Forman JE, Ian D. Walton, David Stern, Richard P. Rava, Mark O. Trulson, *Thermodynamics of Duplex Formation and Mismatch Discrimination on Photolithographically Synthesized Oligonucleotide Arrays*. ACS Symposium Series, 1998. 682: 206-228.

33. Glazer M, Fidanza JA, McGall GH, Trulson MO, Forman JE, Suseno A, Frank CW, *Kinetics of oligonucleotide hybridization to photolithographically patterned DNA arrays*. Anal Biochem, 2006. 358: 225-238.

34. Wang Y, Miao ZH, Pommier Y, Kawasaki ES, Player A, *Characterization of mismatch and high-signal intensity probes associated with Affymetrix genechips*. Bioinformatics, 2007. 23: 2088-2095.

35. Li ESY, Liu W-T, *DNA microarray technology in microbial ecology studies-principle, applications and current limitations*. Microbes and Environments, 2003. 18: 175-187.

36. Naef F, Magnasco MO, *Solving the riddle of the bright mismatches: labeling and effective binding in oligonucleotide arrays*. Phys Rev E Stat Nonlin Soft Matter Phys, 2003. 68: 011906.

37. Peplies J, Glockner FO, Amann R, *Optimization strategies for DNA microarray-based detection of bacteria with 16S rRNA-targeting oligonucleotide probes*. Appl Environ Microbiol, 2003. 69: 1397-1407.

38. Bhanot G, Louzoun Y, Zhu J, DeLisi C, *The importance of thermodynamic equilibrium for high throughput gene expression arrays*. Biophys J, 2003. 84: 124-135.

39. Khomyakova E, Livshits MA, Steinhauser MC, Dauphinot L, Cohen-Kaminsky S, Rossier J, Soussaline F, Potier MC, *On-chip hybridization kinetics for optimization of gene expression experiments*. Biotechniques, 2008. 44: 109-117.

40. Vainrub A, Pettitt BM, *Coulomb blockage of hybridization in two-dimensional DNA arrays*. Phys Rev E Stat Nonlin Soft Matter Phys, 2002. 66: 041905.

41. Vainrub A, Pettitt BM, *Surface electrostatic effects in oligonucleotide microarrays: control and optimization of binding thermodynamics*. Biopol, 2003. 68: 265-270.

42. Vainrub A, Pettitt BM, *Sensitive quantitative nucleic acid detection using oligonucleotide microarrays*. J Am Chem Soc, 2003. 125: 7798-7799.

43. www.izbi.de/working_papers.html

44. Halperin A, Buhot A, Zhulina EB, *Sensitivity, specificity, and the hybridization isotherms of DNA chips*. Biophys J, 2004. 86: 718-730.

45. Halperin A, Buhot A, Zhulina EB, *Brush effects on DNA chips: thermodynamics, kinetics, and design guidelines*. Biophys J, 2005. 89: 796-811.

46. Halperin A, Buhot A, Zhulina EB, *Hybridization at a surface: the role of spacers in DNA microarrays*. Langmuir, 2006. 22: 11290-11304.

47. Wong KY, Pettitt BM, *Orientation of DNA on a surface from simulation*. Biopol, 2004. 73: 570-578.

48. Wong KY, B.M. Pettitt, *A study of DNA tethered to surface by an all-atom molecular dynamics simulation*. Theoretical Chemistry Accounts, 2001. 106: 233-235.

49. Jayaraman A, Hall CK, Genzer J, *Computer simulation study of molecular recognition in model DNA microarrays*. Biophys J, 2006. 91: 2227-2236.

50. Jayaraman A, Hall CK, Genzer J, *Computer simulation study of probe-target hybridization in model DNA microarrays: effect of probe surface density and target concentration*. J Chem Phys, 2007. 127: 144912.

51. Zeng J, *Interfacial hybridization kinetics of oligonucleotides immobilized onto fused silica surfaces*. Sensors and Actuators B, 2003. 90: 68-75.

52. Owczarzy R, *Melting temperatures of nucleic acids: discrepancies in analysis*. Biophys Chem, 2005. 117: 207-215.

53. Mergny JL, Lacroix L, *Analysis of thermal melting curves*. Oligonucleotides, 2003. 13: 515-537.

54. Panjkovich A, Melo F, *Comparison of different melting temperature calculation methods for short DNA sequences*. Bioinformatics, 2005. 21: 711-722.

55. Breslauer KJ, Frank R, Blocker H, Marky LA, *Predicting DNA duplex stability from the base sequence*. Proc Natl Acad Sci U S A, 1986. 83: 3746-3750.

56. Owczarzy R, Dunietz I, Behlke MA, Klotz IM, Walder JA, *Thermodynamic treatment of oligonucleotide duplex-simplex equilibria*. Proc Natl Acad Sci U S A, 2003. 100: 14840-14845.

57. SantaLucia JJ, *A unified view of polymer, dumbbell, and oligonucleotide DNA nearest-neighbor thermodynamics*. Proc Natl Acad Sci U S A, 1998. 95: 1460-1465.

58. Sugimoto N, Nakano M, Nakano S, *Thermodynamics-structure relationship of single mismatches in RNA/DNA duplexes*. Biochemistry, 2000. 39: 11270-11281.

59. Chou CC, Chen CH, Lee TT, Peck K, *Optimization of probe length and the number of probes per gene for optimal microarray analysis of gene expression*. Nucleic Acids Res, 2004. 32: e99.

60. Peterson AW, Heaton RJ, Georgiadis RM, *The effect of surface probe density on DNA hybridization*. Nucleic Acids Res, 2001. 29: 5163-5168.

61. Peterson AW, Wolf LK, Georgiadis RM, *Hybridization of mismatched or partially matched DNA at surfaces*. J Am Chem Soc, 2002. 124: 14601-14607.

62. Peytavi R, Liu-Ying T, Raymond FR, Boissinot K, Bissonnette L, Boissinot M, Picard FJ, Huletsky A, Ouellette M, Bergeron MG, *Correlation between microarray DNA hybridization efficiency and the position of short capture probe on the target nucleic acid*. Biotechniques, 2005. 39: 89-96.

63. Steel AB, Levicky RL, Herne TM, Tarlov MJ, *Immobilization of nucleic acids at solid surfaces: effect of oligonucleotide length on layer assembly*. Biophys J, 2000. 79: 975-981.

64. Levicky R, Horgan A, *Physicochemical perspectives on DNA microarray and biosensor technologies*. Trends Biotechnol, 2005. 23: 143-149.

65. Podyminogin MA, Lukhtanov EA, Reed MW, *Attachment of benzaldehyde-modified oligodeoxynucleotide probes to semicarbazide-coated glass*. Nucleic Acids Res, 2001. 29: 5090-5098.

66. Steinberg G, Stromsborg K, Thomas L, Barker D, Zhao C, *Strategies for covalent attachment of DNA to beads*. Biopol, 2004. 73: 597-605.

67. Walsh MK, Wang X, Weimer BC, *Optimizing the immobilization of single-stranded DNA onto glass beads*. J Biochem Biophys Methods, 2001. 47: 221-231.

68. Livshits MA, Mirzabekov AD, *Theoretical analysis of the kinetics of DNA hybridization with gel-immobilized oligonucleotides*. Biophys J, 1996. 71: 2795-2801.

69. Sorokin NV, Chechetkin VR, Livshits MA, Pan'kov SV, Donnikov MY, Gryadunov DA, Lapa SA, Zasedatelev AS, *Discrimination between perfect and mismatched duplexes with oligonucleotide gel microchips: role of thermodynamic and kinetic effects during hybridization*. J Biomol Struct Dyn, 2005. 22: 725-734.

70. Su HJ, Surrey S, McKenzie SE, Fortina P, Graves DJ, *Kinetics of heterogeneous hybridization on indium tin oxide surfaces with and without an applied potential*. Electrophoresis, 2002. 23: 1551-1557.

71. Guo Z, Guilfoyle RA, Thiel AJ, Wang R, Smith LM, *Direct fluorescence analysis of genetic polymorphisms by hybridization with oligonucleotide arrays on glass supports*. Nucleic Acids Res, 1994. 22: 5456-5465.

72. Shchepinov MS, Case-Green SC, Southern EM, *Steric factors influencing hybridisation of nucleic acids to oligonucleotide arrays*. Nucleic Acids Res, 1997. 25: 1155-1161.

73. Watterson JH, Paul A. E. Piunno, Christopher C. Wust, Ulrich J. Krull, *Effects of Oligonucleotide Immobilization Density on Selectivity of Quantitative Transduction of Hybridization of Immobilized DNA*. Langmuir, 2000. 16: 4984-4992.

74. Held GA, Grinstein G, Tu Y, *Modeling of DNA microarray data by using physical properties of hybridization*. Proc Natl Acad Sci U S A, 2003. 100: 7575-7580.

75. Skvortsov D, Abdueva D, Curtis C, Schaub B, Tavare S, *Explaining differences in saturation levels for Affymetrix GeneChip arrays*. Nucleic Acids Res, 2007. 35: 4154-4163.

76. Dai H, Meyer M, Stepaniants S, Ziman M, Stoughton R, *Use of hybridization kinetics for differentiating specific from non-specific binding to oligonucleotide microarrays*. Nucleic Acids Res, 2002. 30: e86.

77. Dorris DR, Nguyen A, Gieser L, Lockner R, Lublinsky A, Patterson M, Touma E, Sendera TJ, Elghanian R, Mazumder A, *Oligodeoxyribonucleotide probe accessibility on a three-dimensional DNA microarray surface and the effect of hybridization time on the accuracy of expression ratios*. BMC Biotechnol, 2003. 3: 6.

78. Tawa K, Yao D, Knoll W, *Matching base-pair number dependence of the kinetics of DNA-DNA hybridization studied by surface plasmon fluorescence spectroscopy*. Biosens Bioelectron, 2005. 21: 322-329.

79. Stillman BA, Tonkinson JL, *Expression microarray hybridization kinetics depend on length of the immobilized DNA but are independent of immobilization substrate*. Anal Biochem, 2001. 295: 149-157.

80. Bommarito S, Peyret N, SantaLucia JJ, *Thermodynamic parameters for DNA sequences with dangling ends*. Nucleic Acids Res, 2000. 28: 1929-1934.

81. Marky LA, Breslauer KJ, *Calculating thermodynamic data for transitions of any molecularity from equilibrium melting curves*. Biopol, 1987. 26: 1601-1620.

82. Wick LM, Rouillard JM, Whittam TS, Gulari E, Tiedje JM, Hashsham SA, *On-chip non-equilibrium dissociation curves and dissociation rate constants as methods to assess specificity of oligonucleotide probes*. Nucleic Acids Res, 2006. 34: e26.

83. Wilkins Stevens P, Henry MR, Kelso DM, *DNA hybridization on microparticles: determining capture-probe density and equilibrium dissociation constants*. Nucleic Acids Res, 1999. 27: 1719-1727.

84. Carletti E, Guerra E, Alberti S, *The forgotten variables of DNA array hybridization*. Trends Biotechnol, 2006. 24: 443-448.

85. Marcy Y, Cousin PY, Rattier M, Cerovic G, Escalier G, Bena G, Gueron M, McDonagh L, le Boulaire F, Benisty H, Weisbuch C, Avarre JC, *Innovative integrated system for real-time measurement of hybridization and melting on standard format microarrays*. Biotechniques, 2008. 44: 913-920.

86. Sartor M, Schwanekamp J, Halbleib D, Mohamed I, Karyala S, Medvedovic M, Tomlinson CR, *Microarray results improve significantly as hybridization approaches equilibrium*. Biotechniques, 2004. 36: 790-796.

CHAPTER II

THEORY OF ELECTROSTATIC AND ENTROPIC BLOCKING

2.1 Introduction

With the launch of the microarrays, various question marks have started to come up in different aspects of the technology, and the answers are being sought through extending the investigations made in solution to analyze the behavior of DNA, including the helix-coil transition. However, the hurdles along the way are more tedious than initially thought. The examination of the hybridization and denaturation of DNA on the surface has to take the presence of the surface and the subsequent variables into account. These variables are the determining characteristics of the system, and can be manipulated to change the outcome of the experiment, but the fundamental influences accompanying them are harder to capture.

The major role these surface characteristics play on the surface is a part of the bigger picture that is inherent to the processes taking place with duplex formation reactions on surfaces. Experiments on arrays indicate a decrease in duplex stability on the surface [1], and this trend is explained by the blockage of the hybridization reaction on the surface [2], in other words, progressive hampering of the duplex formation due to repulsive electrostatic and entropic contributions.

In this part of the thesis, electrostatic and entropic blocking of the duplex formation reaction on the surface are investigated through a comprehensive theoretical study.

Electrostatic blocking is a term used to represent the interactions stemming from the charges the ions in the solution, surface and the strands carry. A great deal of experimental and theoretical effort has been put forward to understand the polyelectrolyte behavior of nucleic acids [3-5]. Poisson-Boltzmann theory can be extended to represent the electrical double layer formation occurring on surfaces, in our case, a flat-surface with 1:1 electrolyte present as an infinite liquid layer [6]. The findings through this could assist in simulating any possible surface potential and surface density changes with respect to the different steps of synthesis that can be modeled as a hard surface with no ion penetration, i.e. derivatization. Changes in surface potentials in various synthesis steps will demonstrate the effect of the alterations imposed on the system. Including the spacer and the probe layers as the last steps in synthesis will bring it to a new level where an incorporation of the ion penetration may represent the environment better, through a soft-shell model [6, 7]. Direct measurement of the surface potential has proven itself as an experimental challenge; therefore, alternatively, zeta potentials are measured [8]. These zeta potential values are incorporated into the polyelectrolyte theory, and with various assumptions, surface charges and potentials can be calculated at each synthesis step.

Various effects that can be imposed on the system, i.e. probe length, spacer length, probe density, can affect the surface charge and potential. To be able to monitor the influences of these variables on duplex formation and its stability, their contributions on the free energy of duplex formation need to be calculated. The electrostatic free energy penalty experienced by the hybridizing target can be calculated by an approach proposed by Binder [2] through the Surface Partition Model, when the initial surface potentials and charges are known in the system. The influence of the hybridized duplexes on the surface can be simulated through different hybridization efficiencies. The calculations are further carried out to observe the free energy contributions of two experimental parameters: spacer length and probe density.

The other factor that accompanies the electrostatic blocking on the surface is the entropic blocking. When compared to in-solution, the immobilization of one of the strands on an impermeable surface brings in an additional entropic penalty to the duplex formation. Anchoring one of the strands would reduce the conformational freedom of the duplex due to the restrictions it can impose on the various bonds in the structure. In addition, these structures could be in close proximity within each other, and under certain conditions, their presence is going to influence the neighboring site. A similar phenomenon may also be observed with the presence of an impermeable surface, which would cause excluded volume effects with their repulsive interactions with the duplexes. These two aspects lend themselves as steric effects in the entropic blocking concept. In this chapter, the calculations necessary to simulate the influence of the entropic blocking on the duplex formation on the surface are based on the models proposed by Halperin *et al.* [9, 10] focusing on the problem through polymer physics, and using second virial coefficients to represent the various possible monomer-monomer interactions, without including the effect of electrostatics into the picture. The influence of the duplexes hybridized on the surface can also be simulated through different hybridization efficiencies.

2.2 Materials and Methods

The development of the theory of electrostatic blocking in the system requires the knowledge of the surface potential, Ψ_0, to be able to calculate the free energy penalty term due to the presence of the surface. Having a better representation of the system characteristics requires measurements to be performed at similar conditions to the melting experiments. It is widely accepted that measuring a value for the surface potential is quite a challenge [8]. An easier way to get around the problem is to measure the zeta potential instead, and with applicable assumptions, calculate the surface potential using the polyelectrolyte theories that can similarly represent our system.

Glass beads made of borosilicate with average diameter of 10 μm (Cat no: 07666, Polysciences Inc, PA, USA) were used in the experiments for zeta potential measurements, which were carried out in Zetasizer Nano ZS Series (Malvern Instruments Ltd, UK) instrument through electrophoretic mobility measurements using the concept of Laser Doppler Velocimetry (LDV) [11]. These glass beads are similar to the glass type used in the microfludic chips in which the melting experiments are carried out.

Initial measurements focused on the amount of the glass beads to be used in the future experiments, within the range from 0.0001 mg to 0.01 mg. After the concentration was determined, other zeta potential measurements were performed.

Zeta potential measurements were made at 23°C using 2 ml of SSPE (Saline-Sodium phosphate- EDTA) solutions (pH 6.7) of different concentrations (0.01X (0.0016 M NaCl), 0.1X (0.016 M NaCl), 1X (0.16 M NaCl), 6X (1 M NaCl)) containing 0.0001 mg of glass beads processed at different stages of synthesis (no processing; before derivatization (washing with ammonium hydroxide:hydrogen peroxide:water (1:1:5 by volume) and after derivatization (with the linker, *3-aminopropyltriethoxysilane* (SIA0610.0, Gelest Inc, Pennsylvania, USA)); after synthesis with 15 dT spacer). Glass beads in solution were sonicated in 1.5 ml test tubes, transferred to the appropriate cell for the instrument and the zeta potential measurement was made using the Zetasizer

software (Malvern Instruments Ltd, UK). The result was recorded. Then, the cell was taken out, slowly mixed, and the zeta potential measurement was repeated 2 more times in a similar manner in the same cell for reproducibility.

2.3 Theory

2.3.1 Electrostatic Blocking

2.3.1.1 Calculation of the Surface Potential and Surface Charge Density via Electrical Double Layer Theory

The net charge of a substrate or a colloidal particle in contact with an electrolyte solution gives rise to the formation of an electrical double layer. This layer plays a major role in interfacial electrical phenomena, i.e. the suspension of colloidal particles and their interactions [6]. The net charge density on the surface is usually owed to the adsorption of ions, the desorption of dissociable groups and ionization of surface groups. The electrical field created by the charge density attracts the counterions towards the surface and drives the co-ions away from it, forming a shielding layer, which is known as the electrical double layer (EDL).

The models describing this layer are based on the Gouy-Chapman-Stern (GCS) model [12], in which the double layer is comprised of two layers: Stern layer and a diffuse layer (Figure 2-1).

In the Stern layer, counterions are specifically adsorbed on the surface. They do not move normal to the surface, but rather laterally within the layer [13]. In the diffuse layer, the coions and counterions move around the particle freely in an ionic cloud.

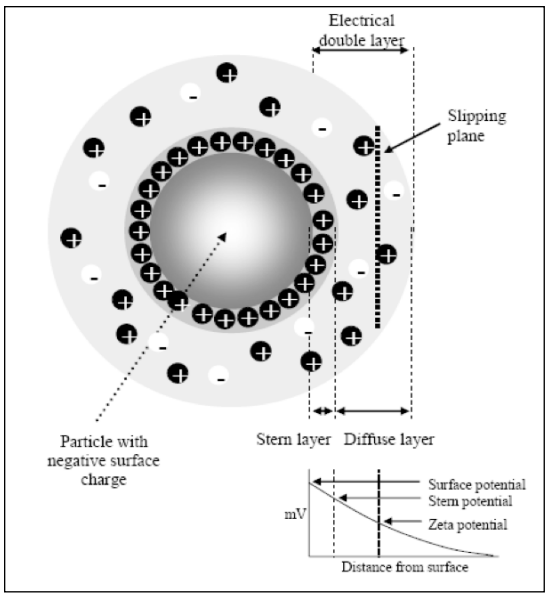

Figure 2-1 Potential distribution around a charged particle in an ionic solution.

The characteristic thickness of the double layer is called the Debye length, κ^{-1}. It is defined as

$$\kappa^{-1} = \sqrt{\frac{\varepsilon_0 \varepsilon_r k_B T}{2 N_A e^2 n}} \qquad \text{Equation 2-1}$$

where ε_0 is the permittivity of free space, ε_r is the dielectric constant, n is the ionic strength of the electrolyte, k_B is Boltzmann constant, T is the absolute temperature, N_A is Avogadro's number and e is the elemental charge.

In addition, the existing potentials on the interfaces are defined between the bulk and the interfacial layer they represent: Surface potential at the surface, Stern potential at the Stern layer, and finally, electrokinetic or Zeta potential at the slipping plane within the diffuse layer. Slipping or shear plane is defined at the hydrodynamic stagnant layer, below the double layer thickness, when there is a tangential liquid flow along the surface (i.e. caused by an external electric field). The ions within this thin layer of fluid act and move with the colloidal particle, with no flow development [14].

Measuring the zeta potential donates with tools to calculate the surface potential, which cannot be measured experimentally [8]. Calculation of the

surface potential could be accomplished via incorporation of the polyelectrolyte theories and equations derived therein.

The theoretical basis of the double layer theory lies mainly on Poisson-Boltzmann equation, which is a differential equation that explains the electrostatic interactions between molecules present in the ionic solutions [15].

When the calculated Debye length is much smaller (0.76 nm – 7.6 nm depending on the electrolyte concentration) than the diameter of the particle used, the potential distribution calculation near the surface is approximated with a plate-like particle immersion in a 1:1 electrolyte applied to the nonlinear form of the Poisson-Boltzmann equation [6] to calculate the potential distribution above the surface (assumed infinite flat plate) and the charge density on the surface in an infinite fluid:

$$\frac{d^2\psi}{dx^2} = \frac{2 * e * n}{\varepsilon_r * \varepsilon_0} * \sinh\left(\frac{e * \Psi(x)}{k_B * T}\right) \qquad \text{Equation 2-2}$$

Boundary conditions:

1) $\psi = \psi_0$ at $x = x_0$

2) $\psi = d\psi/dx = 0$ at $x = \infty$

where ψ_0 is the surface potential, n is the ionic concentration, e is the electron charge, ε_r is the relative permittivity of the medium, ε_0 is the permittivity of the vacuum, k_B is the Boltzmann constant and T is the temperature.

According to Ohshima [6], solving Equation 2-2 with the boundary conditions yields the potential distribution:

$$\psi(x) = \frac{2 * k_B * T}{e} * \ln\left(\frac{1 + \gamma \exp(-\kappa x)}{1 - \gamma \exp(-\kappa x)}\right) \qquad \text{Equation 2-3}$$

with

$$\gamma = \tanh\left(\frac{e * \psi_0}{4 * k_B * T}\right) = \frac{\exp(e * \psi_0 / (2 * k_B T)) - 1}{\exp(e * \psi_0 / (2 * k_B T)) + 1}$$

In addition, the surface charge density on the particle can be calculated by:

$$\sigma = \frac{2 * \varepsilon_r * \varepsilon_{vacuum} * \kappa * k_B T}{e} * \sinh\left(\frac{e * \psi_0}{2 * k_B T}\right) = \left(8 * n * \varepsilon_{r*} \varepsilon_{vacuum} * k_B T\right)^{1/2} * \sinh\left(\frac{e * \psi_0}{2 * k_B T}\right)$$

Equation 2-4

Calculation of the surface potential using Equation 2-3 requires the knowledge of a potential value at a defined distance. Based on the discussion by Hunter [16], the slipping plane is assumed to be present at half of the Debye length from the surface.

2.3.1.2 Calculation of the Surface Potential within the Spacer and Probe Layers

The equations so far are for hard particles with an underlying assumption that there is very little or no sodium ion penetration within the surface layers. Next steps in the process introduce the spacer (a poly-dT sequence used to increase the distance from the surface) and the probe layers in which there is a high probability that the sodium ions will penetrate through the polyelectrolyte layer (Figure 2-2). This case requires a different approach for the surface potential calculation on soft particles with ion penetration.

(a)

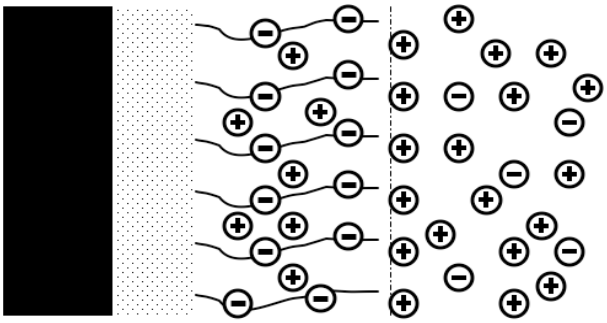

(b)

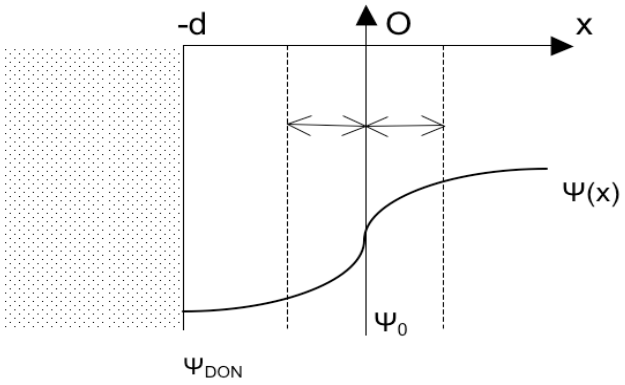

Figure 2-2 (a) The distribution of electrolyte ions (Na^+ and Cl^-) across a negatively charged, ion-penetrable polyelectrolyte layer (i.e. spacer) on a solid planar surface (b) The electric potential distribution across a negatively charged, ion-penetrable polyelectrolyte layer (i.e. spacer) on a solid planar surface.

A planar surface with a polyelectrolyte layer of thickness d is immersed in a symmetrical electrolyte solution with a valence of z and bulk concentration n. It is assumed that the layer thickness d is much larger than 1/κ and the fully ionized groups of valence Z is distributed with a uniform density of N in a surface layer.

According to Ohshima [6], for this case, the Poisson-Boltzmann equation needs to be solved for both above the surface (x>0) and within the surface layer (-d<x<0). The Poisson-Boltzmann equations for the electric potential in the respective regions are given by

$$\frac{d^2\psi}{dx^2} = \frac{2*z*e*n}{\varepsilon_r * \varepsilon_{vacuum}} * \sinh\left(\frac{z*e*\Psi(x)}{k_B*T}\right) \qquad \text{Equation 2-5}$$

at x>0 and

$$\frac{d^2\psi}{dx^2} = \frac{2*e*n}{\varepsilon_r * \varepsilon_{vacuum}} * \sinh\left(\frac{z*e*\Psi(x)}{k_B * T}\right) - \frac{z*e*N}{\varepsilon_R * \varepsilon_{vacuum}}$$ Equation 2-6

at –d< x< 0.

The potential inside the charged layer has a constant potential value called the 'Donnan Potential', ψ_{DON}. Based on the equations above, it can be obtained by setting $d^2\psi/dx^2 = 0$ at the region deep inside the surface layer. Therefore,

$$\psi_{DON} = \frac{kT}{z*e} * \operatorname{arcsin} h\left(\frac{Z*N}{2*z*n}\right) = \frac{kT}{z*e} * \ln\left\{\frac{Z*N}{2*z*n} + \left[\left(\frac{Z*N}{2*z*n}\right)^2 + 1\right]^{1/2}\right\}$$ Equation 2-7

Based on the manipulations proposed by Ohshima [6], equations 2-5 through 2-7 along with the assumption that d>>(1/κ) gives the surface potential:

$$\psi_0 = \psi_{DON} - \left(\frac{kT}{z*e}\right) * \tanh\left(\frac{z*e*\psi_{DON}}{2*kT}\right)$$ Equation 2-8

which is also equal to

$$\psi_0 = \frac{kT}{z*e}\left(\ln\left\{\frac{Z*N}{2*z*n} + \left[\left(\frac{Z*N}{2*z*n}\right)^2 + 1\right]^{1/2}\right\} + \frac{2*z*n}{Z*N} * \left\{1 - \left[\left(\frac{Z*N}{2*z*n}\right)^2 + 1\right]^{1/2}\right\}\right)$$

Equation 2-9

2.3.1.3 Calculation of the Surface Charge Density with the Probes on the Surface

Poisson-Boltzmann equation representing the potential distribution above the surface (above the layer at the free end of the spacers) in the case of the ion penetrable soft shell is the same equation that is used to simulate the potential distribution for the hard impenetrable shell assumption. Therefore, the surface charge calculation equation, Equation 2-4, can be used in the same manner to calculate the surface charge density at the spacer and/or probe layer with the soft shell assumption. Using this approach gives us an initial value of the surface charge density (σ_{q0}), but there is a need for a more comprehensive model to be

able to predict the surface charge density changes as the hybridization takes place.

The simulation of the duplex formation on the surface as it progresses and simulation of the effect of different variables, i.e. probe length, spacer length, target length, probe density, can be done by the theoretical approach proposed by Binder [2], which models the effect of electrostatics near surfaces by the Surface Partition Model. This model requires the knowledge of surface potentials and charges to calculate the free energy experienced by a target penetrating into a charged probe layer.

Using this model, calculation of the surface charge density is achieved through Equation 2-10:

$$\sigma_q = \rho_p * L^P * q_N * (1 + \theta * r_L) \qquad \text{Equation 2-10}$$

where ρ_p is the probe density, L^p is length of the probes on the surface, q_N is the effective charge per nucleotide, θ is the hybridization efficiency, and r_L is the relative length of the target with respect to probes.

This equation is further improved by adding an initial charge density of the surface term, σ_{q0}, that takes into account the effect of the presence of the layers (spacer and the linker) below the probe layer. Therefore, the equation becomes:

$$\sigma_q = \sigma_{q^0} + \rho_p * L^P * q_N * (1 + \theta * r_L) \qquad \text{Equation 2-11}$$

with σ_{q0} representing the initial surface charge density.

Note that at zero hybridization efficiency, where there is no target on the surface, this equation represents the initial surface charge of the probe layer:

$$\sigma_q = \sigma_{q^0} + \rho_p * L^P * q_N \qquad \text{Equation 2-12}$$

According to Bloomfield [17], the binding of counterions is not 1:1 proportional to the phosphate present on the backbone; there is a fraction of charge on DNA that is not compensated by the cations: 0.24 for double stranded DNA and 0.48 for single stranded DNA (the effective charges per nucleotide, q_N). This means that if the salt present is NaCl, then 0.76 Na^+ will be bound to the DNA per phosphate. This is shown to be experimentally accurate: 0.75 Na^+ at all

ionic strengths up to 1.3 M, independent of ionic concentration [17, 18]. As a result, DNA is partially neutralized.

2.3.1.4 Calculation of the Free Energy Penalty due to Probe Layer

Using equations 2-4 and 2-11, surface potential with the probe layer can be obtained. The electrostatic free energy of a charged target of length L^T within the surface potential Ψ_0 can be calculated with the following approximation [2]:

$$G_{el} = F * L^T * q_N * \psi_0 \qquad \text{Equation 2-13}$$

This effect can be included as an additional penalty that needs to be overcome by the target hybridizing with the probe on the surface; in other words, the contribution of electrostatic blocking on hybridization.

Among the various parameters that can be simulated, the effects of spacer length and probe density on the electrostatic penalty are shown in this chapter.

2.3.2 Entropic Blocking

Entropic blocking demonstrates the reduction in the conformational freedom of a duplex formed on the surface. The contributions of the surface result from two main factors: Firstly, the presence of the impermeable solid on which one of the strands is fixed, and secondly, the crowding with the neighborhood probe sites or the targets previously hybridized. Both of these factors bring in additional steric effects that are not present during the duplex formation in solution. This phenomenon is investigated using a polymer physics approach.

The oligonucleotide chips comprise grafted charged polymers, polyelectrolytes, immobilized on one end to a planar surface. A high density of these grafts lead to the formation of a dense turf of chains, in which the anchored strands start to overlap, resulting in a polymer brush [9]. The brush concept brings in three main interactions: hard core repulsion between the monomers supplemented by van der Waals attractions, and electrostatic repulsion. These three interactions are used in the representation of the probe layer on the surface

collectively in the second virial coefficient of monomer-monomer interactions, υ [10]:

$$\upsilon = \frac{2\Pi}{3} a^3 \left(1 - \frac{\theta}{T}\right) + 2\Pi l_b r_D^2 \qquad \text{Equation 2-14}$$

where a symbolizes the spherical monomer radius, l_b is the Bjerrum length (defined as the distance at which the Coulomb interactions between the monomers are equal to the thermal energy kT, represented by $l_b = e^2/\varepsilon kT \approx 7$ Å with e as the charge of an electron, ε as the dielectric constant of the medium, k is the Boltzmann constant, and T is the temperature), r_D is the Debye length (defined as the distance after which the long-range electrostatic interactions are screened, represented by $r_D = 1/\sqrt{8\Pi l_b C_s} \approx 3$ Å with C_s as the ionic concentration, typically 1 M NaCl in hybridization experiments).

The first term in the second virial coefficient equation represents the hard core repulsion between the monomers as modulated by the van der Waals attraction giving rise to the $(1 - \theta/T)$ factor, Θ is the theta temperature at which the interactions between the neutral monomers disappear. The value of this temperature for a single stranded DNA is not established [9]. The second term in Equation 2-14 indicates the screened electrostatic interactions between the monomers. It is important to note that the second virial coefficient does not carry the effects of hydrogen bonding, base-stacking, and structure of the water [9]. With these reservations in mind, one can utilize the second virial coefficients to obtain the interaction free energies of spacer – spacer, probe – probe, probe – spacer contacts and their changes as the target is hybridized with the probes on the surface. The focus on the spacers mainly comes from the interest in the theoretical investigation of the experiments performed with different spacer lengths in Chapter 5 of this thesis.

The dimensions of the double-stranded DNA and single-stranded DNA are significant in these derivations. Double-stranded DNA behaves as a rod-like cylindrical molecule with a helical rise of 3.4 Å per base (assumed to be equal to the spherical monomer diameter), a diameter of ~20 Å, and a cross-sectional area of 284 $Å^2$ [19]. However, the properties of single-stranded DNA are less

clear, with its preferable behavior as a semi-flexible chain, and its swelling capability in a helical rise of 6 Å per base (assumed to be equal to the spherical monomer diameter) [20]. Being in a semiflexible structure, the Flory radius of a single stranded DNA can be expressed as $R_F \approx \left(Na/l_p\right)^{3/5} l_p$ where N equal to the length of the chain, a is the spherical monomer radius, and l_p shows the persistence length, defined as the length at which the correlations in the direction of the tangent are lost [21], or the structure does not demonstrate a stiff elastic rod behavior any more [9]. The persistence length of a single stranded chain is not an established parameter; the reported values range in an interval of 7.5 Å to 35 Å [22]. On the other hand, the persistence length of a double-stranded DNA is ~ 500 Å at moderate to high salt concentrations [21].

To investigate the extent of the brush layer on the surface, one can use the Flory radius of the single stranded chains on the surface, R_F, as a lower limit [23]. For probes (single stranded chains on the surface) and targets (single stranded chains in solution) at equal lengths, the criterion for brush regime is when the surface area per probe, $\Sigma \approx R_F^2$ [9]. Here, the Flory radius includes the total length of the spacer and the probe in its calculation to be more reflective of our system, which is in the brush regime. In this regime, the anchored chains on the surface stretch out normally to the surface [24], to decrease the monomer concentration and the number of repulsive monomer-monomer contacts [23]. Following the approach set by Halperin *et al.* [9], the concentration profile of the monomers is treated in a step-like manner with free ends at the boundary height of H on the surface. This method is a reflection of the Alexander-Flory model with the free energy per site represented as [10, 23]:

$$\frac{\gamma_{site}}{kT} \cong \frac{H}{(N_s + n_p) * a_s^2} + \frac{1}{H\Sigma}\left[\upsilon_s N_s^2 + \upsilon_p n_p^2 (1+x)^2 + \upsilon_{sp} N_s n_p (1+x)\right] + \ldots$$

$$+\left[x\ln x + (1-x)\ln(1-x)\right] + \left[x\frac{\mu_{spt}^0}{kT} + (1-x)\frac{\mu_{sp}^0}{kT}\right] - \ln\left(\frac{H}{(N_s + n_P) * a_s}\right)$$

Equation 2-15

where the numerical prefactors of order unity are omitted for simplicity; and H is the height of the brush layer; N_s is the length of the spacer; n_p is the length of the

probe; a_s is the size of the monomer; Σ is the probe density; υ_s, υ_p, and υ_{sp} are the virial coefficients of spacer-spacer, probe-probe and spacer-probe interactions, respectively; x is the hybridization efficiency; μ^0_{spt} and μ^0_{sp} are the chemical potentials of spacer-probe hybridized with target and spacer-probe, respectively.

The first term in this equation represents the entropic loss due to the stretching of the probe and spacer chain along the normal of the surface in the presence of the neighborhood probes in the brush regime. In other words, it shows the extension of the coil from the ideal unswollen coil dimension $R_0 \cong \sqrt{\left(N_s + n_p\right) * a_s * l_p}$ to H, with the elastic free energy, $F_{el} \approx kT * H^2 / R_0^{\,2}$.

The second term in this equation allows for different types of interactions in the system: spacer-spacer, probe-spacer, probe-probe and the changes incurred by the introduction of the target of the same length as the probe into the system as presented by the increase in the hybridization efficiency, x. Following the description by Halperin *et al* [23], the second virial coefficient equation is modified to include the behavior of a neutral chain only, and the term demonstrating the electrostatic interactions are taken out. In addition, based on the discussion by Rubinstein *et al.* [25] and Halperin *et al* [10], the comparable interactions between the monomer-monomers and monomer-solvent lead to the assumption of a 'good' solvent, in which case, the second virial coefficient or the excluded volume interactions are independent of temperature (T >> Θ). As a result, the second virial coefficient can be re-expressed as:

$$\upsilon \approx \frac{2\Pi}{3} a^3 \qquad \text{Equation 2-16}$$

for all the interactions, and the interaction free energies are formulated as:

$$\frac{F_{\text{int}}}{kT} = H * \Sigma * \upsilon * c^2 \qquad \text{Equation 2-17}$$

where $c = n(1+x)/(H * \Sigma)$, the number concentration of monomers within the layer with x being the fraction of duplexes on the surface (if the chain is involved in the hybridization process), and n being the length of the chain under question. Equations 2-16 and 2-17 are used to represent the individual interactions: spacer

- spacer, spacer - probe and probe - probe, and their summations are included in the site free energy equation in Equation 2-15.

The third term in the site free energy equation demonstrates the mixing entropy associated with the different possible placements of the spacer - probe and spacer - probe - target chains.

The fourth term in the site free energy equation shows the free energy gain during the hybridization process without including the effect of the surface into the picture. The chemical potentials μ_{spt}^{0} and μ_{sp}^{0} are the standard values of the hybridized and unhybridized chains, respectively.

The effect of the impenetrable wall is included in Equation 2-15 as the final term to account for the possible steric effects of its presence.

The next step in the analysis is to find the equilibrium height of the brush at a given hybridization efficiency. This can be done by proposing $\partial\gamma_{site}/\partial H = 0$ at the equilibrium condition. This yields the equilibrium height of the brush, H_{eq}:

$$H_{eq} \cong \left(\frac{\left(N_s + n_p\right) * a_s}{\Sigma} * \left[\upsilon_s N_s^2 + \upsilon_p n_p^2 (1+x)^2 + \upsilon_{sp} N_s n_p (1+x) \right] \right)^{1/3} \qquad \text{Equation 2-18}$$

In this equation, the contribution of the impenetrable surface is neglected because it is proposed that it has a negligible effect on the equilibrium dimensions of the chains [23]. The equilibrium free energy per site can then be calculated by substituting this equilibrium height into Equation 2-15:

$$\frac{\gamma_{site}}{kT} \cong \frac{1}{((N_s + n_p) a_s^2)^{1/3}} * \left(\frac{\upsilon_s N_s^{\,2}}{\Sigma} \right)^{2/3} * \left[1 + \left(\frac{\upsilon_p}{\upsilon_s} \right) \left(\frac{n_p}{N_s} \right)^2 (1+x)^2 + \left(\frac{\upsilon_{sp}}{\upsilon_s} \right) \left(\frac{n_p}{N_s} \right) (1+x) \right]^{2/3} \ldots$$

$$+ \left[x \ln x + (1-x) \ln(1-x) \right] + \left[x \frac{\mu_{spt}^0}{kT} + (1-x) \frac{\mu_{sp}^0}{kT} \right] - \ln \left(\frac{\upsilon_s N_s^2 + \upsilon_p n_p^2 (1+x)^2 + \upsilon_{sp} N_s n_p (1+x)}{\Sigma} \right)^{1/3}$$

Equation 2-19

Furthermore, a hybridization isotherm equation can be determined by the equilibrium condition of $\partial\gamma_{site}/\partial x = \mu_t^0 + kT \ln c_t$, c_t being the target concentration. When this criterion is applied on Equation 2-19, the following equations are obtained:

$$\left.\frac{\partial \gamma_{site}}{\partial x}\right|_{x=x_{eq}} = \Gamma(x_{eq}) + \ln\left(\frac{x_{eq}}{1-x_{eq}}\right) + \frac{\mu_{spt}^0 - \mu_{sp}^0}{kT} = \frac{\mu_t^0}{kT} + \ln c_t \qquad \text{Equation 2-20}$$

and

$$\frac{x_{eq}}{1-x_{eq}} = c_t * K_{bulk} * \exp(-\Gamma(x_{eq})) \qquad \text{Equation 2-21}$$

where

$$K_{bulk} = \exp\left(-\frac{\mu_{spt}^0 - \mu_{sp}^0 - \mu_t^0}{kT}\right) \qquad \text{Equation 2-22}$$

and

$$\Gamma(x_{eq}) = \left[n_p * \left(\frac{N_s}{N_s + n_p}\right)^{1/3} * \left(\frac{\upsilon_s}{\Sigma * a_s}\right)^{2/3} - \left(\frac{(N_s + n_p) * a_s^2 * (\upsilon_s * N_s^2)}{\Sigma}\right)^{1/3}\right] \cdots$$

$$* \frac{\left(\frac{\upsilon_p}{\upsilon_s}\right)\left(\frac{n_p}{N_s}\right)(1+x) + \left(\frac{\upsilon_{sp}}{\upsilon_s}\right)}{\left[1 + \left(\frac{\upsilon_p}{\upsilon_s}\right)\left(\frac{n_p}{N_s}\right)^2 (1+x)^2 + \left(\frac{\upsilon_{sp}}{\upsilon_s}\right)\left(\frac{n_p}{N_s}\right)(1+x)\right]^{1/3}} \qquad \text{Equation 2-23}$$

Using equations 2-21 through 2-23, the effective equilibrium constant dominated by entropic blocking can be expressed as:

$$K_{spt}^{surface} = K_{bulk} * \exp(-\Gamma(x_{eq})) \qquad \text{Equation 2-24}$$

and the contribution of the entropic blocking on the free energy of transitions as:

$$\Delta G_{entropic\ blocking}^0 \approx + R * T * \Gamma(x_{eq}) \qquad \text{Equation 2-25}$$

Equation 2-25 enables the calculation of the effect of entropic blocking with respect to different parameters on the standard free energy change of coil-to-helix transition. In this chapter, the effects of spacer length and probe density are simulated.

2.4 Results and Discussion

2.4.1 Zeta Potential Experiments

Initial zeta potential measurements were focused on the determination of the amount of glass beads to be used in the experiments. This is essential since each type of sample material has a unique range of sample concentration for optimal results; a low concentration may result in insufficient light scattering, and too high of a concentration may cause light scattered by one particle being scattered by the other: multiple scattering [11]. Therefore, using the concentration criterion set forth in the technical manual (for particles with diameters >1 μm, the recommended minimum concentration is %0.01 mass and the recommended maximum concentration is %1 mass), the optimum concentration range for our glass beads with 2.5 g/cm^3 density corresponds to 0.0005 mg – 0.05 mg in 2 ml SSPE solution. In these experiments, glass bead concentrations of 0.0001 mg, 0.001 mg and 0.01 mg in 2 ml of 1X SSPE (pH 6.7) were examined. Figure 2-3 shows the change in the zeta potential with respect to these three different glass bead concentrations.

The average zeta potential values for the concentrations 0.0001 mg and 0.001 mg in 2 ml are quite similar. However, the average zeta potential value at 0.01 mg in 2 ml is much lower in absolute value. As the concentration of the beads increases in solution, the attenuator reduces the amount of light that passes through the sample to decrease the amount of scattered light that could overload the detector [11]. It seems that this reduction also affected our measurements at the highest concentration tested, and resulted in a low zeta potential value. The concentration to be selected should be minimally influencing the zeta potential measurement in order to avoid any concentration dependent effect. As a result, there are only two values left for concentration based on these measurements: 0.0001 mg and 0.001 mg in 2ml SSPE. 0.001 mg glass beads in 2ml SSPE was chosen for further experimentation; since it falls within the recommended range of concentrations.

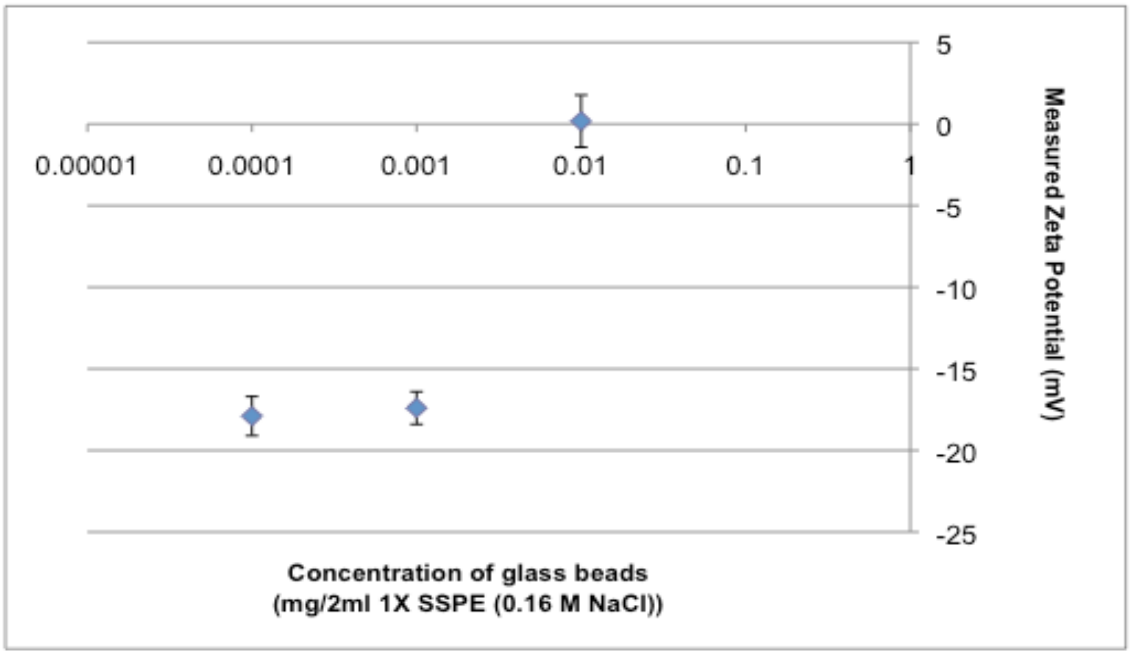

Figure 2-3 Zeta potential measurements with different bead concentrations in 2 ml of 1X SSPE, pH = 6.7 at 23°C.

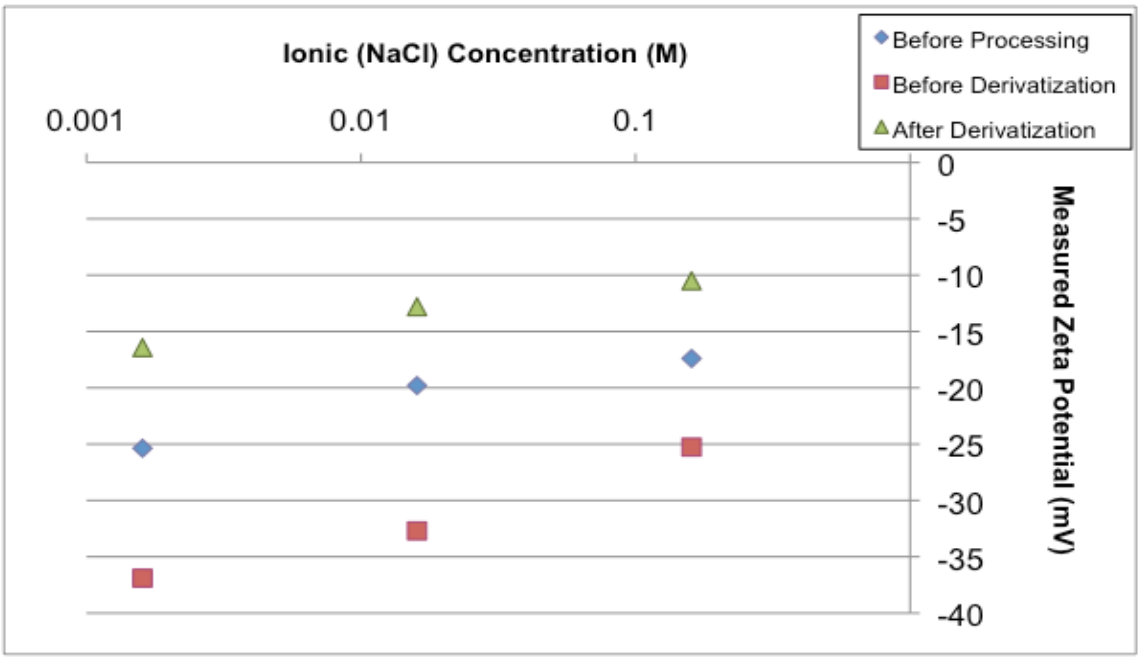

Figure 2-4 Average measured Zeta potential values with 0.001 mg glass beads at different steps during synthesis measured in 2ml of 0.01X (0.0016 M NaCl), 0.1X (0.016 M NaCl), 1X (0.16 M NaCl) SSPE, pH = 6.7 at 23°C.

The next step in the analysis is to look at the variation in zeta potential at different steps of the synthesis: before any processing, before and after derivatization. Figure 2-4 reflects the variations in measured zeta potentials during different steps of synthesis at different salt concentrations.

Among the salt concentrations, 6X SSPE (1 M NaCl) solution did not give reproducible zeta potential measurements. This could be due to the fact that the Debye length is compressed at this ionic concentration (0.76 nm), and any potential measurement at half of this length would be within the detection, or error limits of the instrument. At all other concentrations, 1X SSPE, 0.1X SSPE, 0.01X SSPE, zeta potential values were reproducibly obtained and used in further analysis.

In Figure 2-4, we see that cleaning the glass silica surface from the residual organics with ammonium hydroxide, hydrogen peroxide, water exposes the available sites to the solution. According to the literature [26], it is known that for silica above pH 2, the protonated sites (Si-OH) will be in minority compared to deprotonated ones ($Si\text{-}O^-$). At pH 6.7, the value the experiments were carried out, the density of deprotonated sites will influence the surface charge accordingly, making it more negative. This may lead to preferential concentration of H^+ (H_3O^+) and Na^+ ions near the negatively charged surface. Consequently, the average zeta potential values before derivatization are expected to have more negative zeta potentials when compared to the ones before any processing, as observed in our experiments. The next step, derivatization, would yield $–NH_2$ or amine groups on the surface due to the nature of our linker (*3-aminopropyltriethoxysilane*). Previous studies showed that the pKa of the surface amine groups is 6.0 [26]. At pH 6.7, some deprotonation of the amine groups would occur, and the presence of negative silanol groups underneath would also contribute to the surface charge density. Thus, the average zeta potential value after derivatization would indicate this change as a decrease in negativity, which is in agreement with our experimental observations.

2.4.2 Electrostatic Blocking

The next step in the analysis is to calculate the surface potentials using the average zeta potentials measured at different stages for synthesis via the theory described previously for hard sphere, with no ion penetration assumption. Figure 2-5 shows the values of surface potentials at different salt concentrations calculated through Poisson-Boltzmann theory.

It is observed that the trends in predicted surface potentials at different steps of synthesis are similar to the trends in measured zeta potentials. As the ionic concentration increases, the work required to bring a charged particle from infinity to the surface would decrease, and this will lead to the conclusion that the surface potential would be also lower at higher ionic concentrations [13].

Next step in the analysis is calculating the surface potentials in the presence of the poly dT spacer using the theory based on the polyelectrolytes on a soft particle with ion penetration assumption.

This theory requires the knowledge of the volumetric charge density of the polyelectrolyte, N. It can be calculated using the probe density value published for our system [27] and later modified according to our experimental conditions (1 molecule/2000Å), and the pitch height of single helix assumed to be equal to that of double helix (3.4 Å): 163 mol/m^3.

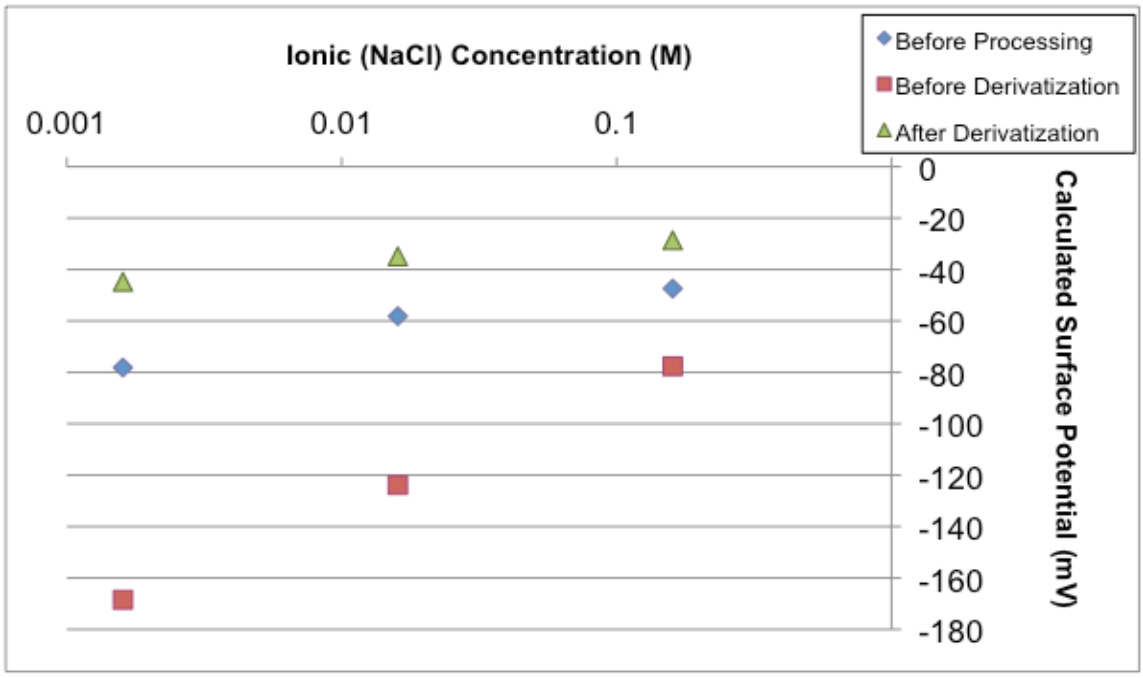

Figure 2-5 Calculated surface potentials for 0.001 mg glass beads at different steps during synthesis measured in 2ml of 0.01X (0.0016 M NaCl), 0.1X (0.016 M NaCl), 1X (0.16M NaCl) SSPE, pH = 6.7 at 23°C, using Poisson-Boltzmann theory for hard spheres without ion penetration.

Table 2-1 shows the predicted surface potential values using the theory of charged soft particle with polyelectrolyte layer at the salt concentrations of 0.0016 M, 0.016 M and 0.16 M after a spacer of length 15 dT was synthesized on the surface.

Table 2-1 Predicted surface potential at salt concentrations of 0.0016 M, 0.016 M, and 0.16 M after the 15 dT spacer synthesis.

	Ionic (NaCl) Concentration (M)		
	0.0016	**0.016**	**0.16**
Surface Potential (mV)	-162.637	-103.807	-47.592

The predicted surface potential change is expected to decrease as the ionic concentrations increases, since the work that is going to bring a unit charge from infinity to the surface is going to be less due to the increasing shielding effect of the ions in the solution.

After the calculation of the surface potential at the spacer layer, predictions of zeta potentials have been made at a distance of half of the Debye length using the Poisson Boltzmann theory with ion penetrable soft shell. These values are compared to the zeta potentials measured after 15 dT spacer synthesis. Figure 2-6 shows the comparison of the predicted potentials at half of the Debye length and zeta potentials for 0.001 mg glass beads after 15 dT spacer synthesis in 2 ml of 0.01X (0.0016 M NaCl), 0.1X (0.016 M NaCl), and 1X (0.16 M NaCl) at pH 6.7 at 23°C.

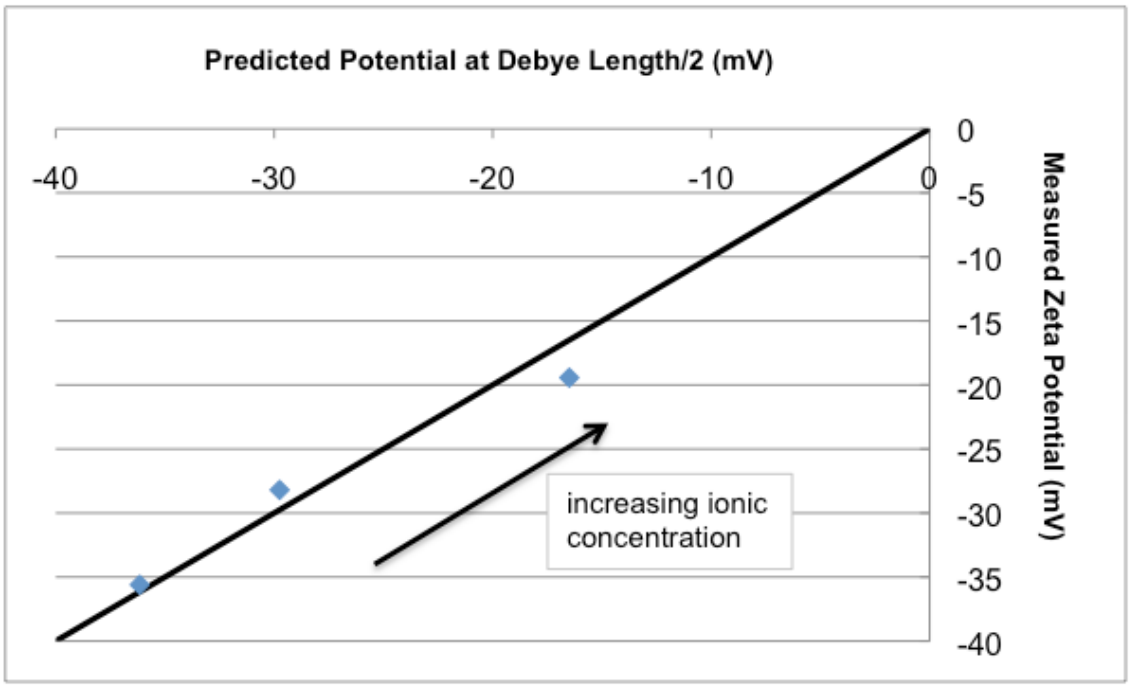

Figure 2-6 The comparison of the calculated potential at the half of the Debye length on a surface with a 15 dT spacer using the Poisson Boltzmann approach with ion penetration, and measured zeta potentials for 0.001 mg glass beads at the end of 15 dT spacer synthesis in 2 ml of 0.01X (0.0016 M NaCl), 0.1X (0.016 M NaCl), 1X (0.16 M NaCl) SSPE, pH 6.7 at 23°C.

Figure 2-6 shows that the predicted potentials at the half of the Debye length are in agreement with the measured potentials at all ionic concentrations; decreasing in negativity with increasing ionic concentration, as expected. This demonstrates that the utilization of the soft-shell ion penetrable theory gives reliable predictions. Even though zeta potential measurements could not be obtained at 1 M ionic concentration, we can conclude that the model can be used to predict the surface potential at this concentration, which is used in all hybridization and melting experiments.

After confirming the reliability of the model, next step in the analysis involves the calculation of the surface potential and surface charge as well as the free energy penalty experienced by a target hybridizing with a probe on the surface. This is accomplished by the Surface Partition Model modified for hybridization between a target and a probe on the array surface, previously introduced in the theory section. It is necessary to use this model at this point, mainly because it gives the flexibility to monitor the change in the surface charge and density with respect to hybridization efficiency, target length, probe density and temperature.

The influences of spacer length and probe density on the electrostatic blocking were simulated. The trends seen with respect to different hybridization efficiencies are presented in the Appendix. For clarity in analysis, the comparison of these effects made at a constant hybridization efficiency of 0.5 is shown in Figure 2-7. Figure 2-7(a) shows that as the spacer length increases, the electrostatic free energy penalty experienced by the incoming target also increases at all probe densities. This would be due to the increased charge density in the probe layer with longer spacer lengths. In Figure 2-7(b), as the probe density increases, the electrostatic blocking term also increases, with a higher surface charge density [28, 29]. However, this increase is more pronounced than the effect of the simulated spacer lengths. This could be because the surface charge density increases more in denser probe layers when compared to layers with longer spacers.

(a)

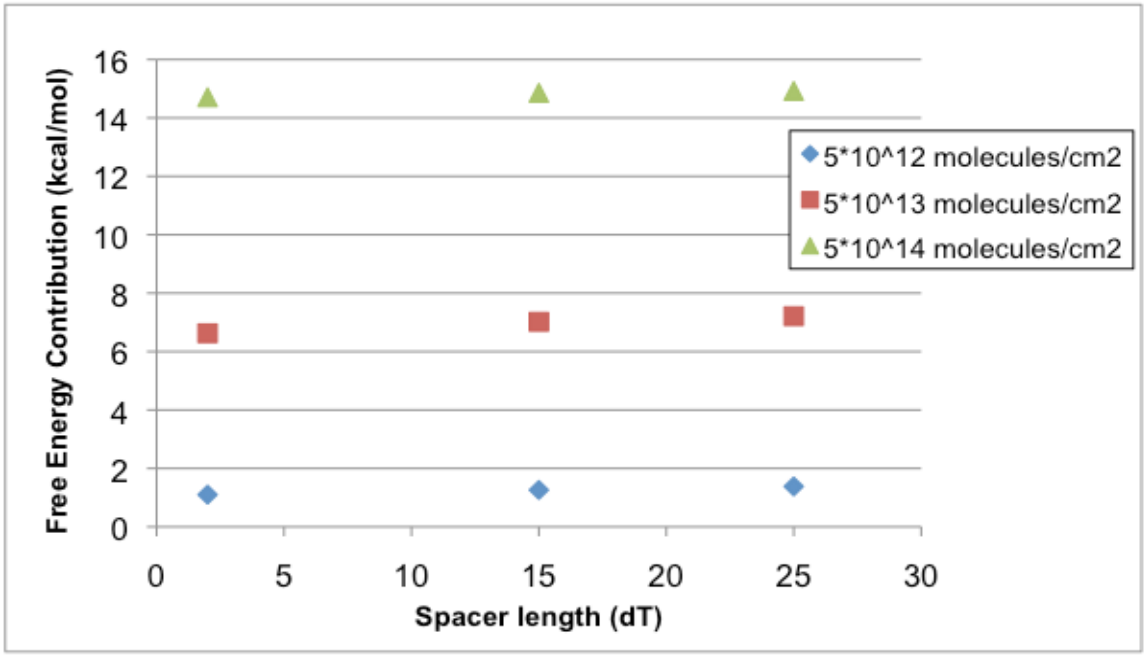

(b)

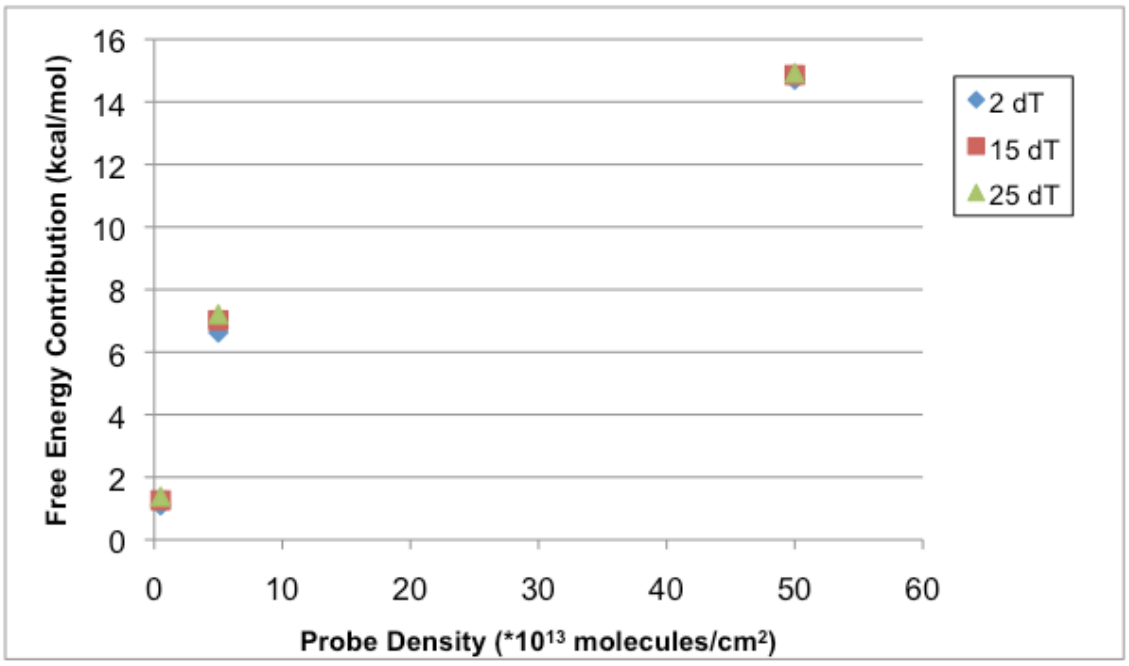

Figure 2-7 Electrostatic free energy penalty experienced by a target hybridizing in a probe layer with a hybridization efficiency of 0.5, at 23°C and 1 M NaCl concentration (a) with respect to spacer lengths of 2 dT, 15 dT, 25 dT at different probe densities, (b) with respect to probe densities of $5*10^{12}$ molecules/cm^2, $5*10^{13}$ molecules/cm^2 and $5*10^{14}$ molecules/cm^2 at different spacer lengths.

These electrostatic blocking terms are accompanied with entropic penalties imposed by the surface on the structure during duplex formation or melting.

2.4.3 Entropic Blocking

In this section, we looked at the effects of spacer length and probe density on the entropic blocking term. The influences of spacer length and probe density on the entropic blocking with respect to different hybridization efficiencies are presented in the Appendix. For clarity in analysis, the comparison of these effects made at a constant hybridization efficiency of 0.5 is shown in Figure 2-8.

In Figure 2-8(a), it can be observed that as spacer length increases, the effect of the surface on the entropic blocking term decreases at all probe densities. This is expected since as the reaction gets far away from the surface, it will start to resemble the solution more [30], and the effect of the surface starts to diminish. We can deduce from Figure 2-8(b) that as the probe density increases, the penalty experienced by the hybridizing target also increases, because of the increased crowding of the probe layer leading to more steric effects on the target. In addition, with increasing probe density, the effect of the spacer length seems to gain more importance. In other words, at denser brush regimes, the farther one gets away from the surface, the less the target will experience the crowding effect of the probe layer as well as the impenetrable surface. This is observed clearly at the higher probe densities, mostly because these phenomena are more pronounced. A comparison between the relative effects of the spacer length and probe density on the entropic blocking concludes that probe density introduces more entropic penalty than short spacer lengths, at the conditions simulated. This suggests that the contribution of crowding probe layer on the entropic penalty seems to be more important.

(a)

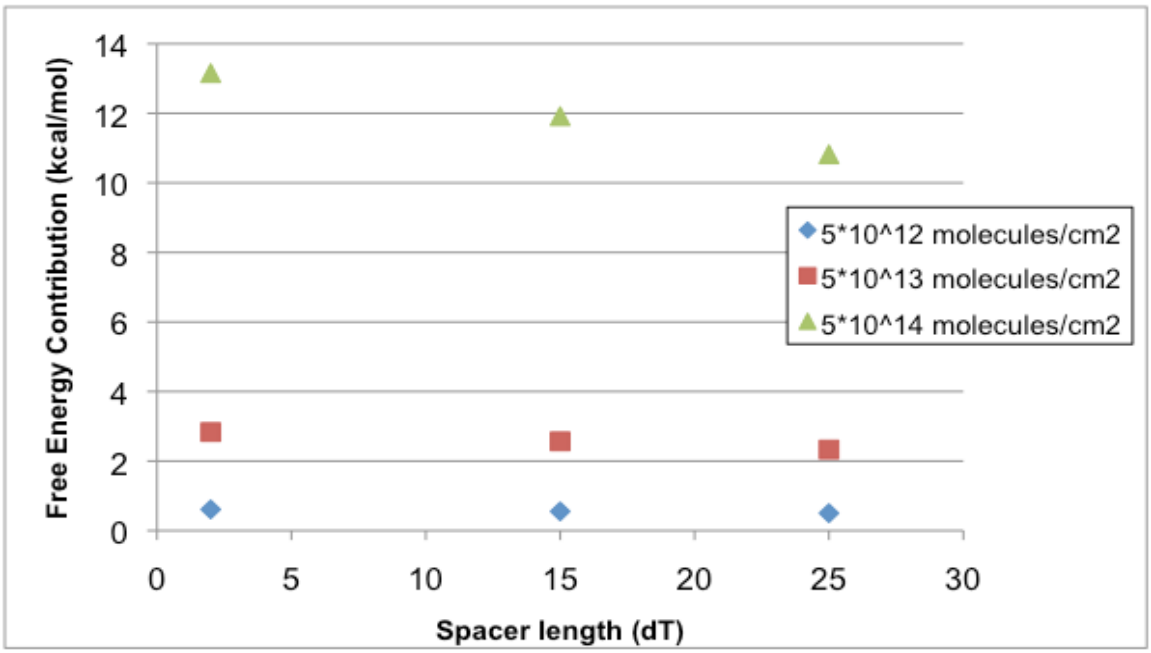

(b)

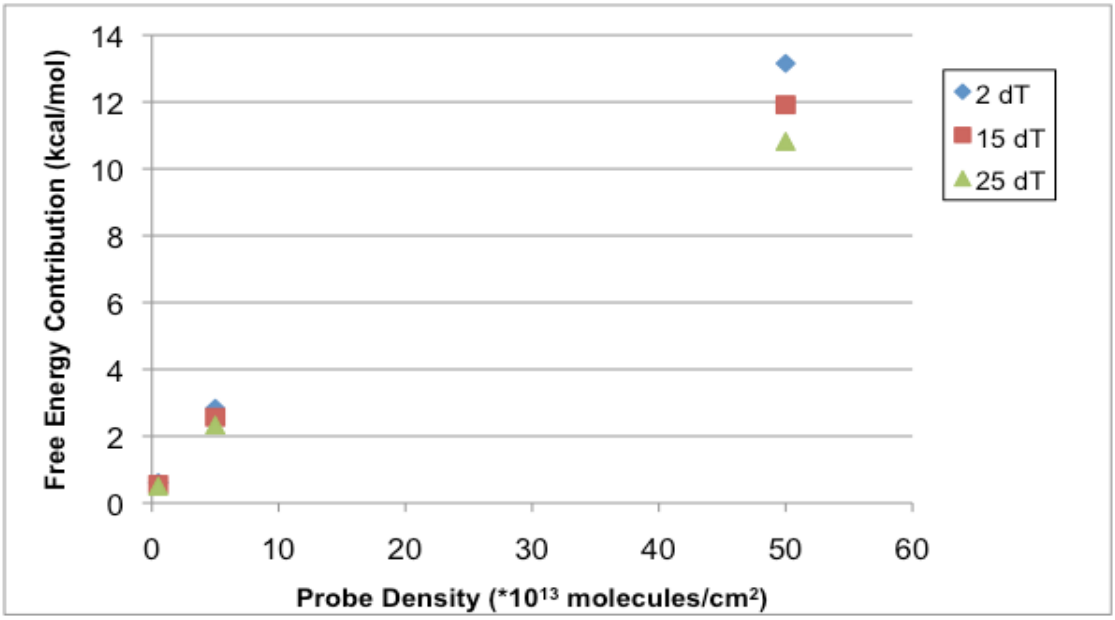

Figure 2-8 Entropic free energy penalty experienced by a target hybridizing in a probe layer with a hybridization efficiency of 0.5, at 23°C and 1 M NaCl concentration (a) with respect to spacer lengths of 2 dT, 15 dT, 25 dT at different probe densities, (b) with respect to probe densities of $5*10^{12}$ molecules/cm^2, $5*10^{13}$ molecules/cm^2 and $5*10^{14}$ molecules/cm^2 at different spacer lengths.

2.5 Conclusion

In this chapter, the theory of electrostatic and entropic blocking was examined. Electrostatic contributions mostly come from the inherent surface charges that are present due to the surface, spacer and probe layers into which the target penetrates to form a duplex. It is calculated via the Electrostatic Double Layer theory and through the adaptation of Surface Partition Model. Electrostatic Double Layer theory provides the means to calculate the initial surface charge before duplex formation by modeling the surface with a penetrable polyelectrolyte layer in the presence of spacer and probes. Using the initial surface charge values and the incremental surface charge changes brought by the targets hybridizing with the probes, it is possible to calculate the surface potential changes as well as the free energy contributions of these changes to reflect on various parameters imposed on the system, i.e. spacer length and probe density. A longer spacer and a denser probe layer lead to an increase in the surface charge and potential. Thus, the free energy penalty experienced by a hybridizing target also increases. The effect of the probe density seems to be more than the spacer lengths examined; which could be mostly due to the higher surface charge introduced into the system with the presence of denser probe layer than the increase in the spacer length by itself.

Entropic blocking takes into account the excluded volume effect due to the presence of the impermeable solid surface and the crowding effect due to the probe layer. This term is calculated theoretically through polymer physics and second virial coefficients to represent the interactions between the spacer, probe and target monomers. Equipped with this model, the effects of the spacer length and the probe density are further screened through their free energy contributions on the duplex formation. An increase in the spacer length results in a decrease in the contribution of the entropic blocking on the surface. As a result, hybridizations with probes on top of longer spacers resemble the in-solution duplex formations more. On the other hand, an increase in the probe density leads to a considerable increase in the entropic penalty contribution to the free energy of duplex formation on the surface; a result of increased crowding and

steric effects within the denser layer. A comparison between the relative effects of the spacer length and probe density on the entropic blocking yields that the influence of the probe density in terms of hindering the duplex formation on the surface is much more pronounced than the effect caused by short spacer lengths at the conditions simulated. In addition, the spacer length effect is observed to be much more apparent when the probe density is higher. The farther the duplex formation is from the surface, the less the target will experience the crowding effect of the probe layer as well as the impenetrable surface. It seems this phenomenon is more pronounced at higher probe densities.

2.6 Appendix

2.6.1 Electrostatic Blocking

Figure 2-9 involves the initial electrostatic blocking of the targets before hybridizing on the surface and an incremental electrostatic blocking due to the targets hybridizing on the surface, which is, in turn, indicated by the hybridization efficiency, and also reflected in the calculation of the surface charge density to estimate the electrostatic free energy contribution.

Increasing hybridization efficiency results in increasing electrostatic penalty since the surface charge increases with duplex formation.

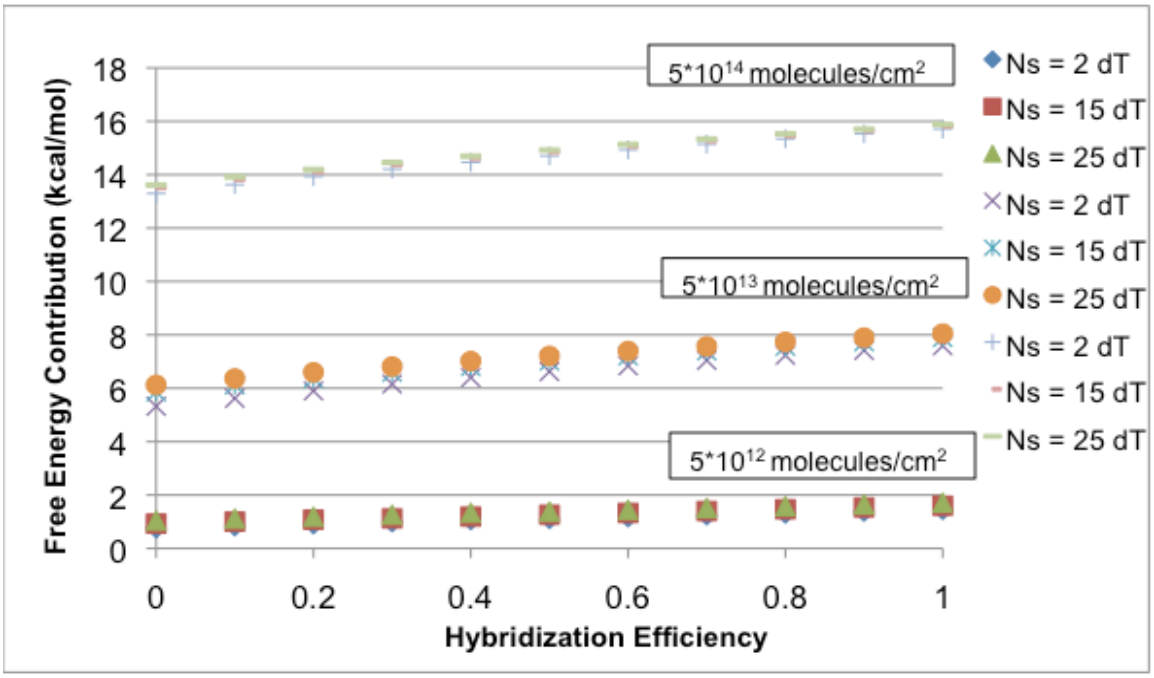

Figure 2-9 Electrostatic free energy penalty felt by a target (25mer) coming into the probe (25mer) layer at different hybridization efficiencies with probe densities of $5*10^{12}$ molecules/cm^2, $5*10^{13}$ molecules/cm^2, $5*10^{14}$ molecules/cm^2 at spacer lengths (Ns) of 2 dT, 15 dT, 25 dT, at 23°C and 1 M ionic (NaCl) concentration

2.6.2 Entropic Blocking

Figure 2-10 demonstrates the free energy contributions of spacer length and probe density with respect to hybridization efficiency. Increasing hybridization efficiencies lead to more entropic penalty with respect to both spacer length and probe density, due to crowding of the probe layer and increasing steric hindrance.

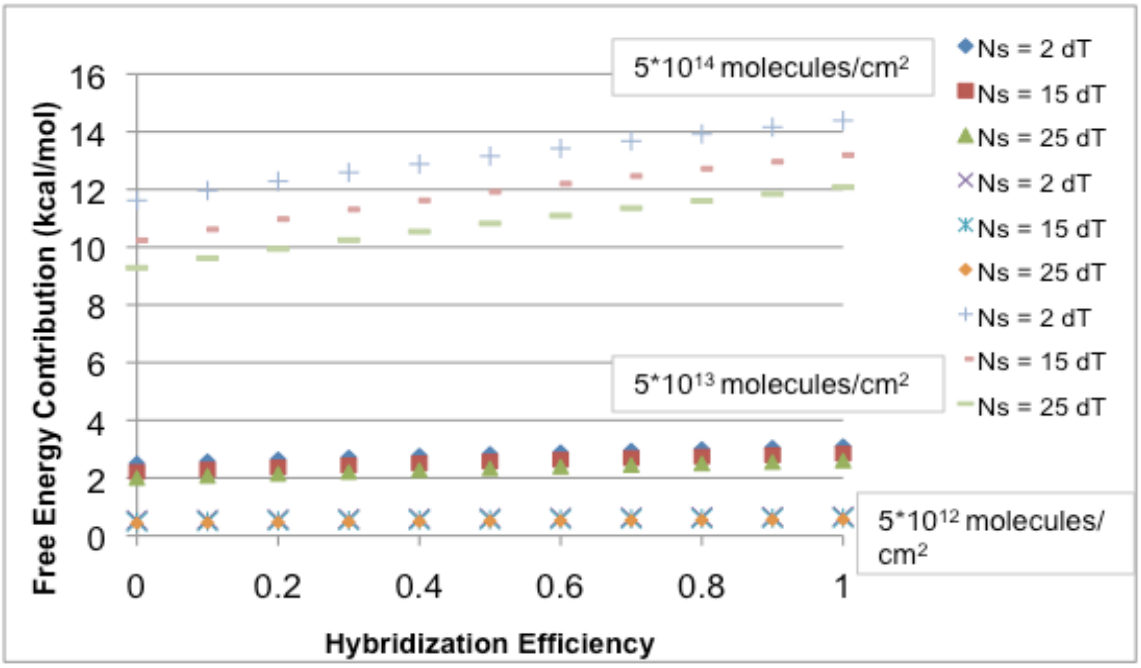

Figure 2-10 Entropic free energy penalty felt by a target (25mer) coming into the probe (25mer) layer at different hybridization efficiencies with probe densities of $5*10^{12}$ molecules/cm^2, $5*10^{13}$ molecules/cm^2, $5*10^{14}$ molecules/cm^2 at spacer lengths (Ns) of 2 dT, 15 dT, 25 dT, at 23°C and 1 M ionic (NaCl) concentration

2.7 Bibliography

1. Southern E, Mir K, Shchepinov M, *Molecular interactions on microarrays*. Nat Genet, 1999. 21: 5-9.
2. www.izbi.de/working_papers.html
3. Wilson RW, Rau DC, Bloomfield VA, *Comparison of polyelectrolyte theories of the binding of cations to DNA*. Biophys J, 1980. 30: 317-325.
4. Gueron M, Weisbuch G, *Polyelectrolyte theory of charged-ligand binding to nucleic acids*. Biochimie, 1981. 63: 821-825.
5. Meyer PI, Wesenberg GE, Vaughan WE, *Dielectric behavior of polyelectrolytes II. The cylinder*. Biophys Chem, 1981. 13: 265-273.
6. Ohshima H, Kunio Furusawa. Electrical Phenomena at Interfaces-Fundamentals, Measurements, and Applications. In: ed. 76. Marcel Dekker, Inc, 1998:1-18.
7. Ohshima H, *Electrophopretic mobility of soft particles*. Electrophoresis, 1995. 16: 1360-1363.
8. Birdi KS. Handbook of Surface and Colloid Chemistry. In: ed. Florida: CRC Press LLC, 2003:396.
9. Halperin A, A. Buhot, E. B. Zhulina, *On the hybridization isotherms of DNA microarrays: the Langmuir model and its extensions*. Journal of Physics: Condensed Matter, 2006. 18: S463-S490.
10. Halperin A, Buhot A, Zhulina EB, *Hybridization at a surface: the role of spacers in DNA microarrays*. Langmuir, 2006. 22: 11290-11304.
11. Instruments M. Zetasizer Nano Series User Manual. In: ed. England: Malvern Instruments Ltd, 2003:15.1-15.11.
12. Hunter RJ. Foundations of Colloid Science. In: ed. 1. Oxford, UK: Oxford University Press, 1989:329.

13. Kirby BJ, Hasselbrink EFJ, *Zeta potential of microfluidic substrates: 1. Theory, experimental techniques, and effects on separations*. Electrophoresis, 2004. 25: 187-202.

14. Delgado, AV, Gonzalez-Caballero F, Hunter RJ, Koopal LK, Lyklema J, *Measurement and Interpretation of Electrokinetic Phenomena*. Pure and Applied Chemistry, 2005. 77: 1753-1850.

15. http://en.wikipedia.org/wiki/Poisson-Boltzmann_equation

16. Hunter RJ. Zeta Potential in Colloid Science- Principles and Applications. In: ed. 2. Oxford, UK: Academic Press, 1981:215-216.

17. Bloomfield VA, Crothers DM, Tinoco JR, Ignacio. Nucleic Acids: Structures, Properties, and Functions. In: Stiefel J, ed. University Science Books, 2000

18. Manning GS, *Electrostatic free energy of the DNA double helix in counterion condensation theory*. Biophys Chem, 2002. 101-102: 461-473.

19. Cantor CR, Schimmel PR. The Conformation of Biological Molecules. In: eds. 1. San Francisco: W.H. Freeman, 1980

20. Smith SB, Cui Y, Bustamante C, *Overstretching B-DNA: the elastic response of individual double-stranded and single-stranded DNA molecules*. Science, 1996. 271: 795-799.

21. http://en.wikipedia.org/wiki/Persistence_length

22. Mills JB, Vacano E, Hagerman PJ, *Flexibility of single-stranded DNA: use of gapped duplex helices to determine the persistence lengths of poly(dT) and poly(dA)*. J Mol Biol, 1999. 285: 245-257.

23. Halperin A, Buhot A, Zhulina EB, *Brush effects on DNA chips: thermodynamics, kinetics, and design guidelines*. Biophys J, 2005. 89: 796-811.

24. Jayaraman A, Hall CK, Genzer J, *Computer simulation study of probe-target hybridization in model DNA microarrays: effect of probe surface density and target concentration*. J Chem Phys, 2007. 127: 144912.

25. Rubinstein M, Colby RH. Polymer Physics. In: eds. Oxford: Oxford University Press, 2003

26. Wang B, Abdulali-Kanji Z, Dodwell E, Horton JH, Oleschuk RD, *Surface characterization using chemical force microscopy and the flow performance of modified polydimethylsiloxane for microfluidic device applications*. Electrophoresis, 2003. 24: 1442-1450.

27. Wick LM, Rouillard JM, Whittam TS, Gulari E, Tiedje JM, Hashsham SA, *On-chip non-equilibrium dissociation curves and dissociation rate constants as methods to assess specificity of oligonucleotide probes*. Nucleic Acids Res, 2006. 34: e26.

28. Vainrub A, Pettitt BM, *Coulomb blockage of hybridization in two-dimensional DNA arrays*. Phys Rev E Stat Nonlin Soft Matter Phys, 2002. 66: 041905.

29. Vainrub A, B. Montgomery Pettitt, *Thermodynamics of Association to a Molecule Immobiized in an Electrical Double Layer*. Chemical Physics Letters, 2000. 323: 160-166.

30. Shchepinov MS, Case-Green SC, Southern EM, *Steric factors influencing hybridisation of nucleic acids to oligonucleotide arrays*. Nucleic Acids Res, 1997. 25: 1155-1161.

CHAPTER III

DEVELOPMENT OF AN EXPERIMENTAL APPROACH TO GENERATE DNA MELTING CURVES ON THE SURFACE

3.1 Introduction

Microarray technology has gained a lot of interest in recent years, and it has been the platform of choice for applications varying from gene expression analysis to biological detection [1, 2]. It is based on the fundamental process of solid-phase hybridization, in which nucleic acid strands tethered to a solid support bind DNA or RNA molecules in the solution. This reaction takes place in a solid-liquid interface, which offers a different environment than a homogeneous solution [3]. The thermodynamics and kinetics of duplex formation have been studied quite extensively for duplex formation taking place in solution [4-7]. Microarray applications use these information in design and experimentation [8, 9].

There has been a recent increase in the number of scientific publications on the physical modeling and experimental investigation of DNA hybridization on the surface [10-13]. Theoretical investigations model the process through various statistical mechanics, molecular physics, kinetic and transport equations [10, 13]. Experimental studies differ in their approaches. Following the procedures set-forth by the array manufacturers (Affymetrix Inc (California, USA), Agilent Inc (California, USA)), some of the studies focus on hybridization techniques in which passive hybridization (with constant amount of target) is improved by the introduction of convection through rotation [14, 15], and investigate the effect of different system variables (i.e. probe density [16], probe length [17]) on the extent of hybridization. Due to the possible limitations of passive hybridization (slow

reaction rates, long hybridization durations [18]), researchers have focused their attention to incorporating microfluidics into the system. Flowing the target solution over the probe layer has shown to improve the reaction kinetics and time considerably [19, 20].

Using this advantage of dynamic hybridization, several studies have been published, looking at the effect of different system variables on the kinetics of duplex formation or the generation of 'non-equilibrium' denaturation curves to aid in the design of experiments [9, 21].

Although 'melting temperature' is commonly regarded as an important experimental design parameter [8, 22], generation of melting curves at equilibrium to determine the melting temperature of the duplex formed on the surface has not been extensively studied.

In this part of the thesis, we introduce an experimental set-up that is capable of real-time monitoring of the hybridization and melting of DNA duplexes formed between labeled targets recirculating through a microfluidic chip and the probes synthesized on its surface using light-directed, *in situ* oligonucleotide synthesis. The introduction of various quality control steps, and a robust analysis method provide us with additional advantages.

3.2 Experimental System Development

3.2.1 Experimental Set-up

The experiments were carried out in a custom designed system that combines microfluidics, microfabrication, *in situ* oligonucleotide synthesis, and real-time image capturing with a fluorescence scanner. The elements included in this system are depicted in Figure 3-1.

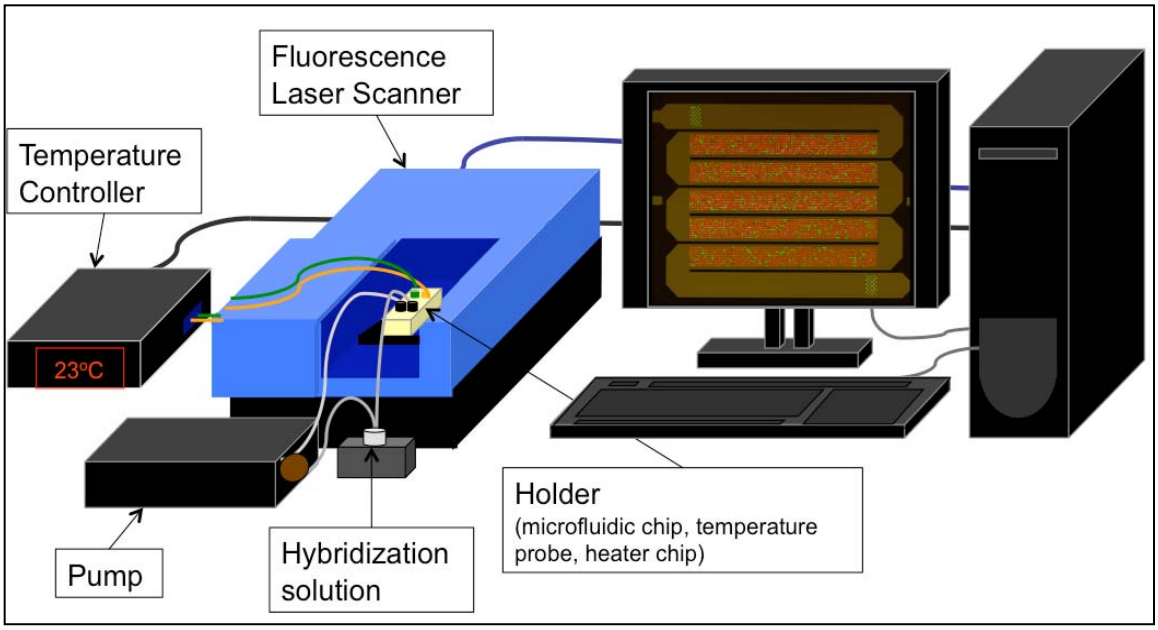

Figure 3-1 The experimental set-up comprising of a custom-designed holder housing a microfluidic chip, heater chip, temperature probe and the necessary fluidic and electrical connections; a temperature controller to check the temperature, a pump to circulate the hybridization solution, and a fluorescence scanner for detection.

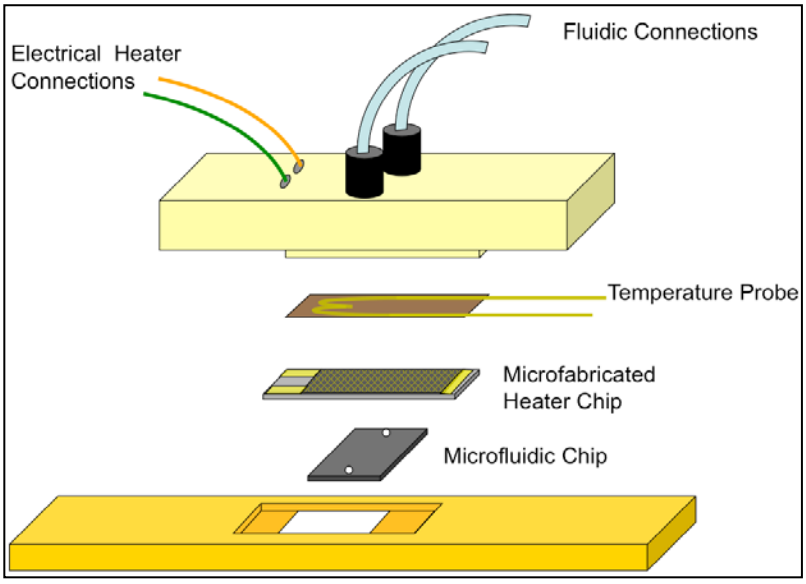

Figure 3-2 The holder housing the microfluidic chip with the probes synthesized; a microfabricated heater chip for heating; a temperature probe for temperature measurement; fluidic connections through which the target constantly recirculates; electrical connections with the temperature controller.

There are five main components in this experimental set-up:

i. A custom-design holder

This holder is specifically designed to capture the real-time hybridization process on the oligonucleotide arrays synthesized in our laboratory. It houses the following units: a microfluidic chip, a temperature probe (CO1-K, Omega Inc, Connecticut, USA) and a heater chip, along with the necessary electrical and fluidics connections. (Figure 3-2)

ii. A temperature controller

The temperature of the microfluidics chip is controlled via a proportional-integral-derivative (PID) temperature controller with autotuning capability (CN9600 Series, Omega Inc, Cincinnati, USA). This controller acts as an intermediary between the computer (the user) and the holder system. It receives the temperature value set by the user on the computer interface; then, reads the current temperature on the system, and acts accordingly to change the temperature by sending the necessary voltage across the heater chip in the holder, and this cycle continues as new temperature values are input by the user in the interface.

iii. A peristaltic pump

An in-house peristaltic pump was used to circulate the target solution through the system during the experiment. A 1,000 μl target solution was prepared in a 1.5 ml eppendorf tube. The pump was connected to the fluidic connection on the holder to draw this solution through the microfluidic chip and pump it back to the same tube for recirculation. A flow rate of 500 μl/min was used in all experiments.

iv. A fluorescence scanner

The housing along with the electrical connections and the fluidic connections is placed into the holder of the fluorescence scanner, GenePix Axon 4000B (Molecular Devices Inc, California, USA) to detect the fluorescence off the labeled target hybridized with the probes on the glass surface as the experiment progresses. These signal intensities are extracted with GenePix 5.0 software,

providing arbitrary units (a.u.) of measurement between 0 and 65,535, with 5 μm resolution. Both of the lasers present in the scanner are used in the experiments: laser exciting at 532 nm, the green laser, and the laser exciting at 635 nm, the red laser, are accompanied with proper emission filters (~557 - 592 nm for green and ~650 - 690 nm for red) to capture the signals from the duplexes formed on the surface as well as the single stranded targets flowing in solution.

The principle behind the detection scheme is similar to the Total Internal Reflection Fluorescence (TIRF) microscopy. To be able to obtain such high resolution (as low as 5 μm), the penetration depth of the signal has to be close to the surface and needs to carry the least interference from the targets flowing free in solution [23]. This can only be achieved by sending in the laser beam at an angle larger than the critical angle of reflection between the glass and the hybridizing solution. Figure 3-3(a) demonstrates the optical set-up within the scanner and Figure 3-3(b) represents this phenomenon on the surface of the glass on which the immobilized probes are hybridizing with the targets flowing freely in the microfluidic channels.

Calculations have been made using the evanescent wave theory to determine the relative contributions of the signal from the surface and the solution on the overall signal intensity. The intensity of the signal detected is represented using:

$$Signal\,Intensity(SI) = \int_{0}^{DNA\,Layer} Surface\,Intensity * C_1 + \int_{DNA\,Layer}^{Pen\,Depth} Intensity * C_2 \qquad \text{Equation 3-1}$$

where DNA Layer is the height of the DNA layer on the surface assuming the strands are standing straight; Pen Depth is the penetration depth of the exiting beam; Surface Intensity is the intensity off the surface, changing exponentially with the depth; C_1 is the concentration of the probes on the surface; Intensity is the signal intensity from the solution immediate to the surface, changing exponentially with depth; C_2 is the concentration of the targets in solution close to the surface. Surface Intensity and Intensity are expressed as $I_o * \exp(-x/\delta)$ with respect to depth (x), where δ is the penetration depth, and I_o is the intensity of the

(a)

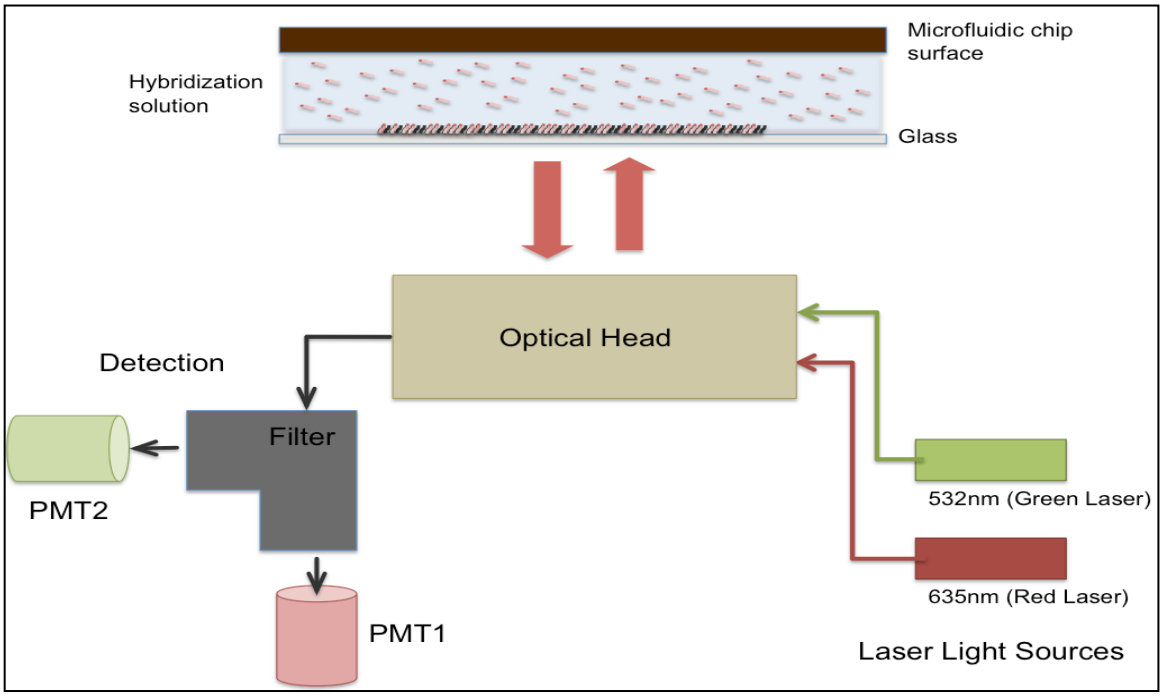

(b)

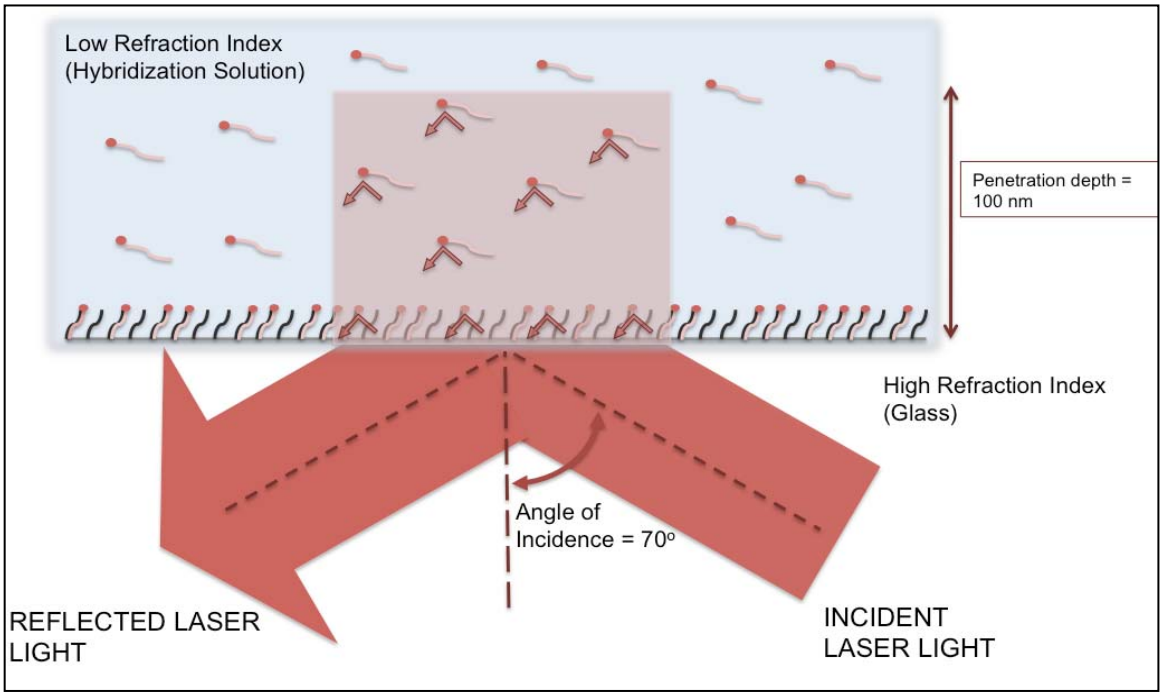

Figure 3-3 (a) Optical set-up within the fluorescence scanner (b) Representation of the TIRF mechanism and evanescent waves on the glass surface during the detection of the fluorescence signal off the targets hybridized with the probes on the glass surface and flowing free in solution.

evanescent wave at the interface between the glass and the solution [24]. DNA Layer is 14 nm (with 15 dT spacer and 25mer probe and assuming 3.4 Å height per monomer) and the penetration depth is calculated using [24]:

$$Penetration\ depth, \delta = \frac{\lambda_0}{4\pi n_2 \sqrt{\left[\sin(\alpha_1)/\sin(\alpha_g)\right]^2 - 1}} \qquad \text{Equation 3-2}$$

with λ_o : wavelength (635 nm), α_1: angle of incidence = 70° (based on TIRF microscopy), α_g : critical angle of total reflection = 60°, n_2: refractive index of less dense medium (assumed to be water at 20°C) : 1.333 [25]. These values result in a penetration depth of 100 nm.

C_1 is calculated to be the concentration achieved when all of the probes on the surface are completely hybridized. Considering the surface density of the probes to be 1 probe in 2000 $Å^2$ (10 times diluted linker ratio in [9]), and the height of the DNA layer to be 14 nm based on the previous calculations, and assuming that there is only one target hybridizing with one probe, C_1 turns out to be $5.933 * 10^{-3}$ M. C_2 is calculated to be $0.26 * 10^{-9}$ M using the observed empty spot intensity in one of the experiments and the fluorescence calibration equation presented later in Equation 3-4. When these values are plugged in Equation 3-1, following equation is obtained:

$$\frac{SignalIntensity(SI)}{I_o} = C_1 * 13.06 + C_2 * 25.53 \qquad \text{Equation 3-3}$$

Concentration terms based on the C_1 and C_2 values are changed simultaneously to simulate different surface coverages (%100 and %10) and solution concentrations ($0.26 * 10^{-9}$ M and $0.26 * 10^{-8}$ M). Table 3-1 shows the effects of these changes on the SI/I_o value.

Table 3-1 Effect of the changes in the concentration of the signal on the surface (C_1) and in solution (C_2) on the SI/I_o value.

C_1(M) \ C_2(M)	$0.26 * 10^{-9}$	$0.26 * 10^{-8}$
$5.933 * 10^{-3}$	0.07748490	0.07748500
$5.933 * 10^{-4}$	0.00774849	0.00774850

It can be inferred from this table that a 10% decrease in the concentration of the hybridized probes on the surface (the concentration in the solution being constant) results in a 10% decrease in the SI/I_o ratio. However, a 10% increase in the concentration of the solution (the concentration on the surface being constant) increases the SI/I_o ratio by only 0.0001%. This demonstrates that the dominant contribution to the overall signal intensity is from the surface rather than the targets in solution.

v. A computer

The temperature ranges and intervals as well as the required equilibrium time(s) are manually entered into an interface designed to integrate and synchronize the scanner and the temperature controller. The interface was written in JavaScript and VBScript, and the communication with the temperature controller is established via a code written in Java programming language.

The temperature input by the user into the interface is sent to the temperature controller, which in turn sends the appropriate signal to the heater chip, and wait for the chip temperature to stabilize within +/- 0.5°C of the set temperature. The system rests till the equilibrium time input by the user expires, during which it periodically checks and records the temperature into a log file. After the set equilibrium time is reached, the scanner scans the chip, and the computer records the image file. At the end of the experiment, all of the images are manually analyzed and the fluorescence intensities are extracted.

The oligonucleotide microfluidic chip used in the experiments constitutes one of the most crucial parts of this study. Therefore, a detailed look at its fabrication, synthesis and design has to be completed before going on further.

3.2.1.1 Microfluidic Chip Fabrication

For a seven-chamber microfluidic chip, a layer of photoresist (PR 1813) is applied by spin-coating at 2000 rpm for 30 s on a silicon wafer. The wafer is soft-baked at 90ºC in an oven for 30 min, and then exposed to UV radiation (404.7 nm, 10 mJ/cm^2, 30 s) to define the chamber pattern. After removal of the activated photoresist by developer solution (MF 319) for 60 s, the wafer is hard-baked at 110ºC for 30 min. The pattern is transferred to the silicon wafer by deep reactive ion etching to obtain 160 μm deep chambers. The photoresist is then removed by a resist stripper (PRS 2000). The new layer of photoresist (AZ9260) is applied at the backside of the wafer by spin-coating at 2000 rpm for 30 s. The wafer is soft-baked at 90ºC in an oven for 30 min and exposed to UV radiation (404.7 nm, 10 mJ/cm^2, 100 s) to define the inlet/outlet holes. The activated photoresist is then removed by a resist developer (AZ400K/H2O, 1:3). Next, the wafer is loaded into the deep reactive ion etcher to create the through inlet/outlet holes.

The silicon wafers containing etched structures are cleaned, and a 0.2 μm thick thermal oxide is grown on the wafers to provide the necessary surface for in situ DNA synthesis. Finally, the silicon wafer is anodically bonded with glass wafer, which is 400 μm in thickness.

3.2.1.2 Heater Chip Fabrication

The fabrication procedure begins with a 4” (100) Si wafer with thermal oxide thickness of 0.6μm. The Cr and Au thin films are then deposited by electron beam deposition (Enerjet Inc, New Hampshire, USA). After the deposition of thin films is completed, the wafers are first primed with hexamethyldisilazane (HMDS). A layer of photoresist (PR 1813, Hoechst Celanese Inc, New Jersey, USA) was then applied by spin-coating at 4000 rpm for 30 s, and the wafers are soft-baked at 90ºC in an oven for 30 min. Later, the

microheater pattern is transferred to the layers of photoresist by photolithography (20 mJ/cm^2, 7 s). The activated photoresist (PR) is removed by developer solution (MF 319, Hoechst Celanese) for 60 s, and the Au and Cr films are then wet-etched using a gold etchant solution (TFA, Transene Company Inc, Massachusetts, USA) for 120 s, and a chromium etchant solution (CR-14, Cyantek Inc, California, USA) for 120 s. To electrically insulate the microheater from the environment, the silicon oxide is deposited by plasma chemical vapor deposition everywhere except the electrical pad.

3.2.1.3 Oligonucleotide Array Synthesis

Oligonucleotide synthesis on the fabricated chips is carried out in three main steps: derivatization, synthesis and deprotection.

i. Derivatization

The surface of the microfabricated chips needs to be further processed to make it clean and ready for synthesis. This requires the introduction of amine sites on the surface, which is accomplished by derivatization. First, the surface is cleaned with an ammonium hydroxide, hydrogen peroxide, water solution (NH_4OH:H_2O_2:H_2O, 1:1:5 in volume) to remove the residual organic materials from the previous fabrication process. Next, the amine groups are introduced on the surface by derivatization using *3-aminopropyltriethoxysilane* solution (SIA0610.0, Gelest Inc, Pennsylvania, USA), which is prepared in different proportions (1 to 0 ratio: 0.4 mM; 1 to 9 ratio: 0.04 mM) in anhydrous toluene (99.8% purity, Sigma-Aldrich Inc, Missouri, USA) under nitrogen, to change the density of the available groups on the surface; thus, changing the probe density on the chip. The dilution of this linker is achieved by adding another linker which provides a non-reactive propyl group on the surface: *n-propyltriethoxysilane* (SIP6917.0, Gelest Inc, Pennsylvania, USA).

ii. Synthesis

ß-cyanoethyl phosphoramidite chemistry (Figure 3-4) constitutes the fundamental chemistry behind the synthesis reactions [26]. It is one of the widely

used methods in oligonucleotide synthesis on solid support, due to its high coupling efficiency, speed, lack of side reactions and the stability of the chemicals used. The basic idea is that the reactive 3’ phosphorus group of one nucleoside, which is delivered in a solution, is coupled to the 5’ hydroxyl of another nucleoside, which is already immobilized on the solid support. Afterwards, 3 more important steps are performed to prepare the growing chain for the next coupling reaction. In this way, a synthesis cycle is completed, adding one monomer at a time, and making the synthesis from 3’ (surface) to 5’.

The first step of the synthesis cycle is deblocking; the removal of the (Dimethoxytrityl) DMT group. This detritylation process is achieved with a dichloroacetic acid solution (DCA), or a trichloroacetic acid solution (TCA) when there is no site addressable synthesis, or i.e. a photogenerated acid, when there is. The cleavage of the DMT cation frees the 5’-hydroxyl for the coupling reaction and produces an orange color that can be used to estimate the synthesis yield and step-wise coupling efficiency spectrophotometrically. Since the DNA bases are acid-labile, this step must only be as long as it is necessary to ensure complete detritylation.

Next step is the coupling of the protected nucleotides or phosphoramidites. While phosphoramidite monomers are protected at the 5’-hydroxyl position with a DMT group, their 3’-phosphite is modified by ß-cyanoethyl and diisopropylamine groups. An activated intermediate is created by simultaneously adding the phosphoramidite nucleoside monomer and tetrazole, a weak acid. The tetrazole protonates the nitrogen of the diisopropylamine group on 3’phosphorous, making it susceptible to nucleophilic attack.

Then, the capping step terminates any chains that did not undergo addition. Since the unreacted chains have a free 5’-hydroxyl group, they can be terminated or capped by acetylation. Capping is done with acetic anhydride and 1-methylimidazole. Since the chains that reacted with phosphoramidite in the previous step are still blocked with DMT, they are not affected by this step. Although capping is not ultimately required for DNA synthesis, it is recommended because it minimizes the length of the impurities.

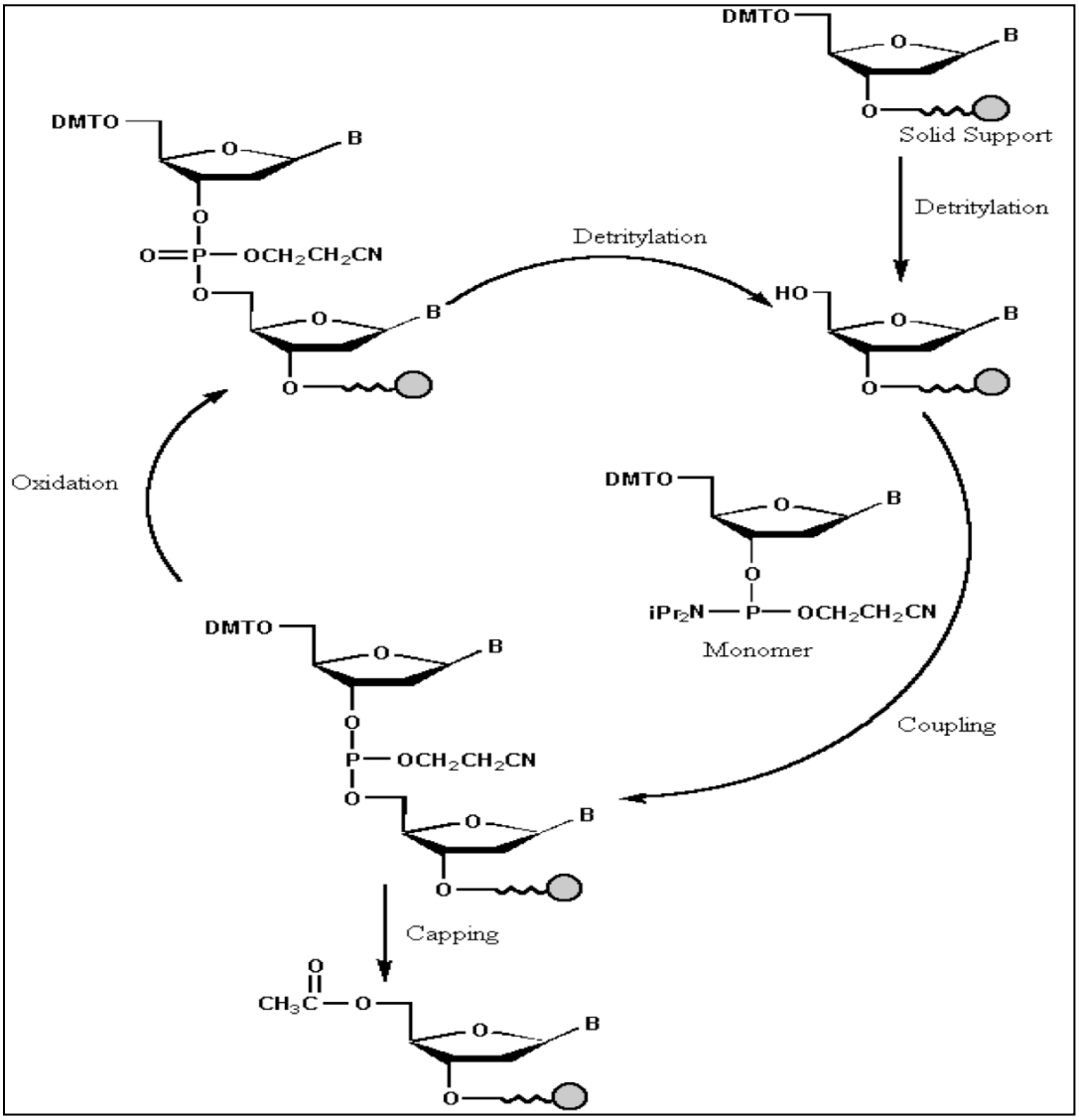

Figure 3-4 A phosphoramidite DNA synthesis cycle.

Finally, the internucleotide linkage is converted from the phosphite to the more stable phosphotriester in the oxidation step. Iodine is used as the oxidizing agent and water as the oxygen donor. This reaction is completed in less than 30 seconds.

After oxidation, cycle restarts from deblocking step for the next nucleotide.

In our laboratory, we have developed a new approach providing a significant improvement over the conventional oligonucleotide synthesis using phosphoramidite chemistry. Addressable site-specificity for the sequence desired combined with coupling yields reaching over 98% was achieved using photogenerated acids (Figure 3-5) [27].

The selective synthesis is accomplished by the utilization of photogenerated acid in the deprotection step. A predetermined light pattern is projected onto the substrate surface to selectively activate the photo-acid precursor (PGA-P), to generate photogenerated acid (PGA) and cleave the DMT protected acid-labile group from the nucleotides on the growing chain on the surface. The terminal 5' hydroxyl groups are now free to react with incoming monomers. At the dark regions, no acid is produced and, therefore, the acid labile protecting groups of the nucleotides remain intact. The substrate surface is then washed, and the monomer is introduced, which adds only to the deprotected molecules under conventional coupling reaction conditions.

The substrate that has the growing sequence is then supplied with consecutive batches of reagents to propagate the chain till the desired lengths and sequences are formed at the selected surfaces, as previously described.

iii. Deprotection

Phosphoramidite chemistry for oligonucleotide synthesis utilizes nucleotides (dA, dC and dG) with extra groups for protection. The exocyclic amines of 2'-deoxyadenosine (dA), 2'-deoxycytidine (dC) and 2' deoxyguanosine (dG) have to be protected during the synthesis process to prevent any side reactions involving these sites. The dA and dC monomers are protected by a benzoyl group at the N6 and N4 positions, respectively, and the dG is protected at the N2 position by an isobutyryl group; whereas dT does not require any extra protection since it

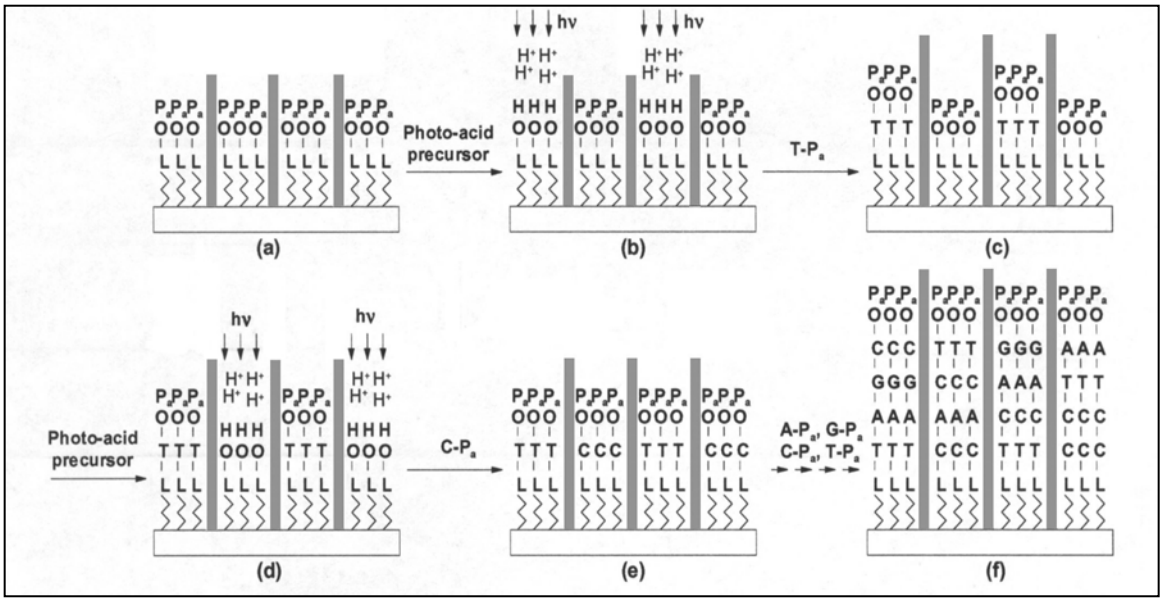

Figure 3-5 Parallel synthesis using acid-labile protecting groups. The DNA chain is deprotected in a spatially controlled manner using photogenerated acid (PGA) (b and d), followed by coupling and oxidation reactions (c and e). This cycle is repeated until the desired lengths and sequences are obtained (f).

does not include any reactive sites that will lead to a side reaction. These groups are removed after synthesis of the oligonucleotide is complete, during the deprotection step.

The protecting groups need to be removed before any hybridization experiment for the best interaction of the oligonucleotide strands on the surface and the oligonucleotide strands in solution. The deprotection is done by treating the oligonucleotides attached to the surface with ethylenediamine – ethanol (50% v/v) solution. If the oligonucleotides are to be removed with ammonium hydroxide, no extra step of deprotection is necessary. Ammonium hydroxide also deprotects the phophorus by ß-elimination of the cyanoethyl group.

3.2.1.4 Probe and Target Design

The length of the probe and target is determined to be 25 nucleotides. Their sequences are complementary to each other.

The sequence design criteria are selected based on the experimental approaches used by Owczarzy *et al.* [28] and SantaLucia, Jr *et al.* [7]:

1. The sequences are to be non-self-complementary, which is valid for both the probe and target sequences.
2. The GC mole fractions of the sequences are to be between 0.2 and 0.8.
3. No hairpins are present in both the target and probe sequences.
4. The target-target dimer formation in solution, and probe-probe dimer formation on the surface are to be negligible compared with the perfect match formation on the surface at the hybridization conditions.
5. There are no long regions of GC and AT base pairs, no more than 2 triplet stretches, 2 doublet stretches and 3 single stretches to reduce any non-two-state melting behavior.
6. The calculated free energies and the melting temperatures are based on in-solution Nearest-Neighbor parameters [6]. The free energies are to be as minimum as possible to create a stable structure at the hybridization temperature and salt concentration, keeping in mind that the presence of the

surface creates a depression in the melting temperature and the free energies of the duplexes, and the magnitude of this depression is unknown.

The probe designed using this criteria is:

5’ – CGCGAGCACTGGACCGGTGTTGGGT – 3’

and the target is:

5’ – ACCCAACACCGGTCCAGTGCTCGCG – 3’

The free flowing target in solution is labeled at 3’ end with Cy5 fluorescence dye (excitation wavelength: 635 nm; emission wavelength range: 650 nm - 700 nm [31]) for detection purposes. The destability imposed with the presence of this dye moiety is assumed to be negligible for sequence design purposes [29]. The labeled target was purchased from IDT Technologies Inc (Iowa, USA) in PAGE purified form. The ozone susceptibility of Cy5 leading to degradation problems observed in hybridization experiments [35] was minimized within the closed system with minimum exposure to ozone.

The perfect match probes are synthesized on the microfluidic chips. These chips comprise of 7 channels continuously connected. In each channel, a set of 1,000 sites is available for synthesis. These 1,000 sites are designed to have perfect match probes, empty spots for background analysis and synthesis controls for intra-normalization. In each channel, the 1,000 spot design is randomly distributed to account for any possible concerns during synthesis and hybridization. Also for the same purpose, first and the last channels are left empty.

Synthesis controls are designed to monitor the unavoidable discrepancies in the system, and the presence of any synthesis and hybridization defects. An intra-normalization step is put in the analysis to screen and take care of these concerns. The synthesis control probes designed for this purpose includes a core 15mer sequence. The corresponding control target is a complementary 15mer, labeled with Cy3 (excitation wavelength: 532 nm; emission wavelength range: 550 nm – 600 nm [31]) on its 3’ end to prevent any interference problems with the main target present in the system. It is designed to have negligible duplex formation with the main probe and target, and self-self duplex formations at the

hybridization conditions. In addition, all different sequential combinations of 1 – 4mers, and random combinations of 5 – 10mers are added at the 3' end of the 15mer core sequence. This creates synthesis control probes of lengths 15-25 nt on the surface, and assists in the analysis of any problems that may occur during the synthesis at different lengths. This designed target control sequence is:

5' – CTCCATACTAGTCAT -3'

This labeled target was purchased from IDT Technologies Inc (Iowa, USA) in PAGE purified form.

3.2.2 Experimental Design

It is important to investigate various experimental variables on the hybridization process to understand their respective influences in the designed set-up. The variables that were examined in this thesis are: target concentration, spacer length and probe density.

The investigation of these variables relies upon the reproduction of melting curves on the surface and extraction of melting temperatures from these graphs, following the examples in in-solution studies [7, 30]. To be able to create melting curves on the surface requires acquiring signal intensity data over a determined temperature range; a heating rate; and time required to reach equilibrium at each temperature step.

The temperature range of 23°C to 85°C was determined based on the restrictions of the experimental set-up. In other words, with the existing experimental system and the cooling capacity, the lowest achievable temperature was 23°C. Therefore, this temperature was set to be the priming (washing with hybridization buffer to establish electrolyte saturation before hybridization) and initial hybridization temperature for all of the experiments. On the other hand, the highest temperature of the experiment was determined from the observed signal intensities of the probe-target duplexes on the surface, and their relative comparison with respect to the background signal. At 85°C, the signal intensities obtained from the spots were at the background level for all of the experiments,

therefore, making it the temperature of choice for the upper end of the temperature range.

The next parameter in the design of the melting curves is the heating rate of the chip. It is a significant parameter because it can contribute to the under-estimation of the reported melting temperature [31]. A lower heating rate is going to result in detection at non-equilibrium conditions at each temperature step, leading to respective shifts in the melting curve. Therefore, in our experiments, keeping the importance of equilibrium in mind [32], the hybridization process at the initial temperature was allowed to reach equilibrium with the recirculating target solution. Then, the temperature was increased one degree, and the process was observed for the time to reach the new equilibrium state. This time period was used as the equilibrium time at temperatures below 65°C, at which the equilibrium was re-observed for the time period and this time period was used all throughout the rest of the experiment. Based on these experimental approaches, the heating rates below 65°C were 3-5°C/h, and above 65°C, they were 5-10°C/h.

Fluorescence signal intensities of a perfect-match duplex formed on the surface with respect to three different temperatures (25°C, 40°C, 55°C), and the resulting melting curve on the surface using this experimental approach are presented in Figure 3-6(a) and (b). The median signal intensities on the surface are captured by creating circular features with a diameter of 35 μm using the Axon GenePixPro software (Molecular Devices Inc, California, USA), and the acquired median intensity values are transferred to Excel (Microsoft Inc, Washington, USA) for further analysis.

One of the main parameters in image acquiring is the value of the photomultiplier tube (PMT) voltage. It determines to which extent the photons sent to the photocathode while scanning the image is going to be proportionally energized and increased in number when they hit the anode [33]. It is necessary to know which value to use; because it determines not only the dynamic range for the signals captured during the experiment, but also the noise level of the measurement, which can exceed the signal intensity at high PMT voltage values.

(a)

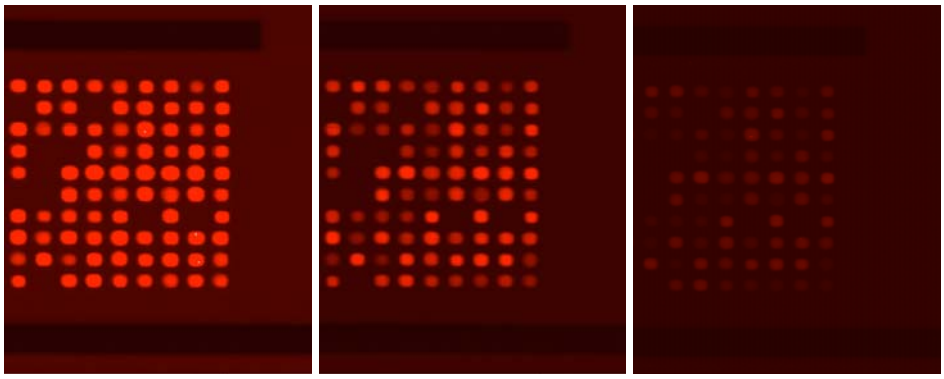

(b)

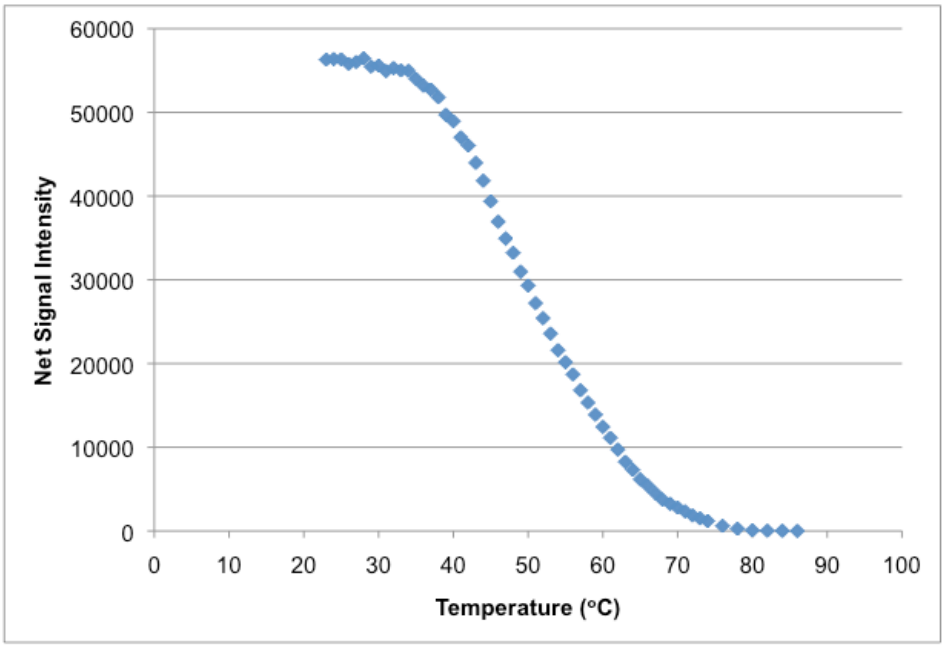

Figure 3-6 (a) Observed changes in the signal intensities on the surface at temperatures of 25°C, 40°C and 55°C at constant PMT voltage, brightness and contrast settings. (b) A melting curve of a perfect match duplex reproduced from the net signal intensities of the duplex at increasing temperatures.

This value was determined at the beginning of each experiment as the value resulting in intensities very close to saturation at the initial hybridization temperature. This value was used all throughout the experiment for consistency.

3.3 Data Analysis and Quality Assessment

3.3.1 Synthesis Quality Assessment

The quality of the synthesized chip needs to be verified to be able to obtain reliable, reproducible data that is representative of the reaction on the surface. Therefore, all of the experiments need to pass these criteria to be used in further analysis.

The first step in the quality assessment of synthesis is looking at the size of the spots at the end of the hybridization at the initial hybridization temperature. It was previously established in studies in our laboratory that a spot size of 50 μm diameter indicated a good quality in synthesis. Not only the spot size but also the signal distribution in the spots is important. The distribution in the spots is expected to be uniform with a flat top when a cross section on the spot is analyzed (in Figure 3-7(a), each pixel corresponds to 5 μm). Secondly, one can also determine the quality of the signal by looking at the signal to noise ratio. Signal is the median intensity measured on the perfect match probes, while the noise is the median intensity obtained at the empty spots. It is an important value because it shows how well one can resolve the true signal from the noise in the system. Higher signal to noise ratios are preferable for the least interference from the background in the experiments.

The final part of the quality control process is carried out after the experiment is finished. It is based on the analysis of the synthesis control signals obtained at the initial hybridization temperature. The signal intensities of the control probes in each channel were analyzed separately with respect to their lengths from 15 nt to 25 nt. All of the distributions are tabulated together, and the ratios are taken with respect to a given channel at each length. The averages of these ratios are taken, and finally, a normalization process is performed based

(a)

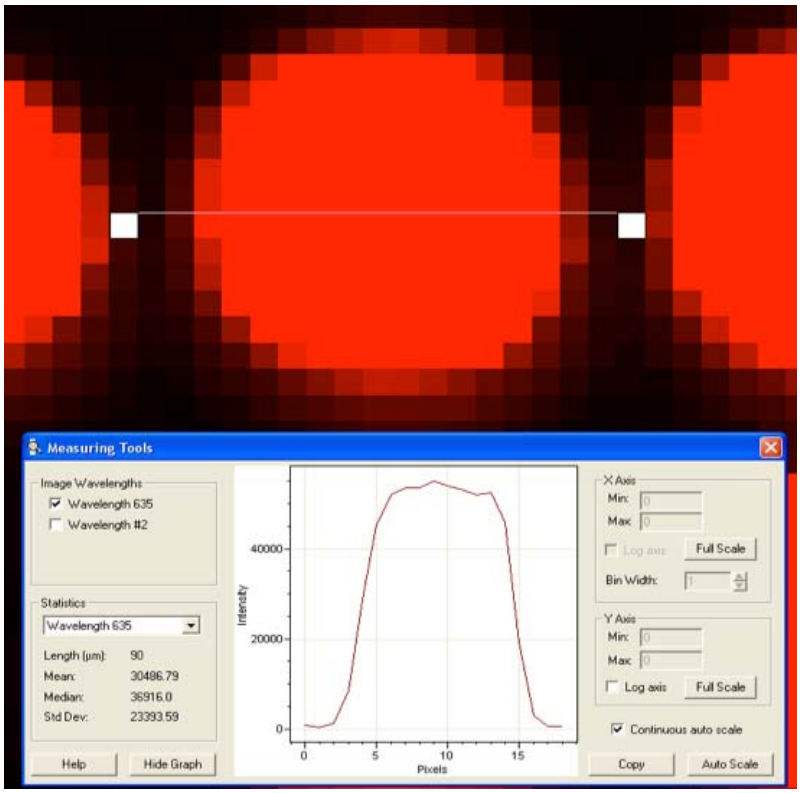

(b)

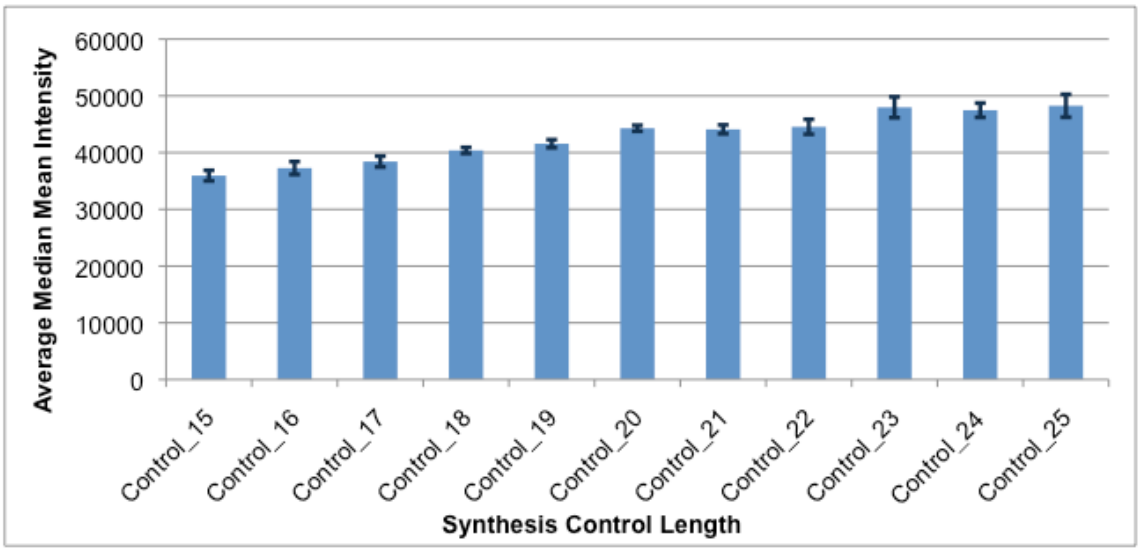

Figure 3-7 (a) The signal distribution within a cross-section of a 50 µm spot with Cy3 labeled targets hybridized with the probes on the surface. (b) The overall signal intensity change on the chip with respect to the length of the Cy3 labeled synthesis controls on the surface.

on the highest of the averaged ratios. Figure 3-7(b) shows an overall signal intensity distribution of synthesis controls with respect to length. The expected observation is that the signal intensity would increase as the probe length increases; in other words, as the probe is further away from the surface. Normalization of the main probe signals (net values) in each channel is performed using the tabulated averaged signal ratios of the synthesis controls. This allows taking into account any deficits that may occur due to synthesis or hybridization in different channels.

3.3.2 Melting Curve Analysis

Initial step in the analysis of the melting curves includes the normalization of the signal intensities in red channel (main probe signals) at all temperatures via the analysis of the synthesis controls in the green channel, as previously described.

The normalized signals are further analyzed in Matlab (The Mathworks Inc, Massachusetts, USA) for faster processing. The analysis steps in Matlab are: background correction of the main probes, and temperature calibration of these fluorescence signals; smoothing and fitting of the experimental melting curve of each probe; extracting the melting temperatures and analyzing them for outliers and standard deviations.

3.3.2.1 Background Correction and Temperature Calibration

Background corrections to the probe signals are required to account for the effects due to autofluorescence of the surface and non-specific binding of labeled targets to the surface. In this case, the background signals are extracted from the signals obtained at the sites which do not have any probe synthesis on them, also called empty spots. The average of all the empty spot intensities in red channel is taken at each temperature, and subtracted from the signal intensities of the probes in the red channel at the same temperature to obtain net signal intensities for the probes.

Another use for the empty spot averages at each temperature is the production of a curve that will represent and approximate the temperature

dependence of fluorescence for the chip under examination. It has been theoretically shown that the intensity of fluorescence is dependent on many factors, including temperature and concentration [34]. The expected trend for the concentration increase would be an increase in the fluorescence intensity, and for the temperature increases, the fluorescence intensity would decrease. The influence of the change in the concentration of the targets in solution and the temperature of the reaction on fluorescence can be simultaneously observed on this reproduced curve (Figure 3-8(a)). The effect of the increasing concentration of the targets as the melting progresses does not seem to be dominant when compared with the effect of increasing temperature.

To prove the usability of the empty spot signal vs. temperature curve in the calibration, an equation that relates the effect of PMT voltage, temperature and concentration to the fluorescence in red channel was reproduced experimentally (Appendix). The designed set of experiments to derive this calibration equation included the free flowing Cy5 labeled target in the microfluidic chip in the absence of any synthesis on the surface. The concentrations used were 0.05 nM, 0.5 nM and 1 nM; the PMT voltages used ranged from 350-1,000 and the temperatures used were 23°C, 50°C and 80°C. The inter-related dependence of fluorescence on PMT voltages, temperature and concentration were expressed as a collective term in the regression equation with their individual dependencies stated using exponential terms [34]. Multiple non-linear regression was carried out using SPSS software (SPSS Inc, Illinois, USA), and the constants were initialized to get the highest R-squared value for the fit at the end of the 999 iterations set by the software.

The reproduced equation is:

$$\text{Fluorescence} = 0.008 * \exp(2426.639 * 1/T) * \exp(0.007 * \text{PMT}) * \text{Conc} - 1.064$$

Equation 3-4

where T is the temperature, PMT is the PMT voltage used and Conc is the concentration of the free target in solution in units of nanomolar. The R-squared fit of this equation to the experimental data is 0.968. Figure 3-8(b) shows the comparison of the experimental background intensity change in Figure 3-8(a)

(a)

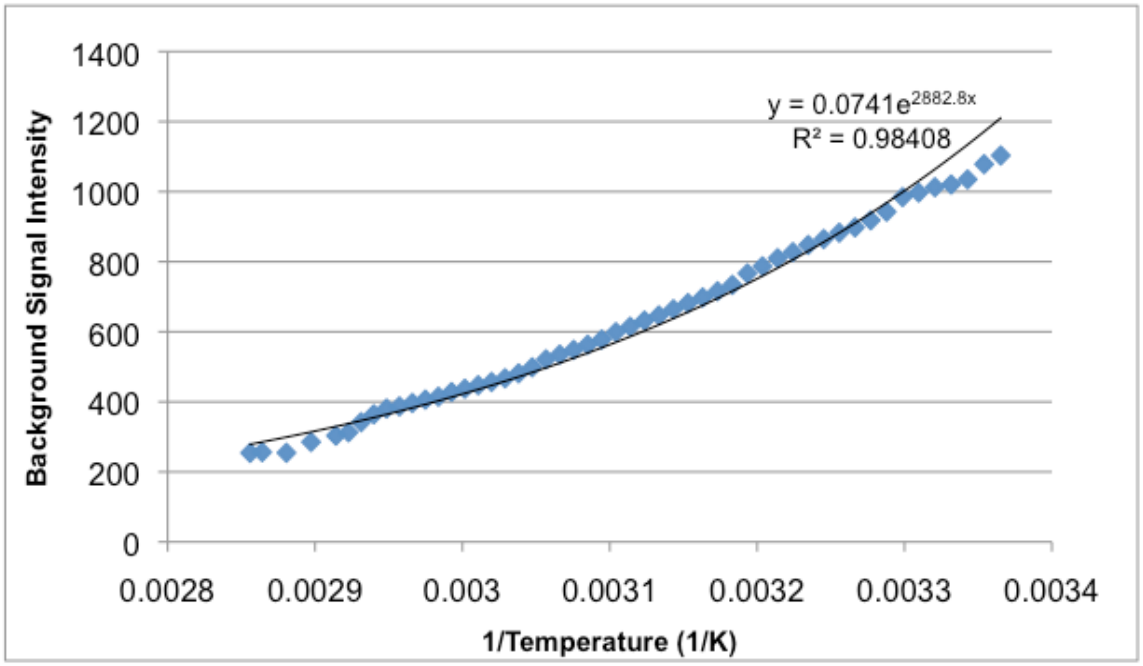

(b)

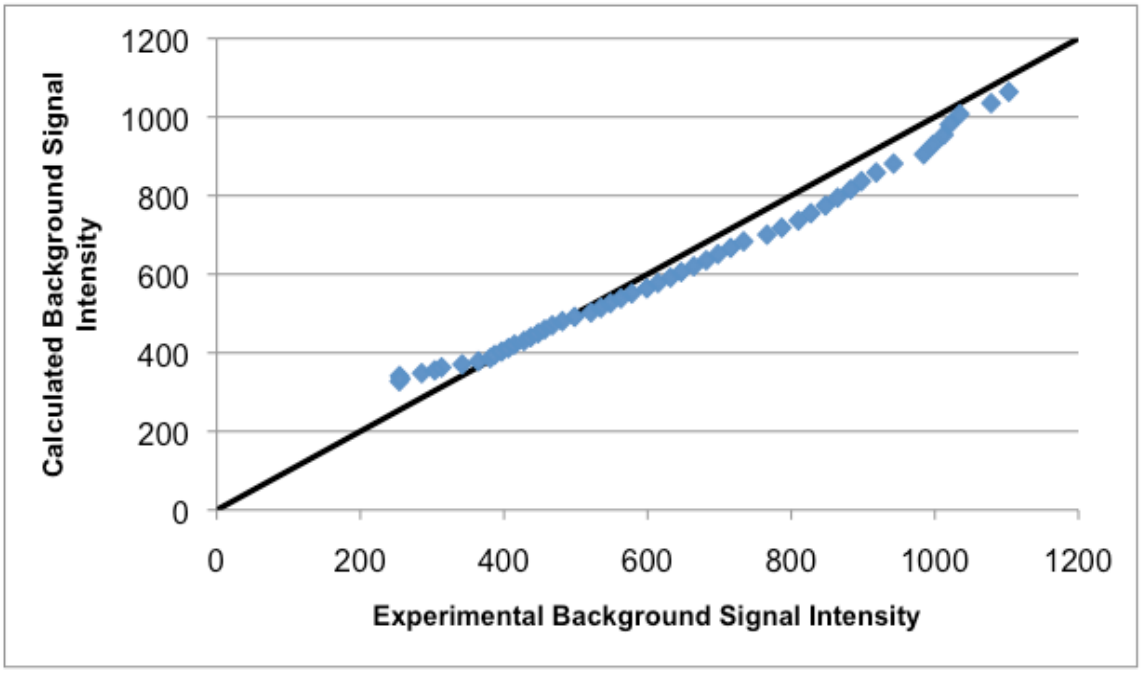

Figure 3-8 (a) An example of the change in the fluorescence signal of the empty spots with respect to temperature. (b) Comparison of the experimental empty spot intensity change with the signal intensities derived from the Equation 3-4 at different temperatures.

with the calculated background intensity change from the calibration equation in Equation 3-4, using the experimental PMT voltage, and assuming a constant target concentration, the concentration obtained at the end of the initial hybridization. This figure shows the negligible effect of the increasing target concentration when the targets were released into the solution as the melting continues at increasing temperatures; therefore, demonstrating that the change in the fluorescence with respect to temperature can be used to show the influence of temperature on the fluorescence and therefore in the calibration.

3.3.2.2 Smoothing and Fitting of the Melting Curve

Due to the presence of unavoidable experimental errors, a smoothing procedure needs to be applied to the original data [30]. For this purpose, a 2nd degree Savitzky-Golay method is used. This method utilizes a polynomial function fit to the signal in a moving window on the curve [35]. The main advantage of this method is that it tends to preserve features of distribution in the data, which are usually flattened by other adjacent averaging approaches [35]. To preserve the relative curvatures at the low temperature and high temperature regions of the melting curve as well as the inflection point in the mid region, this method seems to be a good choice for this purpose. A similar approach is used in the smoothing of the melting curves created in in-solution experiments [36].

Next step in the analysis involves the fitting of the temperature calibrated and smoothed melting curves directly with a function. In this case, the typical S-shape of the melting curve seems to be represented nicely with a Stephen-Boltzmann curve:

$$y = a_2 + \frac{(a_1 - a_2)}{1 + \exp\left(\frac{(x - x_0)}{dx}\right)} \qquad \text{Equation 3-5}$$

where a_1 is the highest signal intensity, a_2 is the lowest signal intensity, x_0 is the estimated inflection point, and dx is the width of the curve.

This curve carries parameters that reflect the individual characteristics of the melting process: the highest and lowest signal intensities help us investigate

the dynamic range we operate in, the inflection point shows the melting temperature, and dx represents the extent of broadening due to the effects of the presence of the surface.

The melting temperatures recorded from the inflection points of each of these curves are tabulated along with the R-squared fit of the equation to the experimental data for each probe analyzed. Next, R-squared values lower than 0.95 are considered bad fits and the remaining melting temperature values are analyzed for outliers within each probe. The criterion for outliers come from the statistical approach of average +/- 1.5 * standard deviation. At the end of the analysis, the average and standard deviations of the melting temperatures are reported.

3.3.3 Performance of the Analysis Method

The performance of this method is tested on error-introduced melting curves with parameters representing different signal to noise ratios, which can be considered as one of the sensitivity and quality indicators of the system. The original curve parameters are set at: a_1 = 55,000, a_2 = 150, x_0 = 57, dx = 5, and errors, which are randomly introduced on this curve to test the performance of the method, fall within five percent of ten percent of the signal intensity at the temperature point in question. Among these parameters, x_0 was modified to simulate the effect of the change in the signal to noise ratio of perfect match intensity (signal) to the background intensity (noise) (Figure 3-9). At each signal to noise ratio modification, 100 melting curves with random errors were reproduced. The quantitative effect of changing x_0 on the signal to noise ratio, as extracted from Figure 3-9 at the initial temperature of 23ºC as signal, and at the final temperature of 85ºC as background, can be observed in Table 3-2.

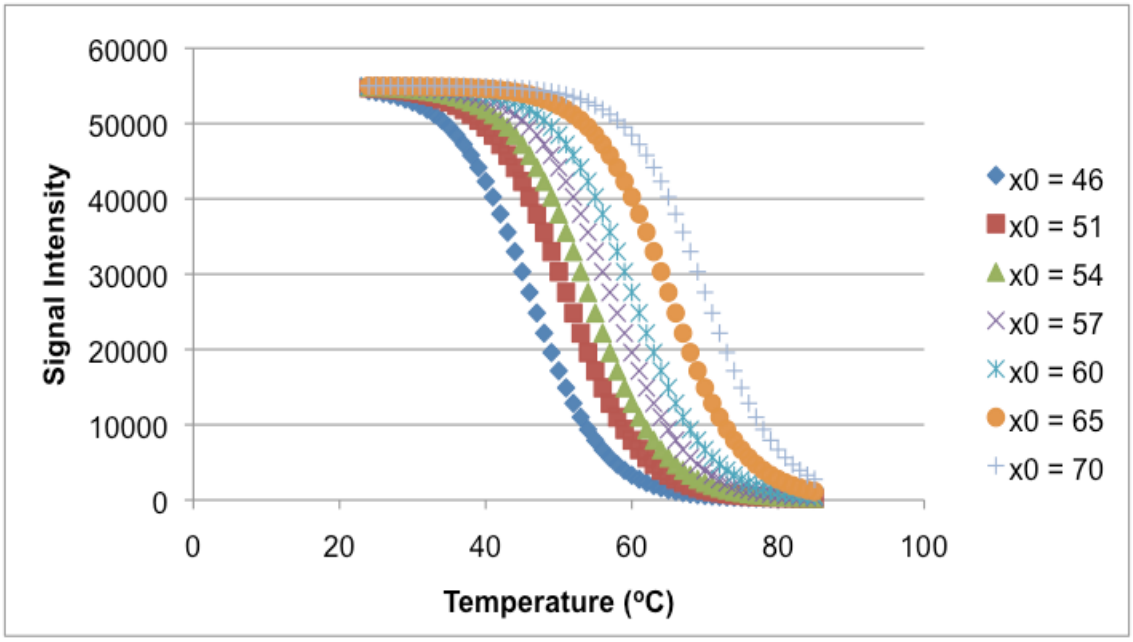

Figure 3-9 Addressing the method performance with simulated data. The originally created curve has the following parameters: a_1 = 55,000, a_2 = 150, x_0 = 57, dx = 5. Various signal to noise ratio values are obtained via assigning the parameter x_0 different values ranging from 46 to 70.

Table 3-2 Signal to noise ratio variation at different simulated x_0 parameters.

	x_0=46	x_0=51	x_0=54	x_0=57	x_0=60	x_0=65	x_0=70
Signal (at 23°C)	52399	54013	54454	54699	54834	54939	54978
Noise (at 85°C)	156	165	177	200	241	397	815
Signal to Noise Ratio	336	326	306	273	227	138	66

The melting temperatures calculated at each x_0 using the method were statistically analyzed, and their averages and standard deviations were calculated. Table 3-3 shows these values along with their correlation coefficient ranges.

Table 3-3 Average, standard deviation and regression coefficients of the melting temperatures calculated from the simulated data using the analysis method.

	x_0=46	x_0=51	x_0=54	x_0=57	x_0=60	x_0=65	x_0=70
Calculated Average Melting Temperature (°C)	46.02	50.99	54.01	57.02	60.00	64.99	70.06
Standard Deviation (°C)	0.23	0.24	0.21	0.23	0.23	0.29	0.36
Regression Coefficients	0.9939-1.000	0.9951-1.000	0.9943-1.000	0.9941-1.000	0.9949-1.000	0.9931-1.000	0.9897-1.000

In Table 3-3, the average of the melting temperatures calculated and their standard deviations and regression coefficients indicate that the analysis method proves to be a robust method for any kind of background noise that can interfere with the measured signal intensity.

3.4 Conclusions

Melting curves represent the change in the signal intensity of the duplexes as they melt, reaching equilibrium at each increasing temperature. Its generation is a necessary step to obtain melting temperature values of these duplexes formed on the surface. In this chapter, a reliable and automated experimental set-up, and a robust analysis method have been developed to create and analyze these melting curves. This experimental set-up integrates microfabrication and microfluidic technology, light-directed *in-situ* oligonucleotide synthesis and a real-time capturing system. The probe and the labeled target sequences are designed with respect to specific thermodynamical parameters set forth for in-solution experiments. The layout for the probe synthesis on the chip surface includes the perfect match sequences, empty spots as well as synthesis controls in each channel. Synthesis and quality controls are in place to monitor and correct the possible synthesis and hybridization discrepancies on the chip. Experimental analysis of the created melting curves includes background subtraction to get rid of interference from any possible autofluorescence of the surface, or dye adhesion on the surface; temperature calibration to take the temperature dependency of the fluorescence into account; smoothing to correct the possible experimental errors; fitting to extract the melting temperature along with the regression coefficient; and finally, the statistical analysis of the melting temperatures of the perfect match probes to determine their averages and standard deviations. This analysis approach has shown great robustness against randomly generated and error introduced melting curves with different signal to noise ratios.

3.5 Appendix

The calibrations with Cy5 labeled target was done at different temperatures (20°C, 50°C, 80°C), different concentrations (0.05 nM, 0.5 nM, 1 nM) and PMT voltages (300 PMT to 1000 PMT). Figures 3-10, 3-11 and 3-12 show the changes in the average median signal intensities at different PMT voltages and temperatures at 0.05 nM, 0.5 nM and 1 nM, respectively.

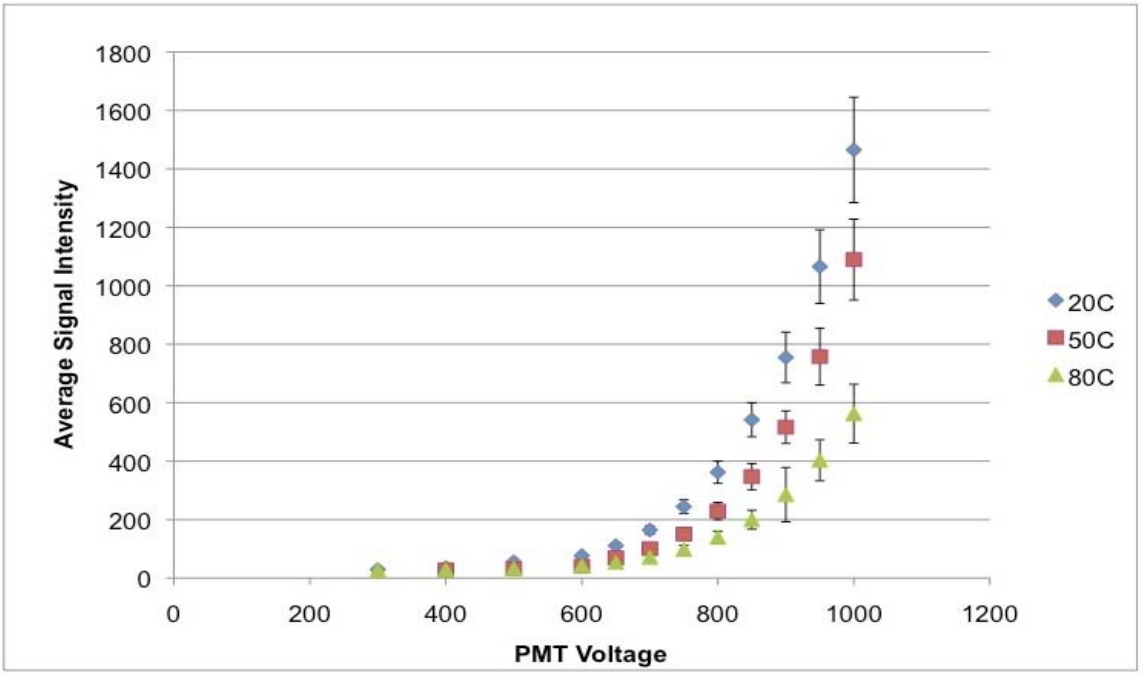

Figure 3-10 The effect of PMT voltage and temperature on the average signal intensity at a target solution concentration of 0.05 nM.

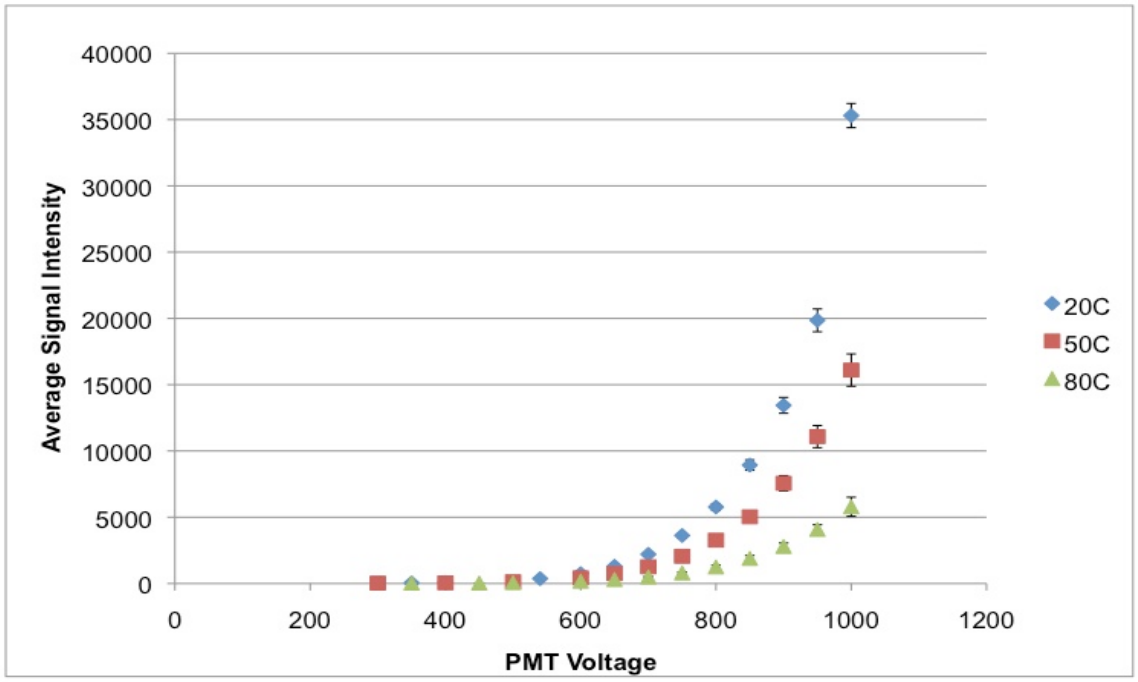

Figure 3-11 The effect of PMT voltage and temperature on the average signal intensity at a target solution concentration of 0.5 nM.

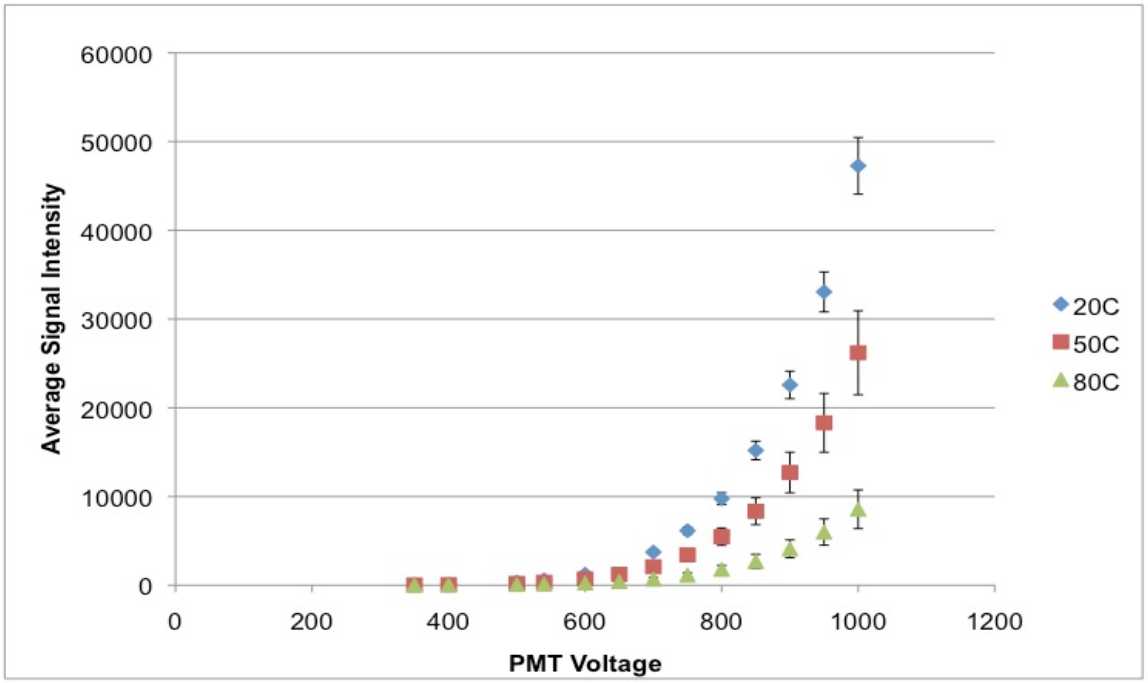

Figure 3-12 The effect of PMT voltage and temperature on the average signal intensity at a target solution concentration of 1 nM.

3.6 Bibliography

1. Absi TS, Sundt TMr, Tung WS, Moon M, Lee JK, Damiano RRJ, Thompson RW, *Altered patterns of gene expression distinguishing ascending aortic aneurysms from abdominal aortic aneurysms: complementary DNA expression profiling in the molecular characterization of aortic disease*. J Thorac Cardiovasc Surg, 2003. 126: 344-57; discission 357.
2. Anguiano A, Nevins JR, Potti A, *Toward the individualization of lung cancer therapy*. Cancer, 2008. 113: 1760-1767.
3. Southern E, Mir K, Shchepinov M, *Molecular interactions on microarrays*. Nat Genet, 1999. 21: 5-9.
4. Owczarzy R, Vallone PM, Gallo FJ, Paner TM, Lane MJ, Benight AS, *Predicting sequence-dependent melting stability of short duplex DNA oligomers*. Biopolymers, 1997. 44: 217-239.
5. Record MTJ, Mazur SJ, Melancon P, Roe JH, Shaner SL, Unger L, *Double helical DNA: conformations, physical properties, and interactions with ligands*. Annu Rev Biochem, 1981. 50: 997-1024.
6. SantaLucia JJ, *A unified view of polymer, dumbbell, and oligonucleotide DNA nearest-neighbor thermodynamics*. Proc Natl Acad Sci U S A, 1998. 95: 1460-1465.
7. SantaLucia JJ, Allawi HT, Seneviratne PA, *Improved nearest-neighbor parameters for predicting DNA duplex stability*. Biochemistry, 1996. 35: 3555-3562.
8. Rouillard JM, Zuker M, Gulari E, *OligoArray 2.0: design of oligonucleotide probes for DNA microarrays using a thermodynamic approach*. Nucleic Acids Res, 2003. 31: 3057-3062.
9. Wick LM, Rouillard JM, Whittam TS, Gulari E, Tiedje JM, Hashsham SA, *On-chip non-equilibrium dissociation curves and dissociation rate constants as methods to assess specificity of oligonucleotide probes*. Nucleic Acids Res, 2006. 34: e26.

10. Gadgil C, Yeckel A, Derby JJ, Hu WS, *A diffusion-reaction model for DNA microarray assays*. J Biotechnol, 2004. 114: 31-45.

11. Hagan MF, Chakraborty AK, *Hybridization dynamics of surface immobilized DNA*. J Chem Phys, 2004. 120: 4958-4968.

12. Sorokin NV, Chechetkin VR, Chechetkin MA, Vasiliskov VA, Turygin AY, Mirzabekov AD, *Kinetics of hybridization on the oligonucleotide microchips with gel pads*. J Biomol Struct Dyn, 2003. 21: 279-288.

13. Held GA, Grinstein G, Tu Y, *Modeling of DNA microarray data by using physical properties of hybridization*. Proc Natl Acad Sci U S A, 2003. 100: 7575-7580.

14. Skvortsov D, Abdueva D, Curtis C, Schaub B, Tavare S, *Explaining differences in saturation levels for Affymetrix GeneChip arrays*. Nucleic Acids Res, 2007. 35: 4154-4163.

15. Pease AC, Solas D, Sullivan EJ, Cronin MT, Holmes CP, Fodor SP, *Light-generated oligonucleotide arrays for rapid DNA sequence analysis*. Proc Natl Acad Sci U S A, 1994. 91: 5022-5026.

16. Wang Y, Li Y, Liu S, Shen W, Jiang B, Xu X, Xie Y, *Study on the dynamic behavior of a DNA microarray*. J Nanosci Nanotechnol, 2005. 5: 1249-1255.

17. Suzuki S, Ono N, Furusawa C, Kashiwagi A, Yomo T, *Experimental optimization of probe length to increase the sequence specificity of high-density oligonucleotide microarrays*. BMC Genomics, 2007. 8: 373.

18. Yuen PK, Li G, Bao Y, Muller UR, *Microfluidic devices for fluidic circulation and mixing improve hybridization signal intensity on DNA arrays*. Lab Chip, 2003. 3: 46-50.

19. Heule M, Manz A, *Sequential DNA hybridisation assays by fast micromixing*. Lab Chip, 2004. 4: 506-511.

20. Peytavi R, Raymond FR, Gagne D, Picard FJ, Jia G, Zoval J, Madou M, Boissinot K, Boissinot M, Bissonnette L, Ouellette M, Bergeron MG,

Microfluidic device for rapid (<15 min) automated microarray hybridization. Clin Chem, 2005. 51: 1836-1844.

21. Li ESY, Liu W-T, *DNA microarray technology in microbial ecology studies-principle, applications and current limitations*. Microbes and Environments, 2003. 18: 175-187.
22. Wei H, Kuan PF, Tian S, Yang C, Nie J, Sengupta S, Ruotti V, Jonsdottir GA, Keles S, Thomson JA, Stewart R, *A study of the relationships between oligonucleotide properties and hybridization signal intensities from NimbleGen microarray datasets*. Nucleic Acids Res, 2008. 36: 2926-2938.
23. Gulari, Erdogan Professor
24. Kramer M, Carl Zeiss, *Evanescent waves in microscopy*. Photonik, 2004. 2: 42-44.
25. http://en.wikipedia.org/wiki/List_of_refractive_indices
26. Caruthers MH, Barone AD, Beaucage SL, Dodds DR, Fisher EF, McBride LJ, Matteucci M, Stabinsky Z, Tang JY, *Chemical synthesis of deoxyoligonucleotides by the phosphoramidite method*. Methods Enzymol, 1987. 154: 287-313.
27. Gao X, Gulari E, Zhou X, *In situ synthesis of oligonucleotide microarrays*. Biopolymers, 2004. 73: 579-596.
28. Owczarzy R, You Y, Moreira BG, Manthey JA, Huang L, Behlke MA, Walder JA, *Effects of sodium ions on DNA duplex oligomers: improved predictions of melting temperatures*. Biochemistry, 2004. 43: 3537-3554.
29. Moreira BG, You Y, Behlke MA, Owczarzy R, *Effects of fluorescent dyes, quenchers, and dangling ends on DNA duplex stability*. Biochem Biophys Res Commun, 2005. 327: 473-484.
30. Owczarzy R, *Melting temperatures of nucleic acids: discrepancies in analysis*. Biophys Chem, 2005. 117: 207-215.

31. Mergny JL, Lacroix L, *Analysis of thermal melting curves*. Oligonucleotides, 2003. 13: 515-537.

32. Bhanot G, Louzoun Y, Zhu J, DeLisi C, *The importance of thermodynamic equilibrium for high throughput gene expression arrays*. Biophys J, 2003. 84: 124-135.

33. www.moleculardevices.com/

34. Yguerabide J MCF, *Theory of Lipid Bilayer Phase Transitions as Detected by Fluorescent Probes*. Journal of Membrane Biology, 1979. 45: 109-123.

35. Press WH, Teukolsky SA, Vetterling WT, Flannery BP, *Savitzky-Golay smoothing filters*. Computers in Physics, 1990. 4: 669–672.

36. www.meltwin.com

35. Yurov YB, Soloviev IV, Vorsanova SG, Marcais B, Roizes G, Lewis R, *High resolution multicolor fluorescence in situ hybridization using cyanine and fluorescein dyes: rapid chromosome identification by directly fluorescently labeled alphoid DNA probes*. Human Genetics, 1996. 97(3): 390-398.

CHAPTER IV

THE EFFECT OF INITIAL TARGET CONCENTRATION

4.1 Introduction

The design of probes on microarrays is currently based on DNA melting temperature predictions, which are made through the utilization of in-solution thermodynamic parameters and correlations [1, 2].

In solution, melting temperature is affected by ionic concentrations, denaturant concentrations, and lengths, sequences and concentrations of the strands involved [3]. An increase in the ionic concentration is expected to increase the melting temperature of the duplex due to less repulsion between more screened negative charges on the strands. A GC rich sequence would give a higher stability in the structure with its 3 hydrogen bonding capability. A longer strand would also be forming more hydrogen bonds with more available nucleotides, therefore increasing the melting temperature.

As the reaction takes place on a solid interface in microarrays, the presence of the surface imposes additional considerations in the design of the experiment: one of the strands is immobilized and highly-packed on a surface, which inherently carries an electrostatic charge. Therefore, the nature and characteristics of the surface gain importance in their individual contributions on duplex formation, and dependence of the melting temperature on its parameters [4-6].

Vainrub and Pettitt theoretically investigate the effect of surface electrostatics on binding thermodynamics and melting temperature of an 8mer duplex [7-9]. In this study, they examine how the salt concentration dependency

duplex [7-9]. In this study, they examine how the salt concentration dependency of the melting temperature is affected by the surface charge. They report that at positive surface charges and 1 M NaCl concentration, the duplex melting temperature is higher than in-solution value. As the salt concentration decreases to 0.01 M, on-surface melting temperature drops to a value much lower than in-solution. On the other hand, at negative surface charges and 1 M NaCl concentration, the melting temperature of the duplex on the surface is lower than in-solution prediction. Decreasing the salt concentration to 0.01 M causes a further decrease in the melting temperature on the surface. When the discrepancies between on-surface and in-solution melting temperatures are compared qualitatively at 0.01 M NaCl for the positively and negatively charged surfaces, it is observed that the effect of the ionic concentration on the melting temperature is pronounced less when the reaction takes place on a positively charged surface. These predictions are supported in an experimental study by Heaton *et al.* using surface plasmon resonance (SPR) spectroscopy [10].

In a study using the same approach, Vainrub *et al.* looks at the effect of probe density on the melting temperature electrostatically [7]. They conclude that as the target-probe layer repulsion increases with the coulomb blockage of hybridization at denser probe layers, melting temperature of the duplex on the surface would decrease. Similar observations were also seen with experiments, where increasing probe densities are accompanied with lower extents of hybridization [11, 12].

In a modeling study, Jayaraman *et al.* investigates the effect of target concentration and probe density on the melting temperature using Monte Carlo simulations [13]. It is observed that when a higher target concentration or probe density is used in the experiment (in other words, higher strand concentrations), the probability of the target binding to more than one probe also increases. This would lead to additional configurational entropy restraints on the duplexes formed, making the structure less stable, and lowering the melting temperature. A similar conclusion is reached in another modeling study by Binder [14], who looks at the effect of target concentration on the surface adsorption of the target to

oligonucleotide probes attached on the surface as a part of the investigation. This different approach models the affinity between the target strand in solution and the probe on the surface by taking into account the changes in the surface charge as more and more duplexes form on the surface. It is suggested that any condition increasing the surface charge would be inversely influencing the duplex formation on the surface, and an increase in target concentration is one of these conditions.

The trends seen in these studies are opposite to what is expected with in-solution melting temperatures. In solution, more strand concentration would lead to higher melting temperatures, because the temperature at which the half of the duplex is denaturated, is going to be higher when more strands are present in solution [3].

These interesting observations in modeling studies have drawn our attention to the examination of the target concentration as one of the factors affecting the duplex formation on the surface. A literature survey yields one study that experimentally looks at its effect on on-surface DNA melting temperature. In their work on the melting of a perfect match duplex on oligonucleotide array, Forman *et al.* concludes that target concentration does not seem to have an influence on DNA melting temperature on the surface [15].

In this chapter, we present an experimental study that examines the influence of surface on the melting temperature dependency on target concentration, and compare our findings with the modeling studies. The results obtained are also alternatively explained with the predictions made using the electrostatic and entropic blocking models developed in Chapter 2.

4.2 Materials and Methods

Following target and probe sequences are designed according to the criteria utilized by SantaLucia, Jr [16] and Owczarzy *et al* [17]:

Target: 5'- ACCCAACACCGGTCCAGTGCTCGCG- 3' -Cy5

Probe: 5'- CGCGAGCACTGGACCGGTGTTGGGT- 3'

The probe sequence has a GC content of 67% and a molecular weight of 7,755.1.

The probe sequence was synthesized on the surface from 3' to 5', and the corresponding PAGE purified target is labeled on 3' end with Cy5 fluorescent dye (Integrated DNA Technologies, Iowa, USA) for detection purposes. The volume of the hybridization solution was 1,000 μl. The target was initially hybridized with the probe on the surface at 23°C till the equilibrium was observed. Then, the melting of this duplex on the surface was monitored at each increasing temperature by using a fluorescence scanner (Axon 4000B, Molecular Devices, California, USA).

In this part of the study, the effect of target concentration on DNA melting temperature is examined in three separate experimental sets, each having a different probe concentration on the surface, with a constant probe density of $5*10^{12}$ molecules/cm^2. These experiments are summarized in Table 4-1.

Each experimental set was designed to have different number of probe spots on the surface, which gives the difference in probe concentrations with the same probe density on the surface.

There are seven channels in each of the microfluidic chips. First and the last channels were left empty to avoid any flow problems within the entrance and exit channels. The probes were synthesized in the remaining five channels, having 1,000 spots in each channel. This 1,000 spot set consists of perfect match probes, synthesis quality controls and empty spots. They were randomized in each channel for redundancy.

Table 4-1 Summary of the Experiments Performed to Address the Effect of Target and Probe Concentrations on the Duplex Formation on the Surface

Concentration of Target in Solution (nM)	Total Amount of Probe on Chip (pmoles on C.S.A[a])	Target to Total Probe Ratio (pmoles/pmoles)
EXPERIMENTAL SET 1:		
15	0.82	18.39 to 1
5	0.82	6.13 to 1
1.39	0.82	1.7 to 1
0.82	0.82	1 to 1
0.5	0.82	0.61 to 1
EXPERIMENTAL SET 2:		
1	0.59	1.7 to 1
0.59	0.59	1 to 1
0.36	0.59	0.61 to 1
EXPERIMENTAL SET 3:		
0.027	0.03	1 to 1
0.0165[b]	0.03	0.61 to 1

(a) C.S.A. = Chip Surface Area = 10^{18} Å^2
(b) Pre-hybridization at 50°C for 5 hours

Synthesis quality control probes have a different design from the main probe. There is a 15mer core probe sequence with which the Cy3 (Integrated DNA Technologies, Iowa, USA) labeled 15mer target hybridizes:

Target: 5’ – ATGACTAGTATGGAG – 3’ – Cy3

Probe: 5’ – CTCCATACTAGTCAT – 3’

Conserving this sequence, sequential combinations of different lengths varying between 1 – 10mers were added at the end of the 3’ of the probe sequence to monitor the synthesis at different steps. These quality control probes were also used in the normalization step in the chip to take into account possible discrepancies within synthesis and hybridization. There are 211 designed probe sequences included in each 1,000 spot set for quality analysis.

The number of empty spots in each channel varies based on the number of perfect matches. Empty spots were used in the background calculations.

All of the experiments in this chapter passed the quality assessment guidelines mentioned in Chapter 3.

The first set of experiments was carried out on a layout with 780 perfect match probes, 211 synthesis control probes and 9 empty spots in each channel. There are 3,900 probes in total on the chip. The target concentration was varied from 15 nM to 0.5 nM, which corresponds to a target to probe ratio range of 18.39:1 to 0.61:1.

The second set of experiments has 720 perfect match probes, 211 synthesis control probes and 69 empty spots in each channel, totaling 3,600 probes on the chip. The target concentration was varied from 1 nM to 0.36 nM, which corresponds to a target to probe ratio range of 1.7:1 to 0.61:1.

The third set of experiments was designed to look at the hybridization process at low probe and target concentrations. There are a total number of 165 perfect match probes on the chip, and the target to probe ratios of 1:1 and 0.61:1 were used.

4.3 Results and Discussion

Figure 4-1 shows the melting temperature trends observed on the surface in comparison with the predicted in solution melting temperatures (using Nearest-Neighbor method, [18]) for each experimental set with different total probe amounts on the surface.

4.3.1 The Effect of Target Concentration on the Melting Temperature on the Surface

There are three main observations one can deduct from the plots:

Firstly, all of the observed melting temperatures on the surface are much lower than in-solution melting temperatures predicted using Nearest-Neighbor method, confirming the conclusion that a lower stability is imposed on the DNA duplex by the surface [4, 5].

(a)

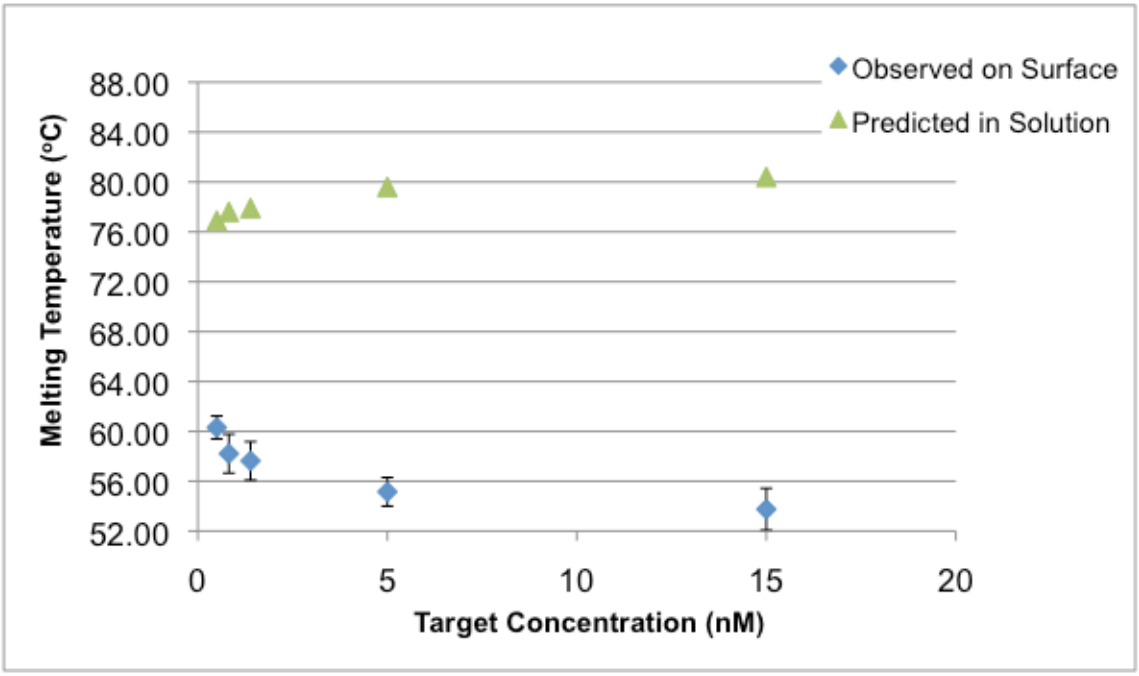
Observed on Surface
Predicted in Solution
Melting Temperature (°C)
88.00
84.00
80.00
76.00
72.00
68.00
64.00
60.00
56.00
52.00
0
5
10
15
20
Target Concentration (nM)

(b)

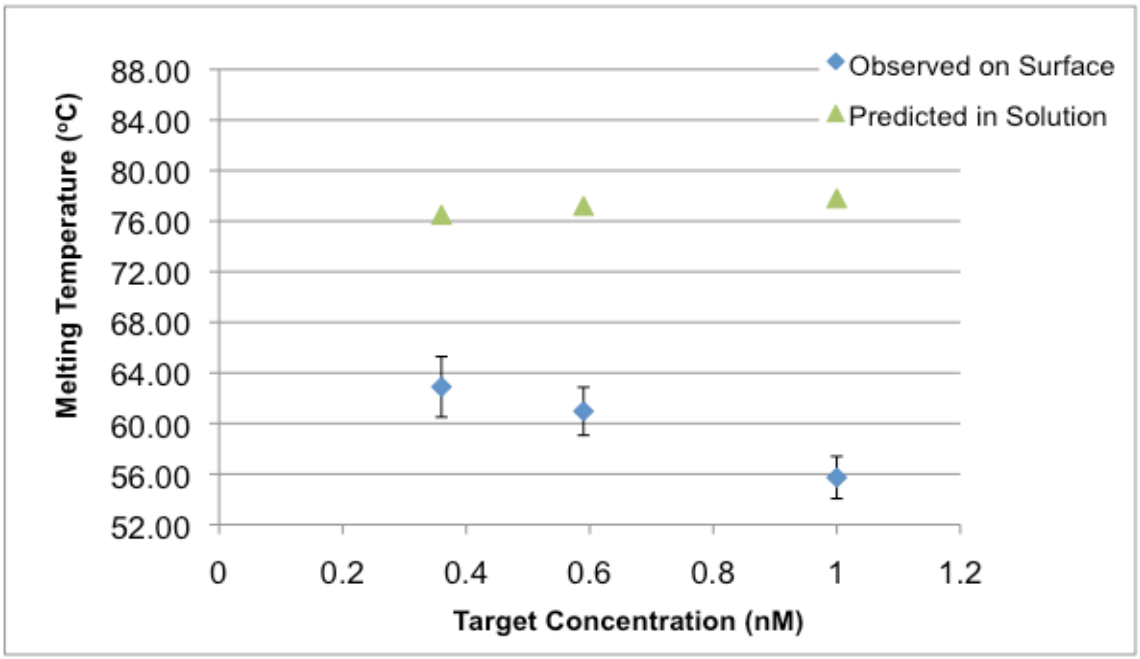
Observed on Surface
Predicted in Solution
Melting Temperature (°C)
88.00
84.00
80.00
76.00
72.00
68.00
64.00
60.00
56.00
52.00
0
0.2
0.4
0.6
0.8
1
1.2
Target Concentration (nM)

(c)

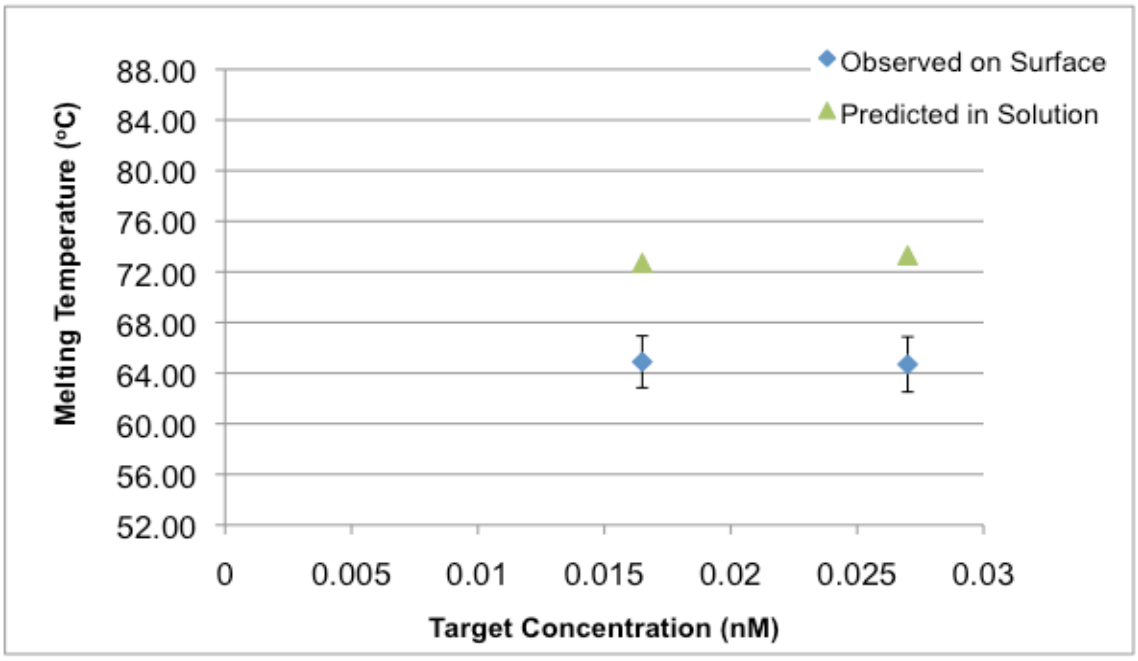

Figure 4-1 The melting temperature trends observed on the surface and predicted in solution (using Nearest Neighbor method) with respect to different target concentrations at perfect match probe amounts of (a) 0.82 pmoles (b) 0.59 pmoles and (c) 0.03 pmoles on 10^{18} $Å^2$ surface.

Secondly, the discrepancy between the predicted in-solution and observed on-surface melting temperatures seems to increase with increasing target concentration. This could be explained by increasing entropic and electrostatic blocking penalties with increasing hybridization efficiencies [14] as well as the higher probability of binding targets to more than one probe as the target concentration increases [13].

Finally, in all of the probe concentrations, an increase in the target concentration is accompanied with a decrease in the melting temperature on the surface. However, in solution, denaturation of the 50% of the duplexes will be observed at a later temperature when, initially, there are more strands present. Our observations on the surface are in an opposite trend with these in solution expectations; but, in agreement with the conclusions presented in the simulations and models by Jayaraman *et al.* [13] and Binder [14]. In their experimental observations, Forman *et al.* [15] arrived at the conclusion that the target concentration does not seem to have an effect on DNA melting temperature. This could be a result of various reasons: low sensitivity in melting curve generation (5°C temperature intervals); the range of target concentrations used could be already saturating the surface at experimental conditions, or the melting curves could be representing the melting of duplexes with the high population of truncated probes as a result of low synthesis efficiency.

Complementary to the findings in modeling studies, it can also be suggested that the influence of the surface and immobilization of one of the strands on DNA hybridization can be a result of the entropic and electrostatic blocking penalties encountered by the target hybridizing with its complementary strand on the surface. Therefore, here, two different alternative approaches will be considered to explain the observed melting temperature trend with respect to target concentration. First one involves an investigation through the kinetics of the reaction on the surface, and the second one involves the application of the entropic and electrostatic blocking models introduced in Chapter 2.

As previously described in Chapter 1, melting temperature is defined as the temperature at which the 50% of the population is single-stranded and 50% is

double stranded [19]. In most of the cases, this definition applies to in-solution bimolecular duplex formation processes in which both of the strands are initially at the same concentration:

	S_1	+	S_2	⇔	D
initial	$S_{1,0}$		$S_{1,0}$		
reacting	$-\theta S_{1,0}$		$-\theta S_{1,0}$		$+\theta S_{1,0}$
final	$S_{1,0}(1-\theta)$		$S_{1,0}(1-\theta)$		$\theta S_{1,0}$

where S_1, S_2 are the single stranded non-self-complementary molecules forming a duplex, D. $S_{1,0}$ is the initial concentration of the each of the targets, which is also equal to the half of the initial total concentration, $C_t/2$; and θ represents the equilibrium conversion reached at any temperature. The association equilibrium constant, K_a, at the initial hybridization temperature (T^0_{hyb}) can be expressed as:

$$K_a(T^0_{hyb}) = \frac{[D]}{[S_1]*[S_2]} = \frac{\theta S_{1,0}}{S_{1,0}{}^2(1-\theta)^2} = \frac{\theta}{S_{1,0}(1-\theta)} = \frac{2\theta}{C_t(1-\theta)} \qquad \text{Equation 4-1}$$

which is equal to

$$K_a(T_m) = \frac{2*0.5}{C_t(1-0.5)} = \frac{4}{C_t}$$

at the melting temperature, where $\theta = 0.5$.

However, when one of the strands is initially present in excess concentration of the other, which resembles the on-surface reaction more with target being in excess of the probes on the surface [20, 21], the definition of the melting temperature becomes the temperature at which the strand with the lower concentration is in 50% single-stranded and 50% double-stranded form. Then, the duplex formation process is represented as:

	S_1	+	S_2	⇔	D
initial	$S_{1,0}$		$S_{2,0}$		
reacting	$-\theta S_{2,0}$		$-\theta S_{2,0}$		$+\theta S_{2,0}$
final	$S_{1,0}1-S_{2,0}\theta$		$S_{2,0}(1-\theta)$		$\theta S_{2,0}$

when S_1 is in excess concentration initially. In this case, the other strand, S_2, becomes the limiting reactant in the reaction. The association equilibrium

constant of this reaction at the initial hybridization temperature can then be formulated as:

$$K_a(T^0_{hyb}) = \frac{[D]}{[S_1]*[S_2]} = \frac{\theta S_{2,0}}{(S_{1,0} - S_{2,0}\theta)*S_{2,0}(1-\theta)} = \frac{\theta}{(S_{1,0} - S_{2,0}\theta)*(1-\theta)} \qquad \text{Equation 4-2}$$

which is equal to

$$K_a(T_m) = \frac{1}{(S_{1,0} - 0.5*S_{2,0})} \qquad \text{Equation 4-3}$$

at the melting temperature, where $\theta = 0.5$.

On the other hand, on-surface applications require further modification in the definition of melting temperature; because the presence of the surface influences the duplex formation and thus, the hybridization efficiency. There are certain cases in which the maximum hybridization efficiency, which is a direct indication of the equilibrium conversion, can be lower than 0.1 [11]. This observation indicates that in-solution melting temperature definition may not be applicable for on-surface applications. Therefore, a new parameter is introduced into the equation: *m*. It is described as the maximum hybridization efficiency achieved at the initial hybridization temperature at equilibrium [22]. Utilizing *m*, the melting temperature definition is adapted to on-surface applications: the temperature at which half of the duplexes formed at the initial hybridization temperature is denatured from the surface, and thus, the fraction this is achieved is 0.5 * *m*. According to the redefinition, the process can then be represented as:

	T	+ P	$\Leftrightarrow$ TP
initial	T_0	P_0	
reacting	$-\theta m P_0$	$-\theta m P_0$	$+\theta m P_0$
final	$T_0 - \theta m P_0$	$P_0(1 - m\theta)$	$\theta m P_0$

where the initial probe concentration, P_0, is the limiting reactant, as in the most cases with target concentration T_0 in large excess. The hybridization efficiency at the end of the process is θ * *m*, and is equal to 1 when all of the probes are available for the duplex formation, as in the case of in-solution reactions.

The association equilibrium constant of this reaction can be formulated as:

$$K_a(T) = \frac{[TP]}{[T]*[P]} = \frac{P_0 m\theta}{(T_0 - P_0 m\theta)*P_0(1-m\theta)}$$ Equation 4-4

at the initial hybridization temperature. It is also equal to

$$K_a(T_m) = \frac{m*0.5}{(T_0 - P_0 m*0.5)*(1-m*0.5)}$$ Equation 4-5

at the melting temperature, where $\theta = 0.5$.

Equation 4-4 requires the knowledge of the maximum extent of hybridization, *m*, and the initial target-to-probe concentration ratio, T_0/P_0, to calculate the association equilibrium constant at the duplex fraction desired. Obtaining this value at the initial hybridization temperature will allow us to compare the stability of a duplex formed on the surface with the one formed in solution, through the relationship between the association equilibrium constant and the free energy change of duplex formation at the standard temperature:

$$\Delta G^0 = -R*T*\ln(K_a)$$ Equation 4-6

Even though the values of *m* and the real initial target-to-probe concentration ratio on the surface are unknown, we attempted to relate the equilibrium constants at initial and melting temperatures through thermodynamic relationships, and observe how different values of *m* and initial target-to-probe concentration ratio will affect the melting temperature, with the initial hybridization temperature set constant and same as the experiments, 23°C.

For systems at constant pressure and temperature, change in the Gibbs free energy of reaction can be expressed as [23]:

$$\Delta G^0 = \Delta H^0 - T*\Delta S^0$$ Equation 4-7

where ΔH^0 is the standard enthalpy change of reaction and ΔS^0 is the standard entropy change of reaction at the reference temperature (T_0). Recent studies have shown that for in-solution duplex formation reactions, the enthalpy and entropy changes are temperature dependent [24]. This temperature dependency can be incorporated into the equation by including the specific heat capacity change, ΔC_p^0:

$$\Delta H^0(T) = \Delta H^0(T_0) + \int_{T_0}^{T} \Delta C_p{}^0 dT$$ Equation 4-8

$$\Delta S^0(T) = \Delta S^0(T_0) + \int_{T_0}^{T} \Delta C_p{}^0 \frac{dT}{T}$$ Equation 4-9

Equations 4-7 through 4-9 can be combined to obtain the temperature-dependent van't Hoff equation [23]:

$$\frac{\Delta G^0(T)}{RT} = \frac{\Delta G^0(T_0) - \Delta H^0(T_0)}{RT_0} + \frac{\Delta H^0(T_0)}{RT} + \frac{1}{T}\int_{T_0}^{T} \frac{\Delta C_p{}^0}{R} dT - \int_{T_0}^{T} \frac{\Delta C_p{}^0}{R}\frac{dT}{T}$$ Equation 4-10

The specific heat capacity change can be assumed independent of temperature [25]. After the integrations are carried out, the relationship between the association equilibrium constant and the free energy change (Equation 4-6) can be incorporated into the van't Hoff equation at any temperature:

$$\Delta G^0(T_0) = RT_0 * \left[-\ln K(T) + \frac{\Delta H^0(T_0)}{R}\left(\frac{1}{T_0} - \frac{1}{T}\right) - \frac{\Delta C_p{}^0}{RT}\left(T - T_0\right) - \frac{\Delta C_p{}^0}{R}\ln\left(\frac{T}{T_0}\right)\right]$$

Equation 4-11

The standard Gibbs free energy change at the standard temperature (T_0) is going to be the same at the initial hybridization temperature (T^0_{hyb}) and the melting temperature (T_m). Expressions derived from Equation 4-11 at these two temperatures can be equilibrated with respect to the standard Gibbs free energy change at the standard temperature. This yields an equation which demonstrates the relationship between the association equilibrium constants at the initial hybridization temperature and the melting temperature:

$$\ln\left(\frac{K(T_m)}{K(T^0_{hyb})}\right) = \frac{\Delta H^0_o}{R}\left(\frac{1}{T^0_{hyb}} - \frac{1}{T_m}\right) + \frac{\Delta C_p{}^0}{R}\ln\left(\frac{T_m}{T^0_{hyb}}\right)$$ Equation 4-12

Inserting in the association equilibrium constant expressions at the initial hybridization and melting temperatures including the maximum extent of hybridization, *m*, and the initial target-to-probe concentration ratio (T_0/P_0) (Equation 4-4 (at $\theta = 1$) and Equation 4-5), and rearranging, results in the final equation:

$$R*\left[\ln\left(\frac{(1-m)*(T_0/P_0-m)}{(1-0.5m)*(T_0/P_0-0.5m)}*0.5\right)-\frac{1}{R}\left(\frac{\Delta H_o^0}{T_{hyb}^0}-\Delta C_p{}^0\ln(T_{hyb}^0)\right)\right]=\Delta C_p{}^0\ln(T_m)-\frac{\Delta H_o^0}{T_m}$$

Equation 4-13

The conditions imposed by Equation 4-13 are:

1) $m \neq 1$
2) $T_0/P_0 \neq m$
3) $T_0/P_0 > m$
4) $0 < m < 1$

To be able to use Equation 4-13, one needs to know the standard enthalpy change of coil-to-helix transition on the surface, ΔH^0, at the reference state; and the standard specific heat capacity change on the surface, $\Delta C_p{}^0$, in addition to the maximum extent of hybridization, *m*, and initial target to probe ratio values, T_0/P_0. Our main goal in this derivation is to observe the melting temperature behavior with respect to different *m* and T_0/P_0 values. Therefore, the following discussion focuses on the standard enthalpy change of coil-to-helix transition and specific heat capacity change on the surface.

In solution, the standard enthalpy change of coil-to-helix transition of our duplex at 23°C is - 209.4 kcal/mol, which is calculated using Nearest-Neighbor method and the improved parameters of SantaLucia, Jr [16] and the range of published values for specific heat capacity change is 7 – 332 cal/mol.bp.K in solution [25].

The enthalpy change of transition represents how well the molecules interact in the two conformations. Each hydrogen bond between the base pairs (which are almost inaccessible to water) contributes to the enthalpy by 2-3 kcal/mol; other interactions such as chain rigidity, dipole/induced-dipole stacking forces contribute 2 to 4 kcal/mol [26]. The strength of the individual hydrogen-bonds will depend on their accessibility to water, i.e. the middle hydrogen bond in the GC base pair might be stronger because it is inaccessible to water [26].

When one of the strands is immobilized on the surface, there is a considerable configurational entropy penalty imposed on the duplex formation in

addition to the double-stranded structure with a stiff backbone allowing a few conformations. As a result, the amount of water molecules displaced with the duplex formation [3] will be much less on the surface, which, in turn, will lower the contribution of the hydrophobic forces stabilizing the structure, and decrease the freedom of water caused by stacking. Furthermore, the strength of the hydrogen bonds holding the base pairs together will be lowered due to their increased accessibility to water. A collection of these factors would play a role in reducing the solution enthalpy change of transition value on the surface. According to a study by Watterson, the standard enthalpy change of coil-to-helix transition on surface is decreased to a half or one-thirds of its value in solution [27].

The specific heat capacity change represents the combinatorial effect of solvent interactions (both solute-solvent and solvent-solvent), conformational entropy, electrostatics and others; solvent effect being more dominant [25]. With the relative changes in the solvent accessible surface areas during folding, the exposure of the structure to water and subsequent hydration play differently on the polar and non-polar surfaces in the two conformations. The presence of the surface and the decreased displacement of water during transition can be accompanied by a less reduction in the contact of the non-polar surfaces with water or more increase in the contact of the polar surfaces with water; both of which results in a smaller increase in the specific heat capacity compared to what might be happening in solution [25]. However, there is no study that specifically looks at the effect of the surface on the specific heat capacity change.

Consequently, following values of standard enthalpy change of coil-to-helix transition and specific heat capacity change are used to simulate the trend in melting temperature with respect to extent of hybridization, *m*, and initial target to probe concentration ratio (T_0/P_0): ΔH^0(23°C) = - 104.7 kcal/mol (half of the solution value), $\Delta C_p^{\ 0}$ = 12.5 cal/mol.bp.K (a value closer to the lower end of the range).

With all the necessary parameters, Equation 4-13, the equation describing the relationship between the association equilibrium constants at the initial hybridization temperature and the melting temperatures, can be plotted with

respect to different initial target-to-probe concentration ratios and maximum extend of hybridization values to observe the behavior of melting temperature (Figure 4-2). The values of the initial hybridization temperature (23°C), the standard enthalpy change of transition and specific heat capacity change are fixed at the indicated values.

A more specific investigation of Figure 4-2 can be made by extracting the melting temperature trends at two initial target-to-probe concentration ratios from Figure 4-2, and plotting them with respect to different possible maximum extents of hybridization. To be able to see the differences in melting temperature trends more clearly, two extreme values of initial target-to-probe ratios are selected from Figure 4-2 : 0.5 and 5, and these trends are plotted in Figure 4-3. The analysis will be carried out based on the assumption that the probe concentration is the same in both.

For a constant probe density and probe concentration, an increase in the target concentration is expected to result in a higher maximum extent of hybridization at the initial hybridization temperature with all other parameters being the same [28]. This is what we observed in our experiments as well. For the experimental set 1, in which we varied the target concentration from 0.5 nM to 15 nM and kept the probe concentration constant at 0.82 pmoles on 10^{18} $Å^2$ chip, the PMT voltage values we used to obtain the maximum dynamic range in detection were accordingly increasing with decreasing target concentration (Table 4-2). The increase in PMT voltages, while keeping the average mean intensity of the perfect match signals at the initial hybridization temperature constant, proposes that there are less targets hybridizing with decreasing target concentration, and therefore, more PMT voltage is necessary to capture the highest intensity for the perfect match probes without saturation, for a higher dynamic range.

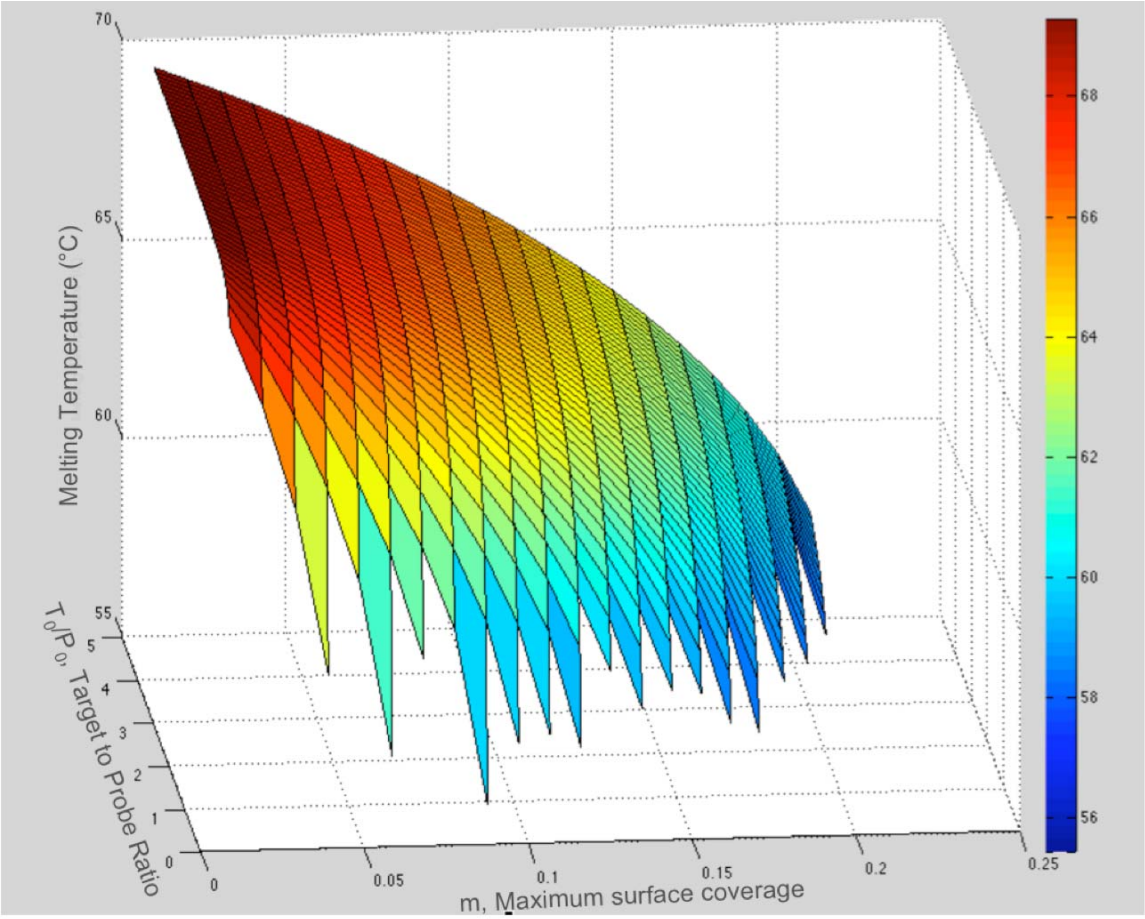

Figure 4-2 3-dimensional representation of the variation in melting temperature of a duplex formed on surface as a function of the maximum extent of hybridization and initial target-to-probe concentration ratio at fixed initial hybridization temperature (23°C), standard enthalpy change of transition (ΔH^0(23°C) = - 104.7 kcal/mole) and specific heat capacity change (ΔC_p^0 = 12.5 cal/mole.bp.K).

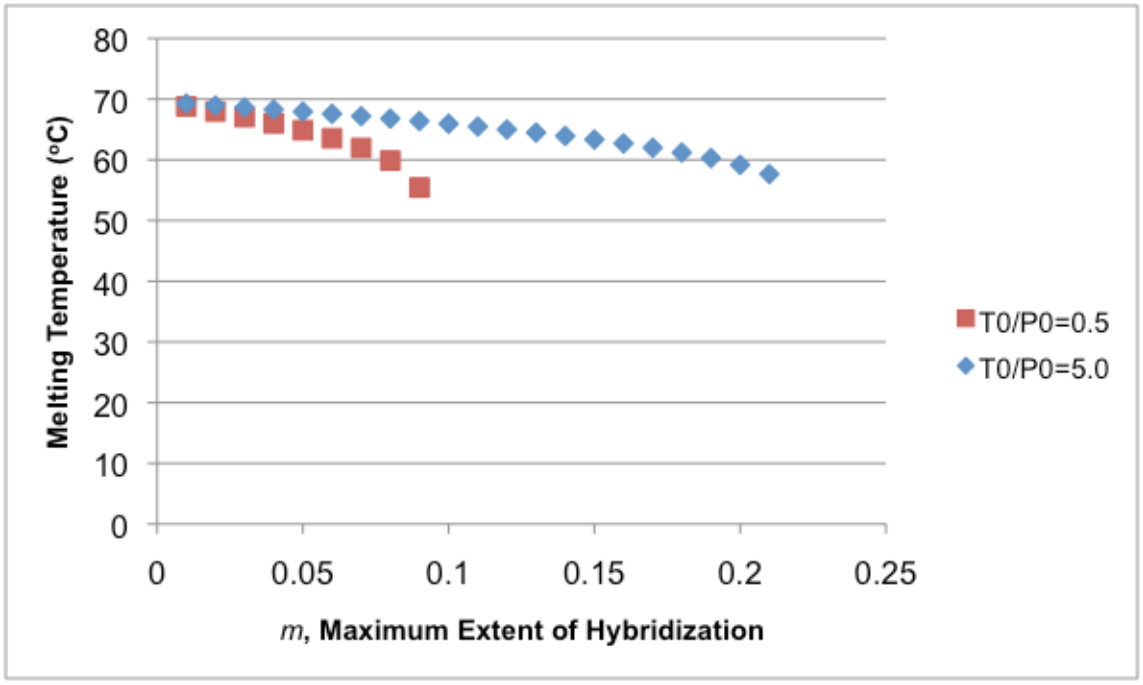

Figure 4-3 Trends in melting temperature with respect to maximum extents of hybridization at two different initial target-to-probe ratios, as extracted from the plot in Figure 4-2.

Table 4-2 PMT Voltages Used in Experimental Set 1.

Concentration of Target in Solution (nM)	PMT Voltage Used at 635 nm Excitation Wavelength	Average Net Median Probe Intensity at 23°C in 635 nm Channel
EXPERIMENTAL SET 1:		
15	460	56378
5	470	59076
1.39	480	58868
0.82	485	58273
0.5	490	57484

This means that, in Figure 4-3, the low initial target-to-probe ratio (0.5) would have a low maximum hybridization efficiency. In this case, looking at the melting temperature trends for both target-to-probe ratios in the same figure, we can conclude that the melting temperature of a duplex formed in the presence of lower target concentration could be higher than that with higher target concentration. This inference from Figure 4-3, and in turn, Figure 4-2, supports our experimental finding that decreasing target concentration could lead to increasing melting temperature for a duplex formed on the surface.

Another explanation for the melting temperature trend seen here could be deducted by looking at the relative free energy contributions of the electrostatic and entropic blocking terms encountered by the hybridizing target at different target concentrations. Figure 4-4 shows the electrostatic and entropic blocking terms reproduced from the theoretical study previously presented in Chapter 2, with the system parameters applied (spacer length = 15 dT, probe length = target length = 25 nt, probe density = $5*10^{12}$ molecules/cm^2). At higher target concentrations, with the probe concentration constant, a higher maximum extent of hybridization would be expected on the surface, leading to higher free energy penalties, and thus, less duplex stability on the surface. This could result in observable duplex denaturations occurring at lower temperatures than more stable duplexes on the surface as the melting progresses with increasing temperatures. Figure 4-5 demonstrates this phenomenon by two experimentally

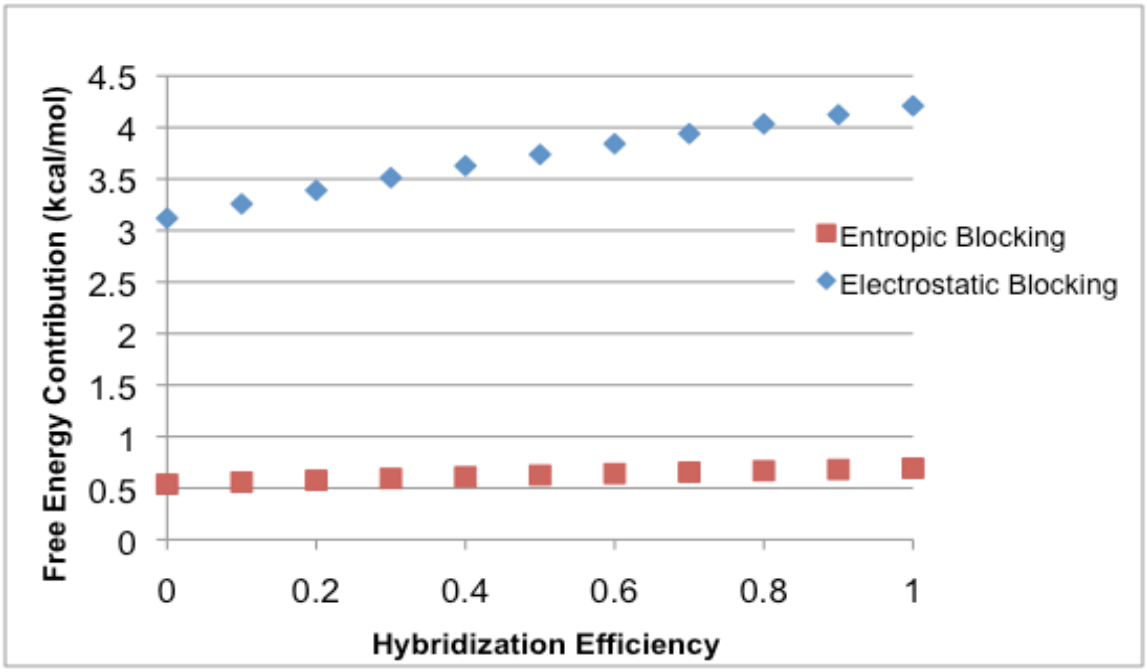

Figure 4-4 Free energy contribution of electrostatic and entropic blocking encountered by a hybridizing target, as reproduced from the theoretical model presented in Chapter 2; simulated with Experimental Set 1 system parameters (spacer length = 15 dT, probe length = target length = 25 nt, probe density = $5*10^{12}$ molecules/cm^2, at melting temperature of Initial Target to Probe Ratio = 1).

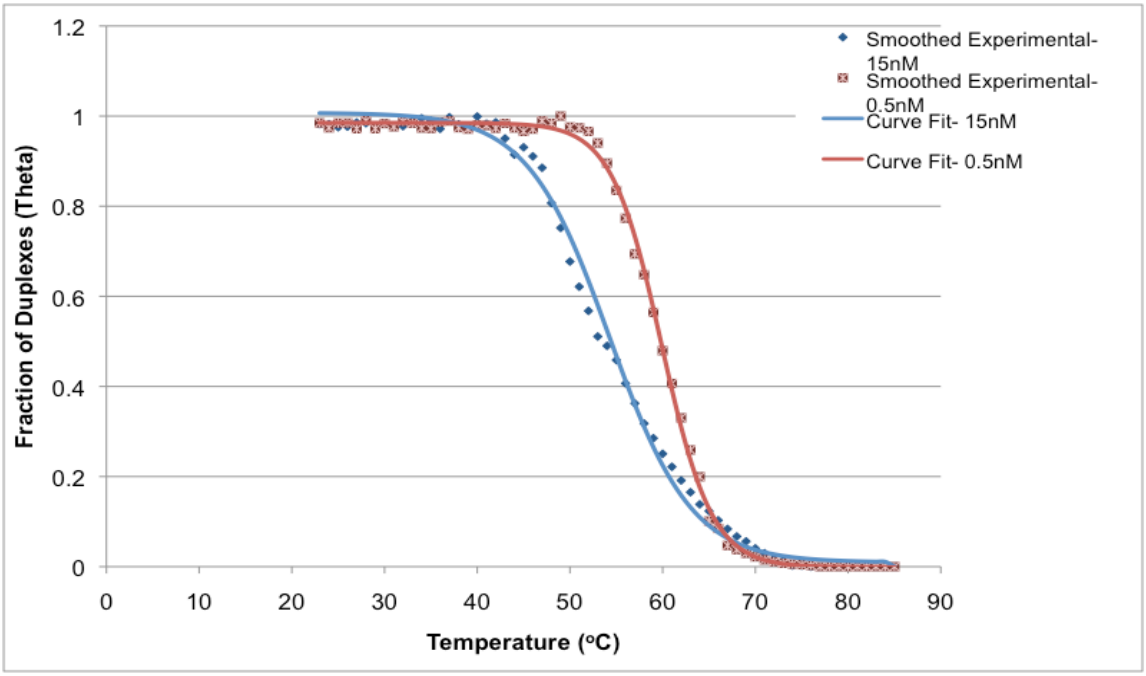

Figure 4-5 Experimentally observed melting curves of two duplexes formed on the surface with target concentrations of 15 nM and 5 nM with a constant probe concentration of 0.82 pmoles in 10^{18} Å^2 (from Experimental set 1).

observed melting curves of duplexes formed with two different target concentrations (15 nM and 0.5 nM) and a constant probe concentration (0.82 pmoles on 10^{18} $Å^2$) (from Experimental set 1). Duplexes start to melt at a lower temperature when the hybridization is performed with 15 nM of target concentration, indicating their lower stability. On the other hand, the duplexes formed in the presence of a lower target concentration, 0.5 nM, prove to be more stable, and start to show observable denaturation at a higher temperature.

4.3.2 Assessing the Synthesis Imperfections using Melting Curves

Experiments in Set 3 were designed to investigate the melting temperatures at very low initial target and probe concentrations on the surface. The target concentrations were 0.027 nM and 0.0165 nM, and the probe concentration was kept constant at 0.0165 pmoles on the chip area of 10^{18} $Å^2$.

We made an interesting observation with the melting curves reproduced at these concentrations. The experiments with 0.027 nM and 0.0165 nM initial target concentration showed melting curves different from what was observed in the experimental sets 1 (Figure 4-5) and 2. Figure 4-6 demonstrates a representative melting curve of a perfect-match probe-target pair (without any high temperature pre-hybridization) on the surface at this target and probe concentration.

It is a distinctive melting curve, because it does not show the typical S-shaped curve observed in the melting experiments with higher target and probe concentrations. A careful look at the low temperature domain in the melting curve suggests that there could be multiple melting processes taking place before the perfect match pair melts at a higher temperature. A similar observation was made in studies on single nucleotide polymorphism genotyping experiments by generating high resolution melting curves in solution [29, 30]. A mixture of heteroduplex (with single nucleotide polymorphism) and perfect match (wild-type) samples is shown to reproduce melting curves with distinctive shapes in low temperature domains. With the presence of single base mismatch, the duplex with lower stability melts at a lower temperature than the perfect match; yielding a melting curve similar to our observations.

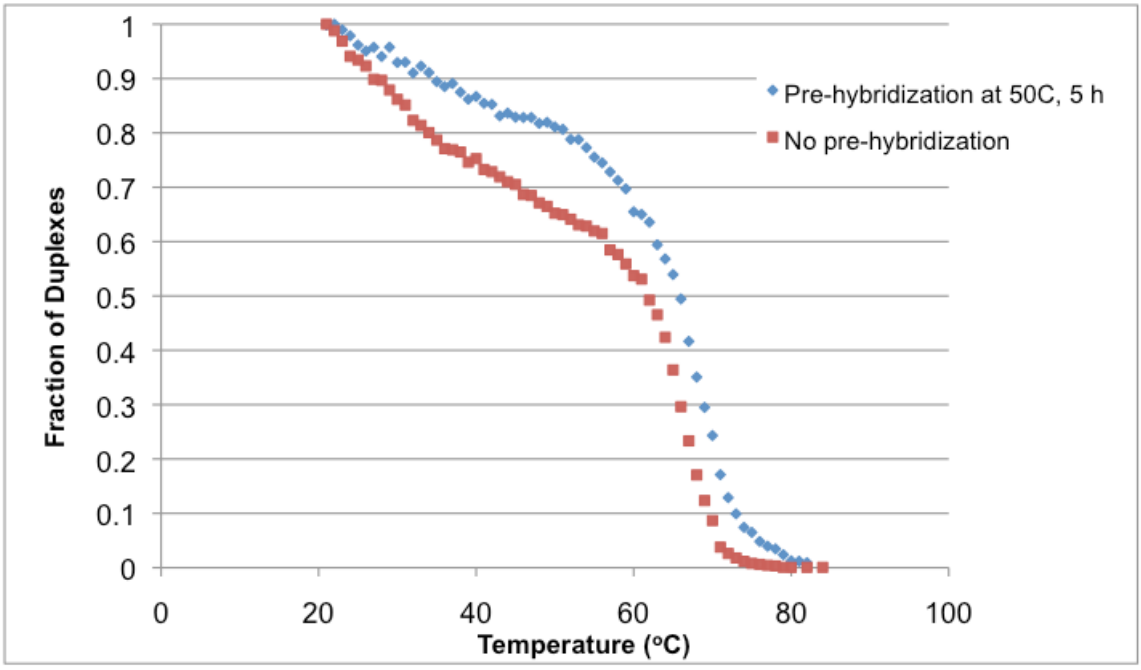

Figure 4-6 A representative perfect-match duplex melting curve and the effect of pre-hybridization at 50°C for 5 h observed in Experimental Set 3 with target concentration of 0.0165 nM and probe concentration of 0.0165 pmoles in 10^{18} Å^2.

In our case, multiple melting processes in the low temperature domain of the melting curve would indicate the presence of sequences which form less stable duplexes than the perfect match itself, truncated probe sequences which are an inherent result of *in situ* oligonucleotide synthesis [15, 31]. A possible reason of observing them in this target concentration but not in the higher ones can be explained by looking at the expected value for the maximum hybridization efficiency term. At this low target concentration, the anticipated extent of hybridization would be low. However, the presence of the truncated sequences can create a competitive environment for the full length probes at the initial hybridization temperature [14, 15]. Under these circumstances, with the initial low amount of target available to react and an assumed even distribution among the probe population on the surface, the maximum extent of hybridization would reach lower coverages than initially predicted. Therefore, any melting curve reproduced in these conditions would represent melting of truncated, less stable sequences in lower temperatures (in the low melting temperature domain) and the perfect match, full length probe itself at a higher temperature.

These sequences with lower stabilities would be inherent results of in-situ light-directed combinatorial oligonucleotide synthesis [15, 31], namely 5'-truncated probes. These sequences are shorter in length and irreversibly blocked in the capping step during synthesis. The population of these truncated probes can be calculated using the step-wise synthesis yield, which is predicted to be 99.5% in our system [32]. With this value, our 25mer probes are expected to be 88% of the population in each spot; the rest having a dispersion of shorter lengths with a distribution of smaller Gibbs free energies in absolute value [15].

To test our hypothesis of polydispersity in synthesized probe lengths and their melting; we tried to reduce the observed multi-melting process at the low temperature domain by initially carrying out the hybridization at a higher temperature, 50°C, for a certain period of time (5 h), and then bringing it down to the regular hybridization temperature of 23°C, and continue hybridization till the equilibrium was reached. Figure 4-6 shows the effect of high temperature pre-hybridization for 5 h on the melting curve.

At high temperatures, the hybridization reaction would be favorable towards the more stable duplex, due to comparably lower association equilibrium constants of low stability duplexes [22]. After pre-hybridization at 50°C, as the temperature was decreased and hybridization was carried out at 23°C, there would be fewer targets in solution available for hybridization with the truncated probes, since perfect match sequences are more stable and would retain more of the targets. This results in less number of duplexes formed with lower stabilities on the surface. As the melting experiment is carried out with increasing temperatures, the imperfect duplexes, which are now less in number, will melt in the low temperature domain of the melting curve; but the slope of the curve in this region would indicate a smoother transition than the case without any high temperature pre-hybridization.

4.4 Conclusion

This chapter describes the effect of target concentration on the duplex formation and melting on the surface, and more indicatively, melting temperature. It is experimentally observed that the melting temperature decreases on the surface with respect to in-solution, with more restrictions imposed on the structure by the presence of the surface. This discrepancy is found to increase with increasing target concentration, which could be due to increasing probability of targets binding to more than one probe as well as more electrostatic and entropic penalties experienced by the hybridizing targets with increasing hybridization efficiencies.

It is also interestingly seen in the experiments that at constant probe concentrations, a decreasing target concentration trend can be accompanied with increasing melting temperature. This is an opposite trend to what is expected in solution, but in agreement with the models and simulations published in the literature. As a result of more possibility of target binding to more than one probe with increasing target concentration as well as the additional electrostatic and entropic penalties imposed on the structure, melting duplexes can exhibit lower melting temperatures. With the introduction of the maximum extent of hybridization term, *m*; modification of the equilibrium constant expressions at the initial hybridization and melting temperatures; and temperature dependent van't Hoff equation, we were able to demonstrate graphically that it is possible to observe increasing melting temperature trends with decreasing target concentrations, at surface-adapted standard enthalpy change and specific heat capacity change values for duplex formation.

Experiments performed with low target and probe concentrations yielded melting curves different than what was seen with high target and probe concentrations. A possible multiple melting process is observed in the low temperature domain of the curve. This could be attributed to the polydispersity of the probe length on the surface due to the truncated sequences, which is an inherent characteristic of *in situ* combinatorial oligonucleotide synthesis on the surface. These sequences exhibit stabilities lower than the perfect match probes,

resulting in their melting at lower temperatures than the perfect match. This hypothesis is confirmed with pre-hybridization experiments at higher temperature. This finding can play its role as an important tool to further assess the quality of the probes synthesized on the surface.

4.5 Bibliography

1. Pozhitkov A, Noble PA, Domazet-Loso T, Nolte AW, Sonnenberg R, Staehler P, Beier M, Tautz D, *Tests of rRNA hybridization to microarrays suggest that hybridization characteristics of oligonucleotide probes for species discrimination cannot be predicted*. Nucleic Acids Res, 2006. 34: e66.
2. Rouillard JM, Zuker M, Gulari E, *OligoArray 2.0: design of oligonucleotide probes for DNA microarrays using a thermodynamic approach*. Nucleic Acids Res, 2003. 31: 3057-3062.
3. Bloomfield VA, Crothers DM, Tinoco JR, Ignacio. Nucleic Acids: Structures, Properties, and Functions. In: Stiefel J, ed. University Science Books, 2000
4. Shchepinov MS, Case-Green SC, Southern EM, *Steric factors influencing hybridisation of nucleic acids to oligonucleotide arrays*. Nucleic Acids Res, 1997. 25: 1155-1161.
5. Southern E, Mir K, Shchepinov M, *Molecular interactions on microarrays*. Nat Genet, 1999. 21: 5-9.
6. Southern EM, Case-Green SC, Elder JK, Johnson M, Mir KU, Wang L, Williams JC, *Arrays of complementary oligonucleotides for analysing the hybridisation behaviour of nucleic acids*. Nucleic Acids Res, 1994. 22: 1368-1373.
7. Vainrub A, Pettitt BM, *Coulomb blockage of hybridization in two-dimensional DNA arrays*. Phys Rev E Stat Nonlin Soft Matter Phys, 2002. 66: 041905.
8. Vainrub A, Pettitt BM, *Surface electrostatic effects in oligonucleotide microarrays: control and optimization of binding thermodynamics*. Biopolymers, 2003. 68: 265-270.
9. Vainrub A, B. Montgomery Pettitt, *Thermodynamics of Association to a Molecule Immobiized in an Electrical Double Layer*. Chemical Physics Letters, 2000. 323: 160-166.
10. Heaton RJ, Peterson AW, Georgiadis RM, *Electrostatic surface plasmon resonance: direct electric field-induced hybridization and denaturation in*

monolayer nucleic acid films and label-free discrimination of base mismatches. Proc Natl Acad Sci U S A, 2001. 98: 3701-3704.

11. Peterson AW, Heaton RJ, Georgiadis RM, *The effect of surface probe density on DNA hybridization*. Nucleic Acids Res, 2001. 29: 5163-5168.
12. Peterson AW, Wolf LK, Georgiadis RM, *Hybridization of mismatched or partially matched DNA at surfaces*. J Am Chem Soc, 2002. 124: 14601-14607.
13. Jayaraman A, Hall CK, Genzer J, *Computer simulation study of probe-target hybridization in model DNA microarrays: effect of probe surface density and target concentration*. J Chem Phys, 2007. 127: 144912.
14. www.izbi.de/working_papers.html
15. Forman JE, Ian D. Walton, David Stern, Richard P. Rava, Mark O. Trulson, *Thermodynamics of Duplex Formation and Mismatch Discrimination on Photolithographically Synthesized Oligonucleotide Arrays*. ACS Symposium Series, 1998. 682: 206-228.
16. SantaLucia JJ, Allawi HT, Seneviratne PA, *Improved nearest-neighbor parameters for predicting DNA duplex stability*. Biochemistry, 1996. 35: 3555-3562.
17. Owczarzy R, Vallone PM, Gallo FJ, Paner TM, Lane MJ, Benight AS, *Predicting sequence-dependent melting stability of short duplex DNA oligomers*. Biopolymers, 1997. 44: 217-239.
18. SantaLucia JJ, *A unified view of polymer, dumbbell, and oligonucleotide DNA nearest-neighbor thermodynamics*. Proc Natl Acad Sci U S A, 1998. 95: 1460-1465.
19. Mergny JL, Lacroix L, *Analysis of thermal melting curves*. Oligonucleotides, 2003. 13: 515-537.
20. Chan V, Graves DJ, McKenzie SE, *The biophysics of DNA hybridization with immobilized oligonucleotide probes*. Biophys J, 1995. 69: 2243-2255.
21. Khomyakova E, Livshits MA, Steinhauser MC, Dauphinot L, Cohen-Kaminsky S, Rossier J, Soussaline F, Potier MC, *On-chip hybridization*

kinetics for optimization of gene expression experiments. Biotechniques, 2008. 44: 109-117.

22. Glazer M, Fidanza JA, McGall GH, Trulson MO, Forman JE, Suseno A, Frank CW, *Kinetics of oligonucleotide hybridization to photolithographically patterned DNA arrays*. Anal Biochem, 2006. 358: 225-238.
23. Smith JM, HC Van Ness, MM Abbott. Introduction to Chemical Engineering Thermodynamics. In: ed. New York: McGraw Hill Inc, 1996:565-571.
24. Holbrook JA, Capp MW, Saecker RM, Record MTJ, *Enthalpy and heat capacity changes for formation of an oligomeric DNA duplex: interpretation in terms of coupled processes of formation and association of single-stranded helices*. Biochemistry, 1999. 38: 8409-8422.
25. Mikulecky PJ, Feig AL, *Heat capacity changes associated with nucleic acid folding*. Biopolymers, 2006. 82: 38-58.
26. Levitt M, *Folding of nucleic acids*. Ciba Found Symp, 1972. 7: 147-171.
27. Watterson JH, Paul A. E. Piunno, Christopher C. Wust, Ulrich J. Krull, *Effects of Oligonucleotide Immobilization Density on Selectivity of Quantitative Transduction of Hybridization of Immobilized DNA*. Langmuir, 2000. 16: 4984-4992.
28. Guo Z, Guilfoyle RA, Thiel AJ, Wang R, Smith LM, *Direct fluorescence analysis of genetic polymorphisms by hybridization with oligonucleotide arrays on glass supports*. Nucleic Acids Res, 1994. 22: 5456-5465.
29. Gundry CN, Vandersteen JG, Reed GH, Pryor RJ, Chen J, Wittwer CT, *Amplicon melting analysis with labeled primers: a closed-tube method for differentiating homozygotes and heterozygotes*. Clin Chem, 2003. 49: 396-406.
30. Liew M, Pryor R, Palais R, Meadows C, Erali M, Lyon E, Wittwer C, *Genotyping of single-nucleotide polymorphisms by high-resolution melting of small amplicons*. Clin Chem, 2004. 50: 1156-1164.
31. Halperin A, A. Buhot, E. B. Zhulina, *On the hybridization isotherms of DNA microarrays: the Langmuir model and its extensions*. Journal of Physics: Condensed Matter, 2006. 18: S463-S490.

32. Rouillard, Jean-Marie, PhD.

CHAPTER V

THE EFFECT OF SPACER LENGTH AND PROBE DENSITY

5.1 Introduction

Oligonucleotide microarrays utilize terminally anchored, chemically grafted probe sequences on the surface. These probe sequences are designed to capture the targets in solution in a competitive hybridization environment on a microarray. In an application such as gene expression profiling, the identification of differentially expressed genes is influenced by the measured signal intensities [1, 2]. These intensities depend on the efficiency of the hybridization reaction on the surface, which is influenced by the microarray design parameters and experimental conditions. Among these specifications, spacer length and probe density are widely studied in their contributions on DNA duplex formation.

The study by Schepinov *et al.* suggests that that an optimal spacer length of at least 40 atoms in length can be built from a variety of monomeric units that can give an increase in the hybridization yield 150-fold [3]. Concurrent studies by Guo *et al.* and Southern *et al.* observe the signal intensity increase with longer dT spacers (0 to 15 nucleotides) between the probes and the surface [4, 5]. These results propose that accessibility to the probes improves with increased distance from the surface, mitigating the effect of its presence on duplex formation.

However, in addition to the length of the spacers, longer probes can provide higher surface coverage and intensities. It has been demonstrated by Hughes *et al.* [6] and Kane *et al.* [7] that the length of the probes for optimum sensitivity lies between 50 – 60 nt. But, this approach can provide a disadvantage. Further studies by Guo *et al.* [4] and Peterson *et al.* [8] have found that the 10 – 18 nt at

disadvantage. Further studies by Guo *et al.* [4] and Peterson *et al.* [8] have found that the 10 – 18 nt at the tethered end of the probe sequence can be relatively inaccessible to the hybridizing targets due to steric hindrances by the surface [3]. Therefore, utilization of a spacer could render the probe accessible for hybridization and increase the sensitivity level of detection [9].

The effect of probe density on DNA hybridization has been also investigated in terms of hybridization efficiency. Several researchers have concluded in their studies that increasing probe densities results in lower extents of hybridization (Peterson *et al.* [10], Watterson [11], Steel *et al.* [12]). Using Surface Plasmon Resonance, Peterson *et al.* observed that the efficiency dropped from 70% to 5% when the probe density was increased from $2*10^{12}$ molecules/cm^2 to $12*10^{12}$ molecules/cm^2 [10]. This reduction is attributed to the increasing electrostatic and steric effects within a denser probe layer.

In their following study, Peterson *et al.* monitor the hybridization of perfectly matched, and partially matched DNA at different probe densities [8]. A 25mer probe is designed to hybridize with different targets, which include a perfect match; 18mer target hybridizing with the first 18 nucleotides at the tethered end of the probe (18-low), and an 18mer target hybridizing with the last 18 nucleotides at the free end of the probe (18-high). It is observed that at low surface densities ($1.5*10^{12}$ molecules/cm^2), the hybridization efficiencies with both 18mer targets are quite similar. However, a different conclusion is reached in the presence of a denser probe layer ($3*10^{12}$ molecules/cm^2). Partial hybridizations with the 18mer targets are found to be affected by the increasing probe density with 18-low giving a lower hybridization efficiency than 18-high target. Both of these findings are attributed to the increased steric crowding within a denser probe layer.

These studies look at how spacer length and probe density influence the hybridization efficiency on the surface. The duplex signal intensity can be improved with longer spacers or lower probe densities on a surface; but, it would be difficult to control their effects specifically in a microarray environment. They could alter the specific and non-specific hybridization reactions with a particular

probe similarly [13], and the signal intensity measured would be representing both of these competitive reactions, leading to imprecise conclusions [14, 15]. However, knowledge of how the spacer length and probe density influences the stability of the DNA duplex and its melting temperature accordingly could facilitate the design and optimization of the experimental conditions in microarrays for reliable and accurate outcomes of the experiments.

In this part of the thesis, we investigate the impact of the surface on the stability of a DNA duplex formed on the surface by focusing on the effects of spacer length and probe density. Their individual influences are monitored experimentally by generating DNA melting curves and extracting the duplex melting temperatures, and these observations are interpreted in combination with the theoretical predictions made using electrostatic and entropic models presented in Chapter 2.

5.2 Materials and Methods

The sequences used in these experiments were also used in the study on the effect of different target-to-probe ratios on the melting temperature in Chapter 4:

Target: 5'- ACCCAACACCGGTCCAGTGCTCGCG- 3' -Cy5

Probe: 5'- CGCGAGCACTGGACCGGTGTTGGGT- 3'

The GC content of the probe sequence is 67% and its molecular weight is 7,755.1.

The probes were synthesized on the surface in 3' to 5' direction using the combinatorial in-situ synthesis on the oligonucleotide microfluidic arrays. The PAGE purified complementary target was labeled with a Cy5 fluorescence dye on 3' end (Integrated DNA Technologies Inc, Iowa, USA) for detection purposes. The detection on the surface was carried out by monitoring the signal intensity change on the probe sites as the targets were denatured when the temperature is increased, and equilibrium is reached, with the use of a fluorescence laser scanner (Axon 4000B, Molecular Devices Inc., California, USA).

The initial hybridization of the target with the probes was carried out at a low temperature of 23°C to derive the exothermic reaction to the maximum extent achievable at equilibrium. The 1,000 μl hybridization solution was constantly recirculated in the microfluidic chambers till the equilibrium was reached, as designated by negligible signal intensity change with respect to time. Next step was to determine the equilibration time at 24°C by observing the signal intensity change over time. When the new equilibration time was determined, the generation of the melting curves was started using a computer controlled capturing system, which is composed of a temperature controller, a fluorescence laser scanner and a holder, which houses the microfluidic chip, a heater chip and a thermocouple.

All of the experiments in this chapter passed the quality assessment guidelines mentioned in Chapter 3. Created melting curves were analyzed through a series of steps including temperature calibration, smoothing, curve fitting and statistical analysis.

The experimental design in this chapter involves the examination of the influences of spacer length and probe density. The summary of the experiments carried out to address these variables are presented in Table 5-1.

Table 5-1 Summary of the Experiments on Spacer Length and Probe Density.

Concentration of Target in Solution (nM)	Total Amount of Probe on Chip (pmoles on C.S.A[(a)])	Target to Probe Ratio (pmoles/pmoles)
EXPERIMENTAL SET FOR ALL SPACER LENGTHS[(b)]		
1	0.59	1.7 to 1
0.59	0.59	1 to 1
0.36	0.59	0.61 to 1
EXPERIMENTAL SET FOR PROBE DENSITY[(c)]		
10	5.87	1.7 to 1
5.9	5.87	1 to 1
3.6	5.87	0.61 to 1

(a) C.S.A. = Chip Surface Area = 10^{18} Å^2
(b) Probe density = $5*10^{12}$ molecules/cm^2, Spacer Lengths = 2 dT, 15 dT, 25 dT
(c) Probe density = $5*10^{13}$ molecules/cm^2, Spacer Length = 15 dT

The spacer chains are synthesized after the derivatization of the silicon dioxide surface with the *3-aminopropyltriethoxysilane* (Gelest Inc, California, USA) linker. The synthesis of these spacers is carried out with trichloroacetic acid as the deprotection agent, giving the advantage of covering all the surfaces with the same sequence. The spacer we used in our experiments is composed of deoxythymidine (dT) monomer. The respective length of the spacer is therefore determined by the number of these monomers synthesized on the surface. In the experimental set looking at this effect, the spacer lengths selected were 2 dT, 15 dT and 25 dT. The values of these lengths signify how far the probes are away from the surface.

The spacer length effect experiments were carried out on the chips derivatized with a linker concentration of 0.04 mM in anhydrous toluene (Sigma-Aldrich Inc, Missouri, USA). This corresponds to an approximate probe density of $5*10^{12}$ molecules/cm^2, based on the previous measurements on surface density

[16]. The probe concentration was kept constant at 0.59 pmoles on a chip area of 10^{18} $Å^2$. The target concentrations used were varied from 1 nM to 0.36 nM, which correspond to target-to-probe ratios of 1.7:1 to 0.61:1.

The examination of the probe density was carried out by changing the linker concentration with which the microfluidic chips were derivatized. In this part of the study, we increased the concentration of the linker ten times, and assumed ten times concentrated probe spots on the surface, with an approximate probe density of $5*10^{13}$ molecules/cm^2. The probe concentration accordingly increased to 5.9 pmoles on a surface area of 10^{18} $Å^2$. The target concentrations used were varied from 1 nM to 0.36 nM, which correspond to target-to-probe ratios of 1.7:1 to 0.61:1. The spacer length was kept at 15 dT.

The layouts of the chips, the probe map on the surface, include 720 perfect match probes and 211 synthesis quality control sequences out of 1,000 possible spots in each microfluidic channel. The rest of the spots is left empty to be later used in background calculations. The layout is designed to have synthesis only in the 5 mid-channels out of 7 channels on the chip, to decrease the previously observed effect of inlet and outlet flows on the synthesis and hybridization.

5.3 Results and Discussion

5.3.1 Effect of Spacer Length on Melting Temperature

The effect of the spacer length on the melting temperature of the duplex on the surface and its comparison with the predicted in-solution melting temperatures at different initial target-to-probe concentration ratios are presented in Figure 5-1.

Firstly, the observed melting temperatures on the surface are lower than the melting temperatures predicted by Nearest-Neighbor method in solution [17]. Due to the electrostatic and entropic penalties imposed on the duplex by the presence of the surface, the stability of the duplex, and thus its melting temperature, would be lower [13, 18].

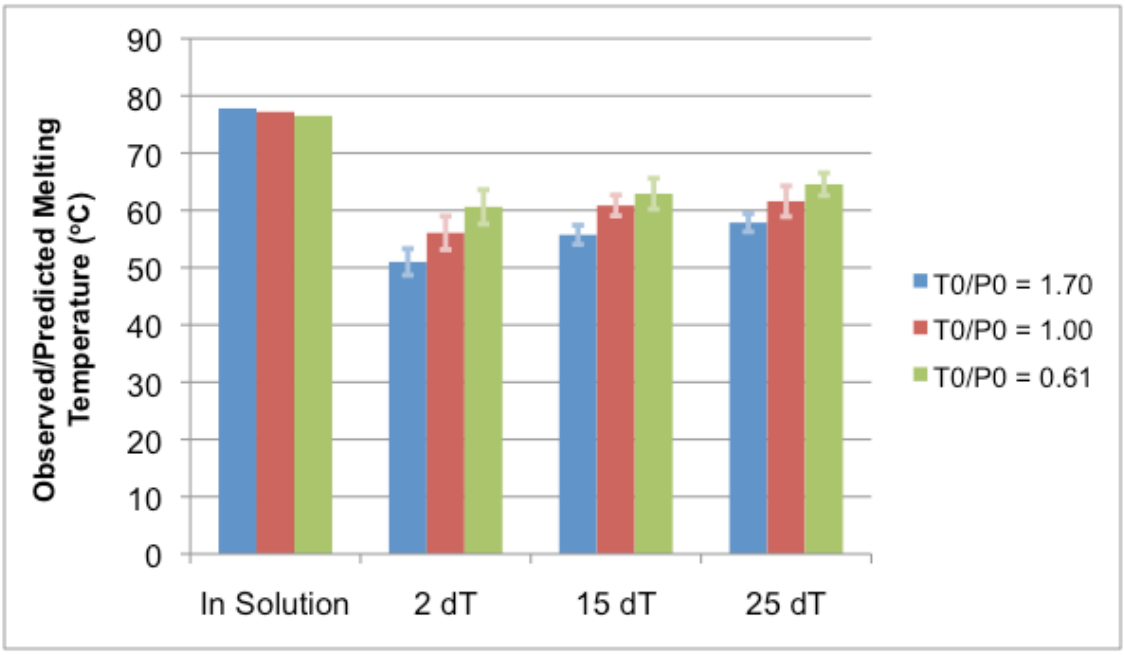

Figure 5-1 The comparison of the effect of spacer length on the melting temperature of the duplex on surface with predicted melting temperatures in solution at the same target-to-probe ratios.

Secondly, as the initial target-to-probe concentration ratio decreases, the melting temperature increases at all spacer lengths; a similar trend observed with our target concentration experiments in Chapter 4, but opposite to what is seen in in-solution studies [19]. This observation was explained theoretically using two strategies: a kinetic and thermodynamic approach that takes into account the effects of the surface, and a modeling approach that incorporates the free energy penalties as a result of entropic and electrostatic blocking proposed in Chapter 2.

To examine if a similar situation is observed with different target concentrations applied in the presence of different spacer lengths, we used our electrostatic and entropic blocking models to simulate the effect of spacer length with respect to hybridization efficiency (see Chapter 2 – Appendix), and demonstrate their relative contributions to the free energy of duplex formation on the surface (Figure 5-2). Figure 5-2 (a) shows the influence of the spacer lengths used in the experiments (2 dT, 15dT, 25 dT) on the hybridization process in terms of the electrostatic free energy penalties they impose on the system, at different hybridization efficiencies, at a fixed probe density of $5*10^{12}$ molecules/cm^2 with probe length equal to the target length, 25; at melting temperatures corresponding to initial target to probe ratios of 1 at each spacer length (as an example) and salt (NaCl) concentration of 1 M. Figure 5-2 (b) demonstrates the effect of spacer length on the free energy of duplex formation through the entropic blocking term with the same system parameters.

To be able to interpret the effect of target concentration on the electrostatic and entropic blocking terms in Figure 5-2, one requires to see the trends in hybridization efficiencies with respect to different target concentrations. Table 5-2 includes the PMT voltages used in 635 nm wavelength to excite the labeled target molecules hybridized on the surface at different target concentrations and spacer lengths. It can be concluded that to keep the dynamic range as wide as possible for detection over the experimental temperature range, PMT voltage values were increased with decreasing target concentration. This may indirectly indicate that there are less target-probe duplexes on the surface with less initial target concentration, designating a lower hybridization efficiency.

(a)

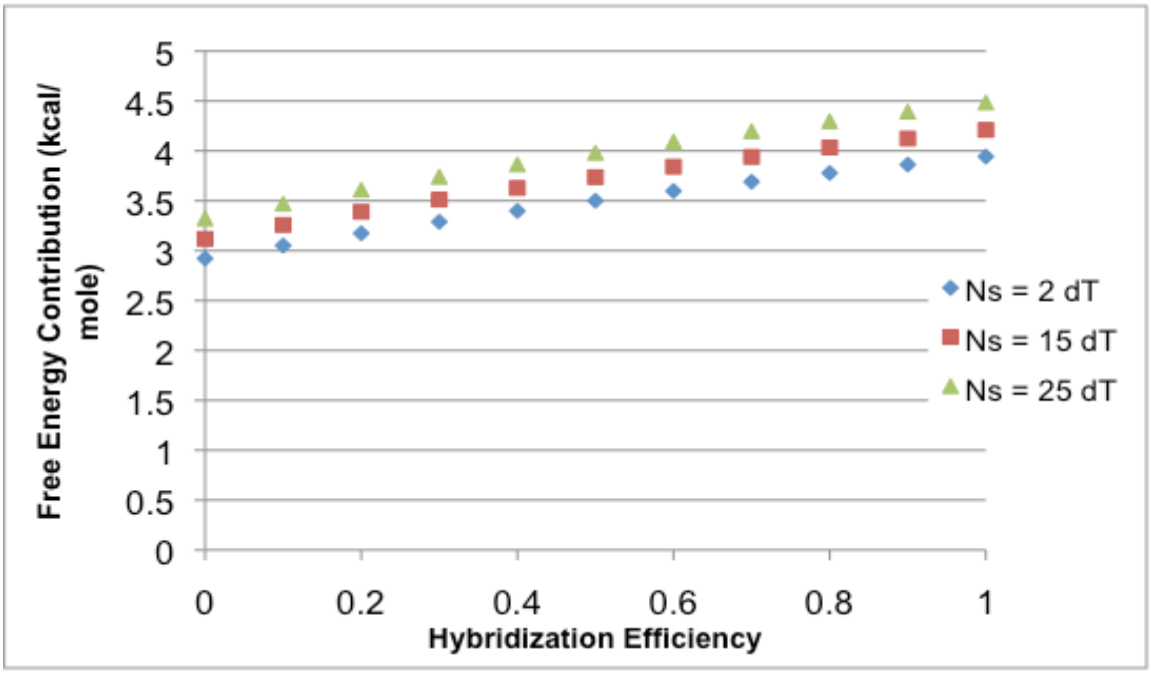

(b)

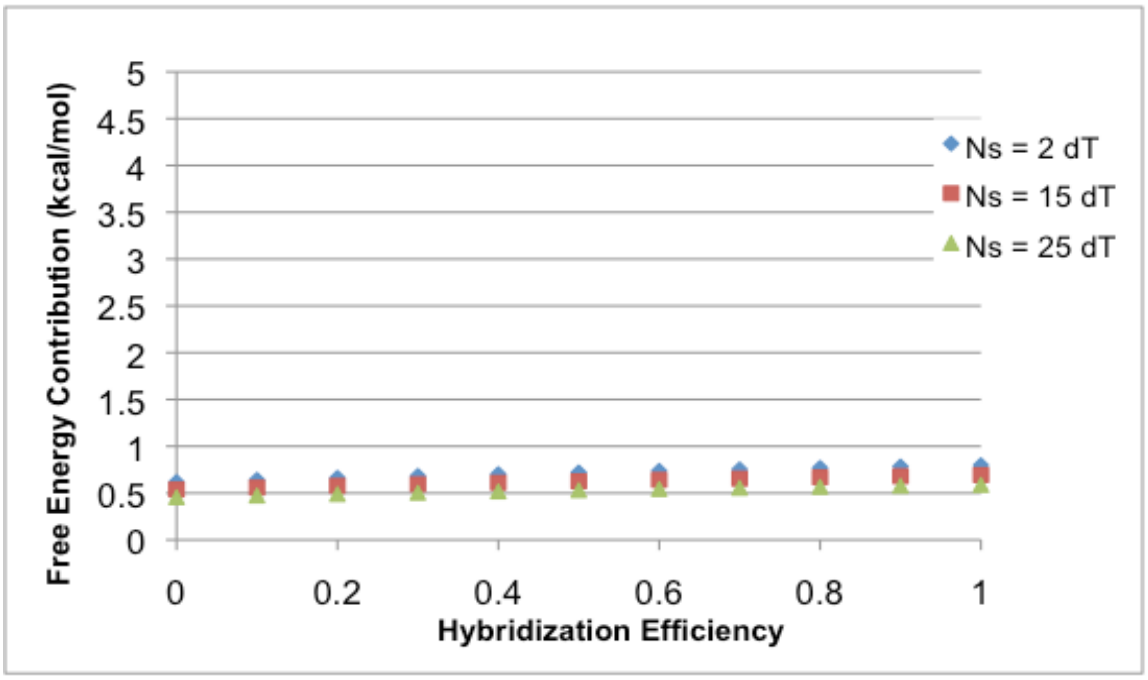

Figure 5-2 Contributions of (a) Electrostatic blocking and (b) Entropic blocking on the free energy of duplex formation on the surface, with spacer lengths (2 dT, 15 dT, 25 dT) used in the experiments with respect to different hybridization efficiencies, a fixed probe density of $5*10^{12}$ molecules/cm^2, a salt concentration of 1M NaCl, at melting temperatures obtained at target to probe ratio = 1.

Table 5-2 PMT voltages used in 635 nm wavelength to detect the probe-target duplex formed on the surface at equilibrium, at the end of initial hybridization, with different spacer lengths and target concentrations (at a probe density of $5*10^{12}$ molecules/cm^2).

Concentration of Target in Solution (nM)	PMT Voltage Used at 635 nm Excitation Wavelength	Average Net Median Probe Intensity at 23°C in 635 nm Channel
EXPERIMENTAL SET WITH SPACER LENGTH = 2 dT		
1	500	54121
0.59	505	53003
0.36	540	51195
EXPERIMENTAL SET WITH SPACER LENGTH = 15 dT		
1	480	51779
0.59	490	52471
0.36	500	50952
EXPERIMENTAL SET WITH SPACER LENGTH = 25 dT		
1	460	55402
0.59	475	52303
0.36	480	56780

It can be inferred from Figure 5-2 that with increasing target concentration and thus, hybridization efficiency, both the electrostatic and entropic penalty terms are expected to contribute to the free energy of duplex formation more positively. As a result, the duplex formed on the surface would be less stable with increasing target concentration, and therefore, the melting temperature would be lower.

The final observation from Figure 5-1 is that the melting temperatures show an increasing trend with increasing spacer length. It has been demonstrated in the studies by Schepinov *et al.* [3] and Guo *et al.* [4] that with increasing spacer lengths, the duplex yield increases on the surface, with all other parameters kept constant. Placing the probes away from the surface would reduce the influence of the surface on duplex formation [9, 18].

Table 5-2 illustrates that effect of the spacer length on the extent of hybridization at all target concentrations. As the spacer length increases, the PMT voltages used in 635 nm wavelength to excite the labeled target molecules

hybridized on the surface decrease to be able to keep the dynamic range as wide as possible for detection over the experimental temperature range. This indirectly indicates that the hybridization efficiency increases with increasing spacer lengths, in agreement with the published studies [3, 4, 9].

Figure 5-2 can also be used to interpret the stability trend seen with different spacer lengths. It is observed in Figure 5-2(a) that the electrostatic penalty increases with increasing spacer length and hybridization efficiency. Since the surface charge increases with the presence of longer spacers and more duplexes on the surface, both of these trends are expected. On the other hand, these are opposite to the stability or melting temperature trends seen with the experiments: the melting temperature increases with increasing spacer length. Therefore, to be able to reach a conclusion on the effect of the spacer length on the free energy of the duplex formation on the surface, we also need to look at the contribution of the entropic blocking term.

Figure 5-2(b) demonstrates that increasing spacer length, which is accompanied with increasing hybridization efficiency, leads to a decreasing entropic blocking penalty on the free energy of duplex formation. Getting far away from the surface would give the immobilized strands more freedom to move, and reduce the conformational restrictions imposed on the structure by the surface [18, 20]. This will facilitate the duplex formation reaction between free targets in solution and immobilized probes on the surface, and would lead to duplexes with higher stabilites. As a result, the trends seen with the entropic blocking term reflect the results we observed experimentally.

The conclusions reached by the analyses of the electrostatic and entropic blocking terms can be combined to propose that at the spacer lengths and experimental conditions tested, the entropic blocking seems to show more dominant effect than the electrostatic blocking term. The stability of the duplex formed on the surface increases with increasing spacer length.

5.3.2 Effect of Probe Density on Melting Temperature

The effect of the probe density on the melting temperature of the duplex on the surface in comparison with the melting temperature prediction in solution using Nearest Neighbor method [17] at different initial target-to-probe concentration ratios is presented in Figure 5-3.

Firstly, the observed melting temperatures on the surface are lower than the melting temperatures predicted in solution. A similar discussion following the experiments with different spacer lengths would conclude that the electrostatic and entropic blocking effects introduced by the presence of the surface leads to a reduction in the stability of the duplex formed on the surface. A lower stability would be accompanied with a lower melting temperature compared with in-solution.

Secondly, as the initial target-to-probe concentration ratio decreases, the melting temperature of the duplexes increases at all probe densities. This observation shows the same trend seen in the previous experiments with target concentration. Therefore, a similar approach can be taken to interpret this finding: examination of the contributions of electrostatic and entropic blocking on the free energy of duplex formation on the surface with respect to the probe density changes. Figure 5-4 demonstrates the behavior of electrostatic and entropic blocking terms modeled through the theory presented in Chapter 2. These plots carry the effects of the applied system parameters, with probe densities of $5*10^{12}$ molecules/cm^2 and $5*10^{13}$ molecules/cm^2, and a constant 15 dT spacer length, a probe length equal to the target length of 25 nt, an ionic concentration of 1 M NaCl, and at melting temperatures corresponding to initial target to probe ratio of 1 at all spacer lengths, as an example.

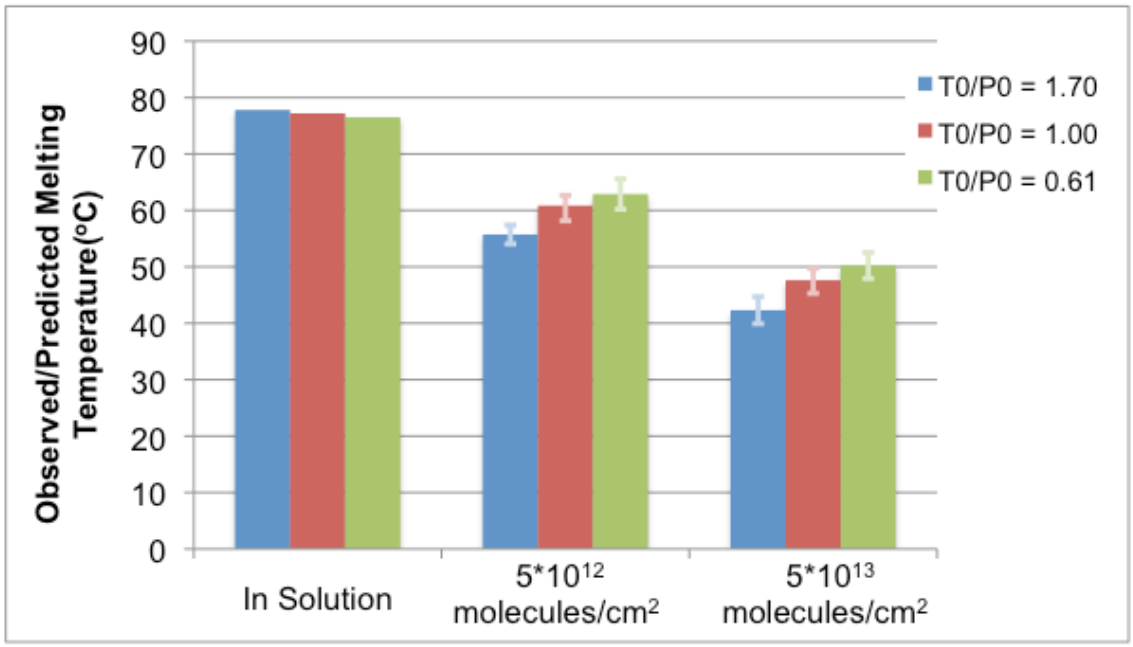

Figure 5-3 The comparison of the effect of probe density on the melting temperature of the duplex on surface with predicted melting temperatures in solution at the same target-to-probe ratios.

(a)

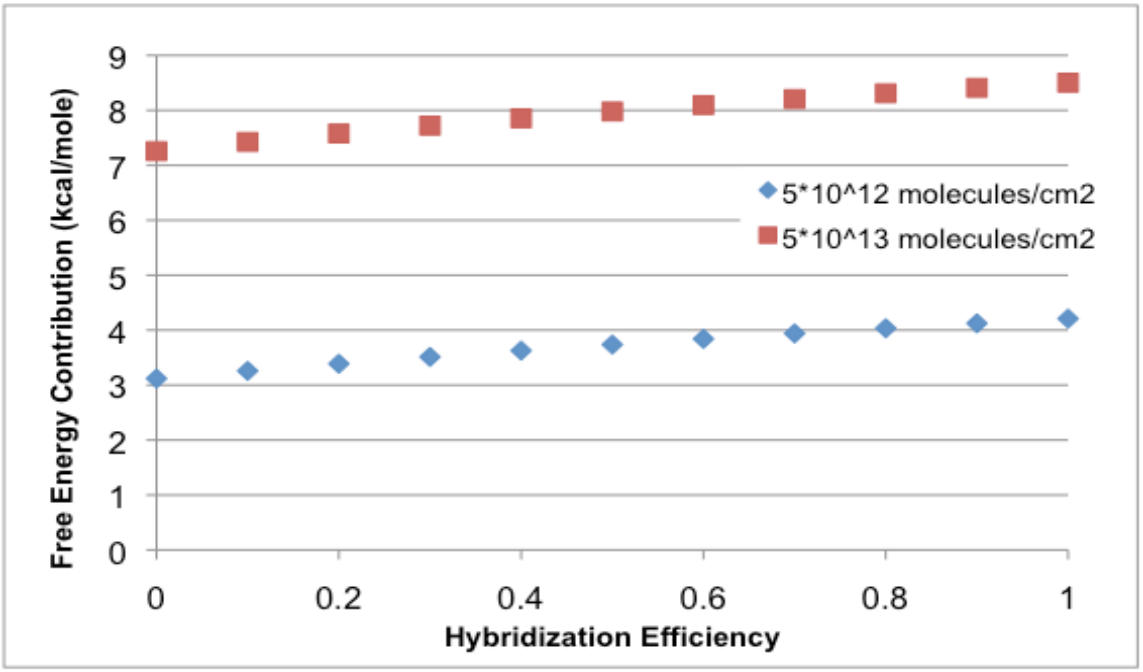

(b)

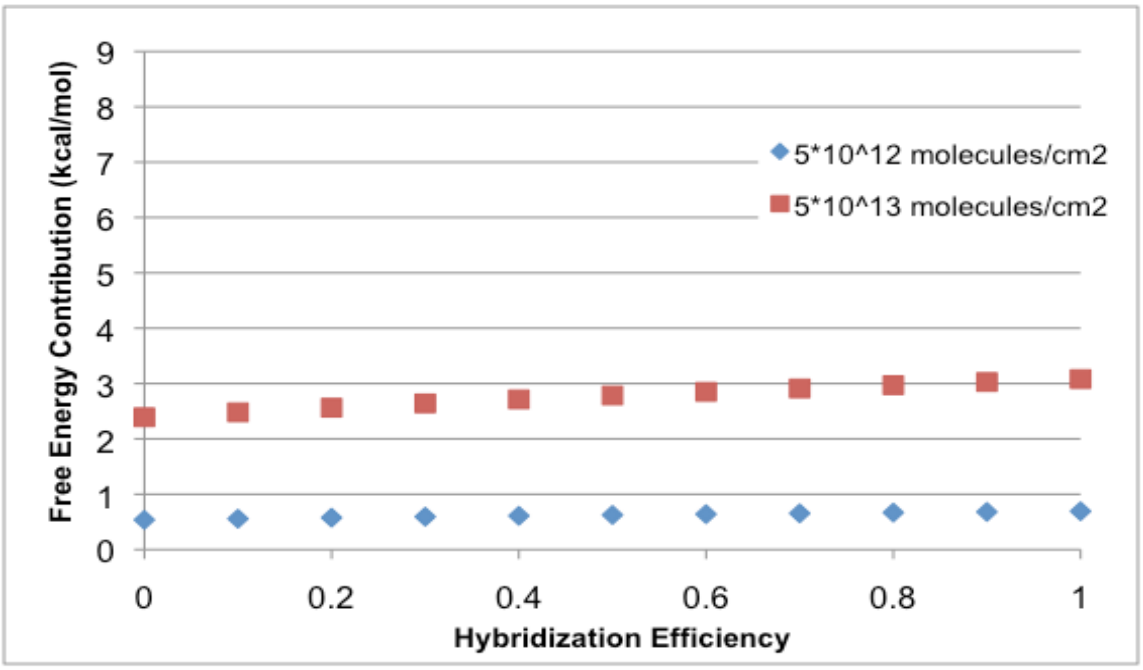

Figure 5-4 The contribution of (a) electrostatic blocking and (b) entropic blocking on the free energy of duplex formation at different, used probe densities ($5*10^{12}$ molecules/cm^2, $5*10^{13}$ molecules/cm^2) with respect to different hybridization efficiencies, a fixed spacer length of 15 dT, a salt concentration of 1M NaCl, at melting temperatures obtained at target to probe ratio = 1.

To be able to see the effect of different target concentrations requires the knowledge of how it is incorporated in the analysis. Table 5-3 is tabulated to show how the hybridization efficiencies change with respect to different target concentrations. This table includes the PMT voltages used in 635 nm wavelength to excite the labeled target molecules hybridized on the surface at different target concentrations and probe densities, and the average net median probe intensities observed in 635 nm channel.

Table 5-3 PMT voltages used in 635 nm wavelength to detect the probe-target duplex formed on the surface at equilibrium, at the end of initial hybridization, with different probe densities and target concentrations.

Concentration of Target in Solution (nM)	PMT Voltage Used at 635 nm Excitation Wavelength	Average Net Median Probe Intensity at 23°C in 635 nm Channel
EXPERIMENTAL SET WITH PROBE DENSITY = $5*10^{12}$ molecules/cm^2		
1	480	51779
0.59	490	52471
0.36	500	50952
EXPERIMENTAL SET WITH PROBE DENSITY = $5*10^{13}$ molecules/cm^2		
10	520	53719
5.9	535	52355
3.6	555	55275

It can be concluded from Table 5-3 that PMT voltages used in the experiments with lower target concentrations were needed to be increased to provide a wider dynamic range to capture the signal intensity change of the duplexes on the surface during the melting experiment. This indirectly indicates that at all probe densities, a decrease in the target concentration leads to a decrease in the hybridization efficiency. This corresponds to lower electrostatic and entropic penalties imposed on the free energy of duplex formation on the surface in Figure 5-4, leading to DNA duplexes with higher stability and melting temperatures on the surface.

Lastly, it can be observed from Figure 5-3 that an increase in the probe density leads to a decrease in the melting temperature of the duplex on the

surface. In this case, the relative effects of the blocking terms in Figure 5-4 are investigated with respect to probe density. Electrostatically, in Figure 5-4(a), it is observed that an increase in the surface density increases the penalty that is going to be experienced by a target coming into the probe layer. This is mostly due to the denser layer of polyelectrolytes, with increased charge density and the negatively increased surface potential. In addition, as it is seen in Figure 5-4(b), the entropic penalty experienced by the target hybridizing would be higher due to denser layer of probes grafted on the surface and the steric effects it experiences while going into this layer. Therefore, both electrostatic and entropic contributions of the increasing probe density will be in the direction to reduce the duplex stability on the surface and the observed melting temperature. In addition, as it can be seen in Table 5-3, the maximum extent of reaction at the initial hybridization temperature also decreases with increasing probe density, which is in agreement with various studies published in literature [10, 21, 22]. The PMT voltages used in the experiments were increased with decreasing probe density to provide a wider dynamic range for the melting temperature experiments.

This trend is observed for the probe densities higher than $5*10^{12}$ molecules/cm^2 mostly due to the entropic crowding effect. However, it is shown in some of the studies that increasing probe density can also result in increasing signal intensities [11]. This contradiction can be investigated further by observing the hybridization signal intensity change on the surface obtained with respect to different probe densities in Figure 5-5 (unpublished data).

This figure demonstrates that there is an optimum probe density in which the observed crowding effect is minimum and therefore the sensitivity, or the detection level of the system becomes maximum. This probe density corresponds to $2.5 * 10^{12}$ molecules/cm^2. When the probe density is increased beyond this value, the entropic crowding effect dominates the reaction, and the expected hybridization efficiency drops. On the other hand, as the probe density is lowered, the number of probes that can hybridized with the targets without the interference from the crowding effect also decreases. This results in a decrease

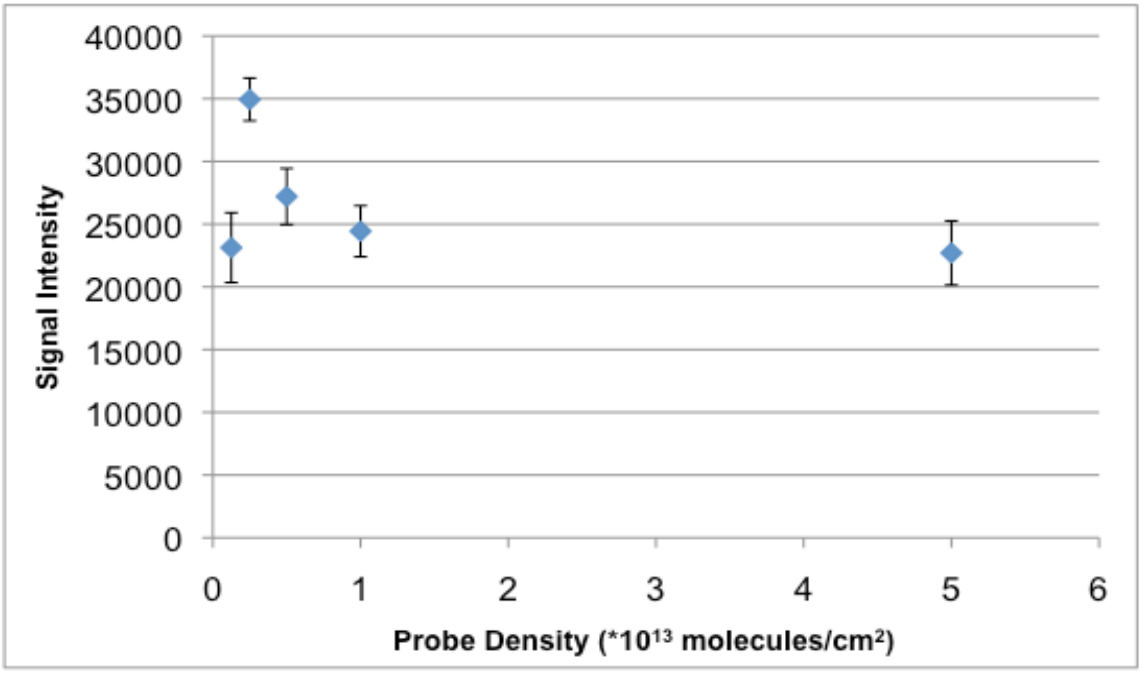

Figure 5-5 Hybridization signal intensity change on the surface with respect to different probe densities. Hybridization conditions were 1 M NaCl, at 23°C and 100 nM target concentration.

in the hybridization signal intensity as it can be observed at the probe density of $1.25*10^{12}$ molecules/cm^2.

Formation of a less stable duplex in denser probe layers has also been predicted in previous Monte Carlo simulation studies [23]. It is pointed out that at high probe densities, or in high brush regime, the targets can bind to more than one probe in the same neighborhood. This would lead to a less stable duplex structure compared to a fully hybridized one, because there would be unbound bases along the sequence, which could be energetically less stable for the structure [24, 25], and additional configurational restrictions would be imposed on it due to stretching [26].

5.3.3 The Comparison of the Effects of Spacer Length and Probe Density on Melting Temperature

The comparison of the effects of spacer length and probe density on the melting temperature of the duplex on the surface and in solution at different initial target-to-probe concentration ratios is presented in Figure 5-6. It can be observed that the effect of probe density is more pronounced in the destabilization of the duplex structure than the spacer length. This could be expected since the entropic and electrostatic blockings seem to create more penalty with increasing probe density than the decreasing spacer length, when the experimental conditions are imposed on the system (Figures 5-2 and 5-4). Electrostatically, a probe density change from $5*10^{12}$ molecules/cm^2 to $5*10^{13}$ molecules/cm^2 would lead to a surface charge and surface potential increase. Since the surface potentials are directly proportional to the free energy penalty experienced by a hybridizing target, this change would increase the electrostatic blocking penalty, i.e. from + 1 kcal/mol to + 5 kcal/mol at no hybridization efficiency (Figure 5-4(a)). However, a similar change in the spacer length from 2 dT to 25 dT would result in a smaller penalty variation, i.e. from + 1.4 kcal/mol to + 1.5 kcal/mol at no hybridization efficiency (Figure 5-2(a)). Comparatively, we can deduce that the electrostatic blocking imposed by creating a denser probe layer is more effective in reducing the stability of the duplex formed than lifting

the duplex higher on the surface. Furthermore, entropically, it can be observed from Figure 5-4(b) that a probe density change imposing a denser grafting layer on the surface would lead to an increase in the penalty from + 0.5 kcal/mol to + 2.25 kcal/mol at no hybridization and same spacer length of 15 dT. However, varying the spacer length from 25 dT to 2 dT at a probe density of $5*10^{12}$ molecules/cm^2 would only increase the penalty from + 0.45 kcal/mol to + 0.55 kcal/mol at no hybridization (Figure 5-2(b)). These arguments would lead us to the conclusion that at the conditions tested, bringing the neighborhood probes closer and creating a crowded environment seems to be more effective in reducing the stability of the duplex formed on the surface than getting far away from the impermeable surface.

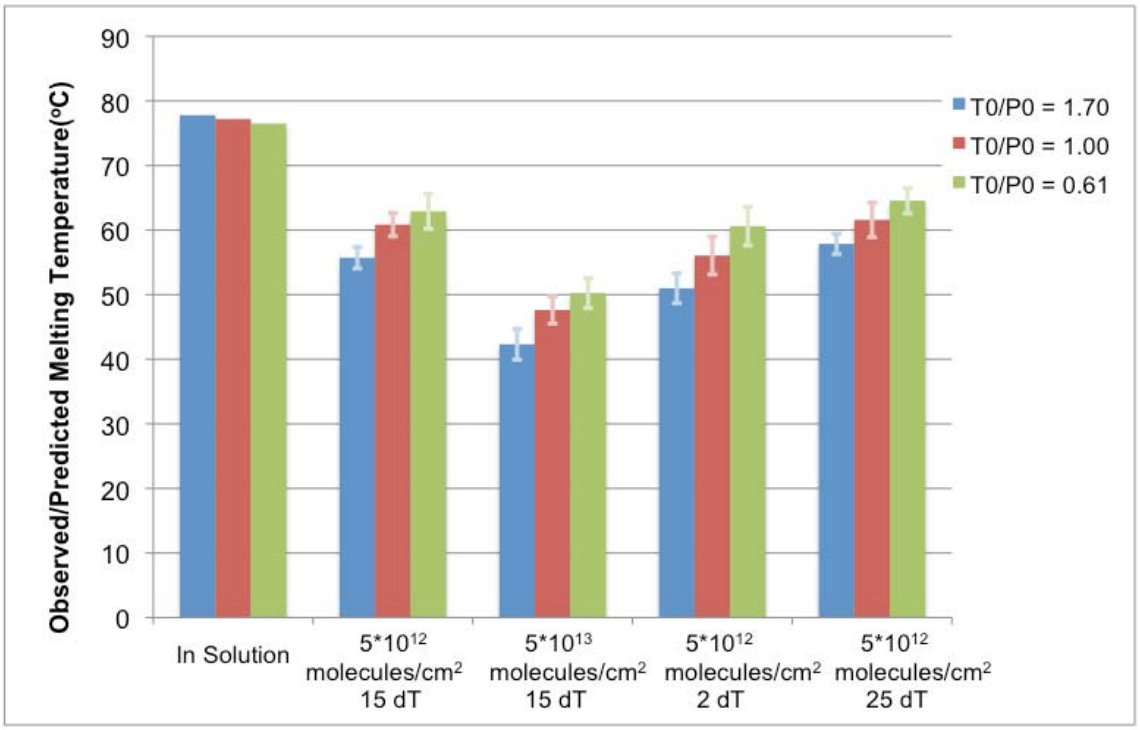

Figure 5-6 The comparison of the effect of spacer length and probe density on the melting temperature of the duplex on surface with predicted melting temperatures in solution at the same target-to-probe ratios.

5.4 Conclusions

This chapter describes the effects of spacer length and probe density on the free energy of duplex formation on the surface, and more specifically, the melting temperature of the duplex, using a combined experimental and theoretical approach. It is experimentally observed that the melting temperature on the surface is lower than in solution. The surface seems to impact the hybridization through its charge as well as the immobilization of one of the strands of the duplex and its impermeability.

Each change imposed on spacer length and probe density was carried out at different target concentrations. In this manner, we were able to confirm our previous finding that an increasing target concentration leads to a decrease in the melting temperature, which was also demonstrated theoretically through the electrostatic and entropic blocking models presented in Chapter 2.

Spacer length experiments focused on varying the distance between the duplex and the surface by changing the number of synthesized dT monomers as spacers. We were able to experimentally demonstrate that, in addition to increasing the extent of hybridization, a longer spacer leads to the formation of a more stable structure with a higher melting temperature. It is also possible to theoretically support this result with the application of the models on contributions of the electrostatic and entropic blocking penalties on the duplex formation. Although an increasing spacer length is found to increase the electrostatic penalty, the reduction of the entropic penalty by moving the duplex away from the surface seems to dominate the hybridization with these system parameters. On the other hand, the experiments with different probe densities showed that a denser surface leads to a lower hybridization efficiency, a decrease in the extent of hybridization on the surface, and also to a structure with a lower stability and a lower melting temperature. The experimental results were supported by the trends seen in the models simulating the electrostatic and entropic blocking penalties; both of which increase with the presence of more grafted probes on the surface. An overall theoretical and experimental comparison of these different design parameters (spacer length and probe density) yields that an increase in

the probe density could have more impact on decreasing the free energy of the duplex formation on the surface than decreasing spacer length. These findings can be used as a guide in the design of experiments and optimization of the hybridization conditions to create a microarray environment that could lead to more accurate outcomes, when spacer length and probe density are considered as design parameters.

5.5 Bibliography

1. Pylatuik JD, Fobert PR, *Comparison of transcript profiling on Arabidopsis microarray platform technologies*. Plant Mol Biol, 2005. 58: 609-624.
2. Schena M, Shalon D, Davis RW, Brown PO, *Quantitative monitoring of gene expression patterns with a complementary DNA microarray*. Science, 1995. 270: 467-470.
3. Shchepinov MS, Case-Green SC, Southern EM, *Steric factors influencing hybridisation of nucleic acids to oligonucleotide arrays*. Nucleic Acids Res, 1997. 25: 1155-1161.
4. Guo Z, Guilfoyle RA, Thiel AJ, Wang R, Smith LM, *Direct fluorescence analysis of genetic polymorphisms by hybridization with oligonucleotide arrays on glass supports*. Nucleic Acids Res, 1994. 22: 5456-5465.
5. Southern EM, Case-Green SC, Elder JK, Johnson M, Mir KU, Wang L, Williams JC, *Arrays of complementary oligonucleotides for analysing the hybridisation behaviour of nucleic acids*. Nucleic Acids Res, 1994. 22: 1368-1373.
6. Hughes TR, Mao M, Jones AR, Burchard J, Marton MJ, Shannon KW, Lefkowitz SM, Ziman M, Schelter JM, Meyer MR, Kobayashi S, Davis C, Dai H, He YD, Stephaniants SB, Cavet G, Walker WL, West A, Coffey E, Shoemaker DD, Stoughton R, Blanchard AP, Friend SH, Linsley PS, *Expression profiling using microarrays fabricated by an ink-jet oligonucleotide synthesizer*. Nat Biotechnol, 2001. 19: 342-347.
7. Kane MD, Jatkoe TA, Stumpf CR, Lu J, Thomas JD, Madore SJ, *Assessment of the sensitivity and specificity of oligonucleotide (50mer) microarrays*. Nucleic Acids Res, 2000. 28: 4552-4557.
8. Peterson AW, Wolf LK, Georgiadis RM, *Hybridization of mismatched or partially matched DNA at surfaces*. J Am Chem Soc, 2002. 124: 14601-14607.
9. Chou CC, Chen CH, Lee TT, Peck K, *Optimization of probe length and the number of probes per gene for optimal microarray analysis of gene expression*. Nucleic Acids Res, 2004. 32: e99.

10. Peterson AW, Heaton RJ, Georgiadis RM, *The effect of surface probe density on DNA hybridization*. Nucleic Acids Res, 2001. 29: 5163-5168.
11. Watterson JH, Paul A. E. Piunno, Christopher C. Wust, Ulrich J. Krull, *Effects of Oligonucleotide Immobilization Density on Selectivity of Quantitative Transduction of Hybridization of Immobilized DNA*. Langmuir, 2000. 16: 4984-4992.
12. Steel AB, Levicky RL, Herne TM, Tarlov MJ, *Immobilization of nucleic acids at solid surfaces: effect of oligonucleotide length on layer assembly*. Biophys J, 2000. 79: 975-981.
13. www.izbi.de/working_papers.html
14. Dai H, Meyer M, Stepaniants S, Ziman M, Stoughton R, *Use of hybridization kinetics for differentiating specific from non-specific binding to oligonucleotide microarrays*. Nucleic Acids Res, 2002. 30: e86.
15. Peplies J, Glockner FO, Amann R, *Optimization strategies for DNA microarray-based detection of bacteria with 16S rRNA-targeting oligonucleotide probes*. Appl Environ Microbiol, 2003. 69: 1397-1407.
16. Wick LM, Rouillard JM, Whittam TS, Gulari E, Tiedje JM, Hashsham SA, *On-chip non-equilibrium dissociation curves and dissociation rate constants as methods to assess specificity of oligonucleotide probes*. Nucleic Acids Res, 2006. 34: e26.
17. SantaLucia JJ, *A unified view of polymer, dumbbell, and oligonucleotide DNA nearest-neighbor thermodynamics*. Proc Natl Acad Sci U S A, 1998. 95: 1460-1465.
18. Southern E, Mir K, Shchepinov M, *Molecular interactions on microarrays*. Nat Genet, 1999. 21: 5-9.
19. Mergny JL, Lacroix L, *Analysis of thermal melting curves*. Oligonucleotides, 2003. 13: 515-537.
20. Halperin A, Buhot A, Zhulina EB, *Hybridization at a surface: the role of spacers in DNA microarrays*. Langmuir, 2006. 22: 11290-11304.

21. Glazer MI, Fidanza JA, McGall GH, Trulson MO, Forman JE, Frank CW, *Kinetics of oligonucleotide hybridization to DNA probe arrays on high-capacity porous silica substrates*. Biophys J, 2007. 93: 1661-1676.
22. Wilkins Stevens P, Henry MR, Kelso DM, *DNA hybridization on microparticles: determining capture-probe density and equilibrium dissociation constants*. Nucleic Acids Res, 1999. 27: 1719-1727.
23. Jayaraman A, Hall CK, Genzer J, *Computer simulation study of probe-target hybridization in model DNA microarrays: effect of probe surface density and target concentration*. J Chem Phys, 2007. 127: 144912.
24. Forman JE, Ian D. Walton, David Stern, Richard P. Rava, Mark O. Trulson, *Thermodynamics of Duplex Formation and Mismatch Discrimination on Photolithographically Synthesized Oligonucleotide Arrays*. ACS Symposium Series, 1998. 682: 206-228.
25. Levicky R, Horgan A, *Physicochemical perspectives on DNA microarray and biosensor technologies*. Trends Biotechnol, 2005. 23: 143-149.
26. Halperin A, A. Buhot, E. B. Zhulina, *On the hybridization isotherms of DNA microarrays: the Langmuir model and its extensions*. Journal of Physics: Condensed Matter, 2006. 18: S463-S490.

CHAPTER VI

CONCLUSIONS AND RECOMMENDATIONS

6.1 Conclusions

In this dissertation, the main objective is to study the impact of surfaces on DNA hybridization between an immobilized probe and a free target, through the investigation of changes imposed on its melting temperature by different system parameters, namely, target concentration, spacer length and probe density. Attachment of one of the strands on the surface introduces a new dimension in which the interactions taking place in a homogeneous solution are further constrained by the surface effects. Here, we looked at these restrictions both theoretically and experimentally.

Chapter 2 theoretically investigates the presence of the surface in terms of the electrostatic and entropic blockage it imposes on the hybridization reaction. Electrostatic blocking stems from the charge of the surface and the probe layer. In this chapter, it is modeled through Electrical Double Layer theory and Surface Partition Model, which take into account the change in the surface potential as the reaction continues, and thus, the free energy penalty on the surface. We were able to verify the application of Electrical Double Layer theory experimentally, and by using the predicted surface potentials, we simulated the effect of spacer length and probe density. A longer spacer and a denser probe layer were found to increase the electrostatic free energy penalty experienced by the hybridizing target. Entropic blocking is a result of the volume exclusion by the impermeable surface, the configurational restrictions due to the attachment of the probes, and the crowding by these probes. This term is modeled through the

polymer physics theory, including the monomer-monomer interactions, entropy of mixing, the stretching of the probes and the influence of the impenetrable wall. These terms are collectively represented to calculate the free energy penalty of entropic blocking. We simulated the effect of spacer length and probe density, and found that as the hybridization moves farther away from the surface, the entropic penalty decreases. However, a highly grafted surface increases the penalty encountered by a hybridizing target.

Chapter 3 reveals the experimental approach we developed to examine the influences of different system parameters (target concentration, spacer length and probe density) on DNA duplex formation through generation of melting curves. This system comprises of a microfluidic chip on which the probes are synthesized using light-directed synthesis, a real-time fluorescence detection system using a scanner, and integration with a computer for control and automation. Duplex formation takes place between the probes on the surface and labeled targets, which are constantly recirculated through the microfluidic channels. The synthesis quality is determined with on-chip controls, and the analysis of the reproduced melting curves and melting temperature extraction are carried out through various steps of background correction, normalization, temperature calibration, smoothing, curve fitting and statistical analysis implemented in Matlab (Mathworks Inc, Massachusetts, USA).

Chapter 4 demonstrates the effect of different target concentrations on the hybridization reaction at different probe concentrations. In all experimental conditions, the melting temperature of the DNA duplex was found to be lower on the surface as compared to in-solution values due to the penalties encountered by the hybridizing target. This discrepancy is found to increase with increasing target concentrations, indicating the increased probability of target binding to more than one probe as well as the steric effects due to the presence of more duplexes formed on the surface at these target concentrations. Through the introduction of different target concentrations at different probe concentrations on the surface, we observed experimentally that a decreasing target concentration leads to increasing melting temperatures at all probe concentrations, a finding

contrary to in solution predictions. Two approaches were devised to investigate this result. First one includes the derivation of association equilibrium constant involving the maximum extent of hybridization term at two temperatures, initial hybridization and melting temperatures. These expressions were then utilized in the temperature dependent van't Hoff equation, and the variation of the melting temperature with respect to maximum extent of hybridization and initial target-to-probe ratios were plotted. It was observed in this graph that with increasing target concentrations corresponding to higher extent of hybridizations, it is possible to observe decreasing melting temperatures. Our second approach includes the utilization of the theoretical models developed in Chapter 2. Simulation of electrostatic and entropic blocking terms with the system parameters used showed separately that with increasing target concentrations and surface coverages, the penalties imposed by the presence of the surface also increase. These would make the duplex formed on the surface less stable, and therefore lead to lower melting temperatures. This decrease in the melting temperature with increasing target concentration is also in accordance with the Monte Carlo simulations by Jayaraman *et al.* [1]. Furthermore, in the experiments with very low target and probe concentrations, we observed melting curves indicative of multiple melting processes at low temperature domains, before the perfect match duplexes melt at a higher temperature. This was interpreted as the melting of low stability duplexes formed between truncated probes, an inherent characteristic of *in situ* synthesis, and the targets. This hypothesis was confirmed with high temperature pre-hybridization study, and it was proposed that the quality of the synthesis can be monitored through the generation of melting curves at very low target and probe concentrations.

Chapter 5 experimentally investigates the effects of spacer length and probe density on DNA melting temperature on the surface. Previously observed low surface melting temperatures, and the influence of target concentration on the melting temperature were verified under different system variables. With increasing spacer lengths, it was found that the melting temperature of the duplex formed on the surface increases. Longer spacer molecules mitigate the

effect of the surface, reducing the entropic penalty encountered by the hybridizing target. On the other hand, increasing lengths of strands bring in more surface charges, therefore, increasing the electrostatic blocking. Based on these two model simulations and the experimental results, it was concluded that the entropic blocking seems to have a more dominant influence on the stability of DNA under these experimental conditions. However, an increasing probe density was found to decrease the stability of the duplex. Due to the increase in the surface charge and potential, and the crowding of the probes, the contributions of both electrostatic and entropic blocking terms increase; leading to much lower stability and melting temperatures. This finding is in accordance with the Monte Carlo simulation studies published in the literature [1]. Examining the relative effects of these terms reveals the comparative influences of spacer length and probe density, and leads us to the conclusion that under the experimental conditions tested, the probe density change seems to be more effective in terms of reducing the duplex stability and melting temperature.

The results of this study form a basis for further investigations of the influences of various system characteristics on duplex stability, and on the dependency of melting temperature on different variables. The knowledge of melting temperature can be used as a guide to design systems and experiments with accurate and reproducible outcomes. Presence of false positives due to non-specific or cross-hybridizations [2-4] can be avoided by carefully selecting the hybridization temperature; a higher hybridization temperature may result in more accurate results; however, this selection needs to be tuned carefully to avoid loss of the intended signal from the perfect matches. In addition, false negative results (i.e. genes with low expression levels [5, 6]) can also be improved by selecting hybridization temperatures depending on the value of the melting temperature of the perfect match duplex on the surface. Another application would be mutation scanning, or single nucleotide polymorphism detection in a parallel fashion by creating and monitoring melting curves on the surface, and comparing them against several reference curves for determination.

This technique has been successfully applied in solution [7-9] using an approach pioneered by Idaho Technologies Inc (Utah, USA).

6.2 Recommendations for Future Work

In this dissertation, the impact of the surface on DNA melting temperature was theoretically and experimentally investigated through three different system parameters: target concentration, spacer length and probe density. However, with the DNA duplex formation taking place on a solid interface, there are various variables that need to be thoroughly studied for the optimum design of the reaction and the system. The dependence of the DNA melting temperature on probe and target length; their sequences, and solution conditions (pH, salt concentrations) could be influenced differently when one of the strands is attached to the surface. Furthermore, this attachment brings an asymmetry to the structure of the probe layer. This suggests that the location of a particular base and mismatch along a probe strand as well as its sequential context might influence their impact on hybridization. Therefore, the design of the system needs to take these into account for the desired level of specificity and sensitivity to be achieved for the objective of the experiment.

For a study that investigates the effect of a mismatch, the stability of the perfect match and mismatch duplexes observed need to be discriminating enough for a plausible distinction. Initially, this requires the determination of the appropriate system parameters such as probe density and spacer length. The selection of the probe density is especially important since an increasing level of detection with higher probe densities does not always result in an observable difference in the perfect match and mismatch signal intensities [10]. This can be determined through experimentation with various system parameters for observable melting temperature differences between the two duplexes. Secondly, the probe sequences play an important role in this distinction. The knowledge of how system parameters affect the melting temperature would yield a melting temperature range to operate in. Within this range, the probes can be designed to specifically demonstrate the effect of a mismatch under the hybridization

conditions (salt concentration, pH) and hybridization temperature (depending on the melting temperature range). This process requires a thorough and vigorous experimentation and melting curve generation for all possible contextual and positional mismatches along the probe sequence. Then, the corresponding melting temperature differences between perfect match and mismatch sequence can be monitored within the study, and it could be possible to comment on the location and type of mismatch on the target sequence based on the designed probe sequence and the observed temperature difference. This study would also allow one to extract dinucleotide thermodynamic base-stacking terms ($\Delta G°$, $\Delta H°$, $\Delta S°$) for a position-dependent nearest neighbor approach, and can be further utilized in the prediction of the stability of the duplex on the surface as well as its melting temperature.

The electrostatic and entropic contributions of the surface can also be monitored individually for their corresponding effects. An experimental approach would be to create an array with the same characteristics, and use peptide nucleic acids (PNA) as the main structure of the spacers, probes and targets. PNA molecules carry no charge [11], and therefore, the electrostatic effect during the hybridization reaction would be quite negligible. As a result, the observed melting temperature on the surface, the stability of the duplexes, will directly indicate the effect of entropic blocking on the duplex formation on the surface, and help us relate the theoretical predictions with the experimental observations more directly.

The real-time capturing capability of our experimental set-up can be further enhanced by monitoring the concentration of the target strands in the bulk solution. This would enable us to calculate hybridization efficiency at different experimental conditions, and extract the kinetic parameters of duplex formation on the surface (i.e. equilibrium association constant). With this approach, we can observe the relative effects of different experimental conditions on the kinetics of duplex formation reaction on the surface as well. This proposed modification could be made by introducing a laser coupled-fiber directed into solution above the hybridization surface to measure the fluorescence of the target in the bulk.

6.3 Bibliography

1. Jayaraman A, Hall CK, Genzer J, *Computer simulation study of probe-target hybridization in model DNA microarrays: effect of probe surface density and target concentration*. J Chem Phys, 2007. 127: 144912.

2. Loy A, Lehner A, Lee N, Adamczyk J, Meier H, Ernst J, Schleifer KH, Wagner M, *Oligonucleotide microarray for 16S rRNA gene-based detection of all recognized lineages of sulfate-reducing prokaryotes in the environment*. Appl Environ Microbiol, 2002. 68: 5064-5081.

3. Naef F, Magnasco MO, *Solving the riddle of the bright mismatches: labeling and effective binding in oligonucleotide arrays*. Phys Rev E Stat Nonlin Soft Matter Phys, 2003. 68: 011906.

4. Wang Y, Miao ZH, Pommier Y, Kawasaki ES, Player A, *Characterization of mismatch and high-signal intensity probes associated with Affymetrix genechips*. Bioinformatics, 2007. 23: 2088-2095.

5. Li ESY, Liu W-T, *DNA microarray technology in microbial ecology studies-principle, applications and current limitations*. Microbes and Environments, 2003. 18: 175-187.

6. Peplies J, Glockner FO, Amann R, *Optimization strategies for DNA microarray-based detection of bacteria with 16S rRNA-targeting oligonucleotide probes*. Appl Environ Microbiol, 2003. 69: 1397-1407.

7. Herrmann MG, Durtschi JD, Bromley LK, Wittwer CT, Voelkerding KV, *Amplicon DNA melting analysis for mutation scanning and genotyping: cross-platform comparison of instruments and dyes*. Clin Chem, 2006. 52: 494-503.

8. Liew M, Seipp M, Durtschi J, Margraf RL, Dames S, Erali M, Voelkerding K, Wittwer C, *Closed-tube SNP genotyping without labeled probes/a comparison between unlabeled probe and amplicon melting*. Am J Clin Pathol, 2007. 127: 341-348.

9. Wittwer CT, Reed GH, Gundry CN, Vandersteen JG, Pryor RJ, *High-resolution genotyping by amplicon melting analysis using LCGreen*. Clin Chem, 2003. 49: 853-860.

10. Peterson AW, Wolf LK, Georgiadis RM, *Hybridization of mismatched or partially matched DNA at surfaces*. J Am Chem Soc, 2002. 124: 14601-14607.

11. http://en.wikipedia.org/wiki/Peptide_nucleic_acid